POLITECNICO DI MILANO
SCUOLA DI INGEGNERIA INDUSTRIALE E DELL'INFORMAZIONE
Dipartimento di Elettronica, Informazione e Bioingegneria
Corso di Laurea Magistrale in Ingegneria Biomedica

A COMPACT AND WIRELESS LUNG FUNCTION TEST DEVICE FOR VETERINARY MEDICINE

Relatore:
Prof. Raffaele Dellacà

Correlatore:
Ing. Davide Bizzotto

Tesi di Laurea Magistrale di:
Thomas Carrassi 944664

Anno Accademico 2020-2021

ABSTRACT

The clinical evaluation of respiratory mechanics in horses is nowadays based on invasive methods that may require sedation. The forced oscillation technique (FOT), known also as oscillometry, is a non-invasive method for lung function testing used in humans that doesn't require subject collaboration. Current FOT devices suitable to be used on horses are complex, cumbersome, expensive, and difficult to be applied in quine veterinary settings. This thesis aims to develop a small, cheap, portable and easy-to-use FOT device according to a novel approach in which the pressure waveforms are generated by a fan moved by the rotational speed of a brushless DC motor. This new approach has been recently demonstrated by a proof-of-concept device. From results of this concept, the detailed specifications of a device for clinical use was defined and both the device and a software application for wireless operations and control were designed and developed. This device was validated in vitro, providing an average error of 0.0789 $cmH_2O \cdot {}^{s}/_{L}$ and 0.2433 $cmH_2O \cdot {}^{s}/_{L}$, respectively, in measuring R and X. The device was also tested in-vivo on five healthy horses and a horse diagnosed with SEA (Severe Equine Asthma), demonstrating good tolerability of the procedure, correct functioning of the device, and reliability in resistance and reactance of horses' respiratory system estimation. This novel approach for applying FOT allowed the development of a compact, wireless, inexpensive, and portable device for the non-invasive evaluation of respiratory mechanics in spontaneously breathing horses, providing a valuable new tool for improving veterinary respiratory medicine.

ABSTRACT IN ITALIANO

La valutazione clinica della meccanica respiratoria nei cavalli si basa attualmente su metodiche invasive che possono richiedere la sedazione. La tecnica delle oscillazioni forzate (FOT), nota anche come oscillometria, è un metodo non invasivo per il test di funzionalità polmonare utilizzato nell'uomo che non richiede la collaborazione del soggetto. Gli attuali dispositivi FOT adatti all'uso sui cavalli sono complessi, ingombranti, costosi e difficili da applicare in ambito veterinario. Questa tesi mira a sviluppare un dispositivo FOT compatto, economico, portatile e facile da usare secondo un nuovo approccio in cui le forme oscillazini pressorie sono generate da una ventola mossa da un motore DC senza spazzole. Questo nuovo approccio è stato recentemente dimostrato da un dispositivo proof-of-concept. Dai risultati di questo prototipo, sono state definite le specifiche dettagliate di un dispositivo per uso clinico e sono stati progettati e sviluppati sia il dispositivo che un'applicazione software per l'elaborazione dei dati e il controllo wireless. Questo dispositivo è stato validato in vitro, fornendo un errore medio di 0,0789 $cmH_2O \cdot s/L$ e 0,2433 $cmH_2O \cdot s/L$, rispettivamente, nella misurazione di resistenza e reattanza. Il dispositivo è stato anche testato in vivo su cinque cavalli sani e un cavallo con diagnosi di SEA (Severe Equine Asthma), dimostrando una buona tollerabilità della procedura, il suo corretto funzionamento e di misurare resistenza e reattanza con una buona affidabilità. Questo nuovo approccio per l'applicazione della FOT ha consentito lo sviluppo di un dispositivo compatto, wireless, poco costoso e portatile per la valutazione non invasiva della meccanica respiratoria nei cavalli durante il respiro spontaneo, fornendo un nuovo prezioso strumento per migliorare la medicina respiratoria veterinaria.

Contents

ABSTRACT **3**

ABSTRACT IN ITALIANO **4**

CONTENTS **6**

SOMMARIO **9**

INTRODUCTION **16**

CHAPTER 1 STATE OF THE ART **18**

1.1 PHYSIOLOGY OF BREATHING IN HORSES 18

1.2 MODEL OF LUNG 22

1.2.1 Airway Resistance *23*

1.2.2 Lung Elasticity *23*

1.2.3 Pulmonary Inertance *24*

1.3 IN VITRO MODEL 24

1.3.1 Axial Fluid Flow *25*

1.3.2 Gas Compression *26*

1.3.3 Distributed Line Model *27*

1.4 PATHOLOGIC HORSE 28

1.5 DIAGNOSIS OF ASTHMA AND PULMONARY TEST IN HORSES 29

1.6 MEASUREMENT OF MECHANICAL PROPERTIES 30

1.6.1 Forced expiration *31*

1.6.2 End-expiratory lung volume *32*

1.6.3 Endoscopy *32*

1.6.4 Immunological Test *32*

1.6.5 Arterial blood analysis *32*

1.7 FORCED OSCILLATION TECHNIQUE (FOT) 33

1.7.1 Impedance *38*

1.8 FOT ON HORSES 39

1.9 A NEW APPROACH 41

CHAPTER 2 A NEW DEVICE FOR PULMONARY ASSESSMENT IN HORSES 43

2.1 REQUIREMENTS 43
2.2 ARCHITECTURE 44
2.3 ESP-32 MICROCONTROLLER 45
2.4 MOTOR UNIT 47
2.4.1 Brushed 48
2.4.2 BLDC 48
2.4.3 Control strategy 52
2.5 AIR COMPRESSION UNIT 55
2.5.1 Motor Housing 55
2.6 SENSOR UNIT 56
2.6.1 Differential pressure sensors 57
2.6.2 Pneumotachograph 58
2.6.3 Monitoring Unit 60
2.7 POWER SUPPLY 62
2.8 CONTROL UNIT 64
2.9 COMMUNICATION 64
2.9.1 Wireless Transmission 65
2.9.2 TCP protocol 68
2.9.3 I2C protocol 69
2.9.4 SPI protocol 71
2.9.5 ESC 72
2.10 HORSE MASK 73
2.10.1 3D-printing Process 75
2.10.2 Silicon components from moulds 76

CHAPTER 3 FIRMWARE AND CONTROL STRATEGY 78

3.1 LOW-LEVEL CONTROL 78
3.1.1 Open loop 79
3.1.2 Closed Loop 79
3.2 CUSTOM CONTROL STRATEGY 81

3.2.1 Offset Control *82*
3.2.2 Sinusoidal Amplitude Control *82*
3.2.3 Intra-breath Baseline Compensation *83*
3.3 FIRMWARE 84
3.3.1 Main Task *86*
3.3.2 Motor Control *87*
3.3.3 Communication Management *90*
CHAPTER 4 SOFTWARE AND USER INTERFACE 91
4.1 ELECTRON FRAMEWORK 91
4.2 APPLICATION ARCHITECTURE 92
4.3 HIGH-LEVEL CONTROL 95
4.4 SOFTWARE ORGANIZATION 96
4.4.1 Main Process *96*
4.4.2 Renderer – menu.html *99*
4.4.3 Renderer – settings.html *100*
4.4.4 Renderer – plots.html *102*
4.4.5 Renderer – dataProcessing.html *103*
CHAPTER 5 VALIDATION 107
5.1 IN-VITRO VALIDATION 107
5.1.1 Sine Generation *107*
5.1.2 Symmetry and Linearity of Pneumotachograph *109*
5.1.3 Mechanical Properties Evaluation *112*
5.2 IN-VIVO VALIDATION 113
CHAPTER 6 CONCLUSIONS AND FURTHER DEVELOPMENTS 121
BIBLIOGRAPHY 128

SOMMARIO

L'asma equina (SEA) è associata all'infiammazione e all'ostruzione delle vie aeree inferiori ed è la condizione respiratoria più frequente nei cavalli. Fino all'80% dei cavalli sarà affetto da SEA almeno una volta nella vita, causando diversi deficit durante l'esercizio fisico [1]. L'ostruzione ricorrente delle vie aeree (RAO), precedentemente nota come broncopneumopatia cronica ostruttiva (COPD) [1], si riferisce a malattie che causano la limitazione al flusso d'aria e problemi respiratori. La patologia può comportare diversi segni clinici, come piccole ostruzioni delle vie aeree, infiammazione, broncospasmo, muco eccessivo e ispessimento della parete delle vie aeree [1]. La diagnosi RAO prevede l'analisi della storia clinica del cavallo e un esame quantitativo. I test di funzionalità polmonare (PFT) valutano oggettivamente le condizioni dei polmoni e delle vie aeree. Il principale svantaggio di questi metodi è legato all'ampia gamma di valori fisiologicamente accettabili, che richiedono competenze altamente specializzate per diagnosticare precocemente la RAO. Inoltre, tali test potrebbero essere basati su procedure invasive che potrebbero richiedere la sedazione dell'animale [2]. Infine, anche le tecniche più utilizzate non sono sufficientemente sensibili da sole, quindi la diagnosi si basa ancora in gran parte sulla storia clinica dell'animale.

Un approccio alternativo, recentemente proposto dal TechRes Lab del Politecnico di Milano, si basa sulla stima delle proprietà meccaniche dell'apparato respiratorio del cavallo mediante la Tecnica delle Oscillazioni Forzate (FOT). La tecnica delle oscillazioni forzate è stata introdotta da Dubois et al. nel 1956. Consiste nel sovrapporre un segnale di piccola ampiezza e alta frequenza all'attività respiratoria spontanea del soggetto in esame. Il rapporto complesso tra pressione e flusso misurato all'apertura delle vie aeree fornisce la cosiddetta “impedenz meccanicaa” del sistema respiratorio. L'impedenza è composta da una parte reale, la resistenza, rappresentativa delle proprietà resistive del polmone, e da una componente immaginaria, la reattanza, che dipende dalle proprietà inerziali ed elastiche del sistema misurato.

Il fatto che la FOT non richieda la collaborazione del paziente, poiché si basa su misurazioni non invasive su soggetti che respirano normalmente, la rende una tecnica ideale per le applicazioni sugli animali. Nel 1989 Young e Hall hanno eseguito test su pony con una configurazione FOT opportunamente modificata utilizzando frequenze di stimolazione da 3 Hz a 40 Hz [3]. Ulteriori studi di Young e Tesarowski sono stati successivamente condotti su cavalli adulti, prima privi di segni clinici di malattie respiratorie, successivamente anche su cavalli con restrizione delle vie aeree. Dai risultati di questo studio Young e Tesarowski hanno concluso che la curva impedenza-frequenza equina può essere simile a quella degli esseri umani ma spostata verso il basso in frequenza a causa della maggiore massa del sistema respiratorio equino [4].

La tecnica delle oscillazioni forzate (FOT) consente dunque di effettuare una valutazione non invasiva della meccanica respiratoria durante la respirazione spontanea; tuttavia, i dispositivi attualmente in commercio sono complessi, ingombranti, costosi e difficili da applicare ai cavalli. Recentemente, un nuovo approccio per le misurazioni FOT è stato proposto e testato su cavalli sani e asmatici dal TechRes Lab del Politecnico di Milano [2]. Il metodo innovativo utilizza un dispositivo basato su microcontrollore che utilizza una compressore assiale per generare le oscillazioni di pressione all'apertura delle vie aeree dell'animale. Questo progetto di tesi mira a migliorare il design del prototipo precedentemente sviluppato. La versione migliorata integrerà tutti i componenti necessari in una maschera facciale personalizzata mentre trasmetterà i dati in modalità wireless a un'interfaccia utente grafica appositamente progettata. Il dispositivo è stato sviluppato secondo alcuni punti cardine. In particolare, il dispositivo deve:

- Sovrapporre oscillazioni di pressione con ampiezza regolabile e frequenza di stimolazione da 1 Hz a 7 Hz al respiro spontaneo dell'animale.
- Misurare correttamente la pressione e il flusso all'apertura delle vie aeree dell'animale.
- Migliorare la portabilità utilizzando la comunicazione wireless con il laptop dell’utente e sviluppando un'applicazione multipiattaforma per il controllo delle misurazioni e l'elaborazione dei dati.

- Essere solido e robusto per lavorare anche dopo bruschi movimenti dell'animale, valorizzando una struttura modulare in modo da poter cambiare i componenti se necessario velocemente.

Il sistema è composto da diversi componenti che possono essere raggruppati come blocchi funzionali. Il componente principale è l'unità di compressione dell'aria, composta da un motore DC brushless (EMAX LS2207-2550KV) azionato da un Electronic Speed Controller (ESC) accoppiato ad un'apposita elica, che è responsabile della generazione di pressione e flusso. Un sensore di pressione differenziale (ELVR-L10D) misura le informazioni sulla pressione all'apertura delle vie aeree del soggetto, mentre un altro sensore (ELVR-L01D) viene utilizzato per acquisire informazioni sulla caduta di pressione a cavallo della resistenza di un pneumotachigrafo personalizzato utilizzato per misurare il flusso d'aria. Per controllare l'erogazione del pattern oscillante di pressione sovrapposto al respiro spontaneo del soggetto, un microcontrollore implementa un controllo ad anello chiuso per correggere la velocità del motore attraverso un regolatore di velocità elettronico (ESC). Un'unità di monitoraggio composta da un sensore di temperatura e umidità (HIH6130/6131) e un sensore di pressione assoluta (MS5637-02BA03) forniscono informazioni sui parametri ambientali in modo che i dati raccolti possano essere compensati per le variazioni ambientali. L'intero sistema è incorporato in una struttura modulare stampata in 3D che compone la maschera del cavallo. Essa integra anche una guarnizione in silicone e una batteria LiPo a tre celle da 12 V, che fornisce l'alimentazione per l'hardware.

Il cuore del sistema è il microcontrollore (Espressif ESP32), che è responsabile del controllo a basso livello del dispositivo e della trasmissione wireless dei dati tra il sistema e il laptop dell'utente. Il firmware è stato sviluppato per garantire che il dispositivo esegua una misura completa in autonomia. Il sistema lavora ad una pressione positiva, necessaria per generare oscillazioni di pressione variando la velocità del motore attorno ad un valore stabile, senza cambiare il senso di rotazione della ventola, che richiederebbe troppa energia. Il controllo è gestito da controllori PID responsabili del raggiungimento e del mantenimento dell'offset di pressione (~ 3 cmH_2O), fornendo un'onda di pressione sinusoidale di ampiezza costante (1 cmH_2O)

sovrapposta al pattern respiratorio del cavallo e compensando la variazione media della pressione all'apertura delle vie aeree del soggetto durante la respirazione spontanea.

Il microcontrollore incorpora un modulo wireless, che consente la connessione Wi-Fi e la trasmissione di dati wireless. Il protocollo TCP consente di stabilire una connessione affidabile tra i due dispositivi collegati alla stessa rete locale (LAN). Un protocollo di comunicazione personalizzato consente alle due macchine di scambiare dati. Un'interfaccia utente intuitiva garantisce il corretto utilizzo del dispositivo ed esegue l'elaborazione dei dati necessaria per valutare le proprietà meccaniche. A questo scopo è stata sviluppata un'applicazione desktop multipiattaforma utilizzando il framework Electron js. L'applicazione è responsabile dell'interazione utente-dispositivo gestendo lo scambio di dati tra laptop e microcontrollore in base alle azioni dell'utente. Al termine della misura, i segnali di pressione e flusso vengono filtrati con un filtro Butterworth passa-banda digitale di 2° ordine con banda 1 Hz centrata alla frequenza delle oscillazioni FOT. Il calcolo dell'impedenza è ottenuto da segnali di pressione e flusso filtrati e sfrutta un algoritmo di stima ai minimi quadrati. La resistenza si ottiene considerando la parte reale dell'impedenza calcolata, mentre la reattanza è costituita dalla parte immaginaria.

A causa della respirazione spontanea del soggetto, sia i segnali di resistenza che di reattanza sono soggetti a brusche variazioni in corrispondenza della fine dell'inspirazione e dell'espirazione. Per questo motivo, il segnale di flusso viene filtrato e integrato ottenendo una traccia di volume da cui vengono determinate le fasi di respirazione considerando i massimi e minimi locali dello stesso. Ogni fase respiratoria è divisa in tre intervalli di tempo uguali; il valore finale di impedenza è calcolato come media dei valori corrispondenti agli intervalli centrali per ciascuna fase respiratoria.

Il dispositivo è stato inizialmente validato in vitro per valutarne le prestazioni. Durante le prove, il dispositivo è stato collegato ad un test-lung realizzato su misura costituito da una damigiana di vetro da 55,75 L, utilizzata per simulare la compliance del sistema respiratorio, collegato ad un resistore di flusso contenente 28 tubi capillari in parallelo, lunghi 15 cm ciascuno con un diametro interno di 2 mm per

simulare la resistenza e l'inerzia. I valori teorici dei parametri meccanici del modello sono stati calcolati secondo il modello proposto da Franken et al. [5]. La configurazione risultante ha una resistenza di 2,57 $cmH_2O \cdot s/L$, una conformità di 0,04 L/cmH_2O e un'inerzia di 0,0274 $cmH_2O \cdot s^2/L$.

La qualità della forma d'onda sinusoidale è stata valutata confrontando le misurazioni di pressione e flusso registrate con una sinusoide ideale. Inoltre, per ciascuna frequenza di stimolazione, è possibile calcolare lo spettro di potenza per analizzare il contenuto in frequenza delle oscillazioni di pressione generate dal dispositivo. Per ogni misurazione sono quindi stati calcolati lo spettro di potenza di Fourier, il Pressure Shape Index e il Flow Shape Index. Lo spettro di potenza di Fourier è stato calcolato per ciascuna frequenza, da 0 a 125 Hz, con una frequenza di campionamento di 250 Hz. L'accuratezza della stima dell'impedenza è stata valutata collegando il dispositivo al test lung utilizzando diverse frequenze FOT, da 1 a 7 Hz, con una risoluzione di 1 Hz. Il tempo di misura per ogni frequenza è stato di 15 s e l'ampiezza picco-picco delle oscillazioni è stata impostata a 0,75 cmH_2O.

Le acquisizioni in vivo sono state effettuate presso la Facoltà di Medicina Veterinaria dell'Università degli Studi di Milano, Lodi. Sono stati eseguiti test per capire se la procedura di misura è fattibile e per valutare la qualità dell'impedenza misurata confrontando i dati raccolti con la valutazione veterinaria delle condizioni dei cavalli. Un ulteriore scopo era la valutazione qualitativa della differenza nelle impedenze respiratorie misurate tra cavalli sani e asmatici. La popolazione dello studio è composta da 6 cavalli: cinque cavalli sani e uno con diagnosi di Asma Equina Grave (SEA). Il protocollo di acquisizione consiste nell’effettuare le misure FOT su una gamma di frequenze da 1 Hz a 7 Hz con un passo di 1 Hz per 30 secondi ciascuna. Le oscillazioni di pressione sono state caratterizzate da un'ampiezza picco-picco di 1 cmH_2O sovrapposta ad una pressione positiva di 3 cmH_20. Le misurazioni sono state ripetute tre volte su ciascun soggetto.

I parametri di impedenza sono stati estratti utilizzando l'algoritmo offline automatico nell'applicazione software. La resistenza e la reattanza sono calcolate a partire da segnali di pressione e flusso filtrati in corrispondenza della sezione centrale sia della fase espiratoria che di quella inspiratoria. Le misurazioni sono state ripetute tre volte

in giorni diversi per ciascun cavallo. Inoltre, analizzando separatamente la reattanza espiratoria e inspiratoria, è possibile calcolare il ΔXrs, che è stato dimostrato essere un indicatore della limitazione del flusso espiratorio (EFL) nei pazienti con COPD. Non c'è differenza tra la reattanza inspiratoria ed espiratoria di cavalli sani (ΔXrs ~ 0 per ciascuna frequenza). Al contrario, il cavallo asmatico ha mostrato un ΔXrs più alto, in accordo con l'EFL associato alla COPD umana e alla SEA nei cavalli.

L'asma equina è una patologia debilitante che si verifica nell'80% dei cavalli almeno una volta. Dato l'impatto di tali disturbi sulle prestazioni fisiche dei cavalli, è fondamentale avere accesso a sistemi di diagnosi precoce che potrebbero essere utilizzati per strategie di trattamento preventivo. A causa della mancanza di dispositivi simili disponibili in commercio, questo lavoro di tesi mirava a progettare e realizzare un dispositivo portatile per la misure dell'impedenza respiratoria nei cavalli tramite Tecnica delle Oscillazioni Forzate.

Il dispositivo è stato sviluppato e validato in vitro presso il TechRes Lab del Politecnico di Milano. I test in vitro hanno dimostrato la possibilità di trasmettere e ricevere dati sfruttando una comunicazione Wi-Fi tra il dispositivo e un'interfaccia utente grafica appositamente progettata. Inoltre, le prove meccaniche hanno mostrato buoni accordi tra le proprietà meccaniche del test lung stimate utilizzando il dispositivo e quelle teoriche.

Tutta l'elettronica, l'alimentazione e la strumentazione necessaria sono state progettate per essere montate su una maschera stampata in 3D che ricorda la faccia del cavallo. L'intera maschera del cavallo, l'unità di compressione dell'aria e il pneumotach sono stati progettati per costituire una struttura solida e compatta. La PCB è stata progettata per ospitare tutti i componenti necessari riducendo al minimo le dimensioni. L'intero sistema è alimentato da una batteria ai polimeri di litio, che può essere facilmente rimossa dalla custodia per essere cambiata o ricaricata. La tecnologia wireless e l'alimentazione portatile consentono di utilizzare il dispositivo in un contesto diverso dalla normale sala medica.

La portabilità e la facilità d'uso del dispositivo sviluppato hanno consentito un primo lotto di misurazioni in vivo che hanno consentito di valutarne le prestazioni nel campo di applicazione. La validazione in vivo ha confermato la fattibilità della

procedura, dimostrando che il dispositivo non interferisce con la respirazione spontanea dei cavalli. Le proprietà meccaniche sono state valutate correttamente in 6 cavalli, mostrando la possibilità di ottenere una misura affidabile con una procedura non invasiva, veloce e semplice. È stata esplorata la possibilità di distinguere tra cavalli sani e menomati, confermando la fattibilità della valutazione.

L'innovazione di questo lavoro si basa sulla non invasività e semplicità della tecnica, consentendo di eseguire prove in un ambiente non controllato, fondamentale per questa applicazione. Inoltre, l'interfaccia utente grafica sviluppata aiuta il clinico durante l'acquisizione, estendendo la possibilità anche a personale non altamente qualificato di gestire il test. Queste due caratteristiche del dispositivo possono consentire un ampio utilizzo per monitorare la meccanica polmonare dei cavalli, aiutando il veterinario a eseguire diagnosi più rapide, accurate e obiettive.

Anche se la popolazione di cavalli utilizzati per la validazione in vivo era limitata ed era incluso un solo cavallo asmatico, i risultati hanno confermato la fattibilità dell'estrazione di parametri meccanici significativi utilizzando il dispositivo sviluppato in un contesto in vivo. Il dispositivo sarà impiegato in uno studio clinico in collaborazione con l'Università di Montreal (Canada) e l'Università Degli Studi di Milano. Il protocollo include misurazioni su un campione esteso di cavalli, che tenga conto della variabilità morfometrica degli animali e che includa soggetti asmatici sintomatici e soggetti asmatici in fase remissiva.

INTRODUCTION

Respiration is one of the most important processes in animals as it is responsible for gas exchange, which in turn provides oxygen to the blood and allows tissues to proliferate.

The breathing process involves the contraction of the muscles that impose a movement to the lung, which has a passive response during the process. The horse's respiratory system is a well-organized apparatus, able to modify its behavior during normal breathing and physical exercise. At rest, horses exchange 60 to 80 L/min of air; during exercise, the minute ventilation increases up to 1600 L/min. In these conditions, obstructions and inflammation of the respiratory system may impair the animal's activity, which may lead to asthma episodes in critical situations.

Equine asthma is associated with lower airway inflammation and obstruction and is horses' most frequent respiratory condition. Up to 80% of horses will be affected by at least one asthma episode in their life, causing clinical signs associated with a lower airway condition such as exercise intolerance [49]. Recurrent airway obstruction (RAO) refers to a group of diseases that cause airflow blockage and breathing-related problems [14]. The pathology can involve different clinical signs, such as small airway obstruction, inflammation, bronchospasm, excessive mucus, and thickening of the airway wall [14].

RAO diagnosis involves the analysis of the clinical history of the horse and a physical examination. Nevertheless, additional tests are required to define RAO with certainty. Pulmonary Function Tests (PFT) objectively evaluate the lung and airway conditions. PFTs are used to assess different parameters such as volume of air breathed, effort realized, gas exchange, air distribution in the lung, and other parameters. The main disadvantage of the procedure is linked to the wide range of physiologically acceptable values hence, PFTs are not indicated for single measurement and might require repeated measurements. Furthermore, the procedures are usually based on the insertion of an esophageal balloon in the horse's esophagus, which requires the sedation of the animal[49]. Consequently, the lack of non-

invasive procedures to assess lung mechanics in horses causes the diagnosis to be largely based on the patient's history and clinical evaluation of symptoms.

The forced oscillation technique (FOT) was first described by DuBois et al. in 1956 [21]. The working principle is based on the superimposition of small-amplitude, high-frequency pressure oscillation to the normal breathing pattern, while both pressure and flow are measured. By acquiring these parameters, it is possible to compute the system impedance as their complex ratio. From impedance, it is possible to extract the resistance and the reactance, representative of the resistive and elastic properties of the respiratory system under analysis [11]. FOT does not require the collaboration of the patients, making this technique very interesting in the veterinary field.

Tests performed on human subjects confirm the possibility of accurately assessing the respiratory system's mechanical properties with FOT[10]. Over the years, FOT has been occasionally applied also to horses, showing trends of resistance and reactance comparable to the ones obtained in human studies[11][12]. However, these studies were performed only in very well-controlled environments with complex and cumbersome set-ups. Recently, *TechRes Lab* of *Politecnico di Milano* exploited a novel approach in which the pressure waveforms are generated by a servo-controlled ducted fan, allowing the design of more sturdy, compact, and portable devices compared to already existing approaches [49].

Starting from the prototype developed at *TechRes Lab*, this thesis work aimed to design and develop a novel wireless version of a fan-based FOT device, integrating a simple-to-use graphic interface developed as a cross-platform desktop application to improve the device portability and facility of use.

The device has been realized and validated in-vitro at *Politecnico di Milano* with the faculty of veterinary medicine faculty of *Università degli Studi di Milano*, where in-vivo tests were performed on a small group of horses.

CHAPTER 1 STATE OF THE ART

1.1 Physiology of breathing in horses

Respiration is one of the most important processes in animals as it is responsible for gas exchange, which in turn provide oxygen to the blood and allows tissues to proliferate. Respiratory system function is strictly correlated to the circulatory apparatus; together they ensure the correct provision of oxygen to the organism, according to the physiological requirements.

The process of respiration can be articulated in repeated acts. A breathing act can be in turn divided in two phases named inspiration and expiration. The first one is responsible for collecting air from the environment and gather it inside the lungs, whereas the expiratory phase, on the contrary, empties the lung from air. The process of ventilation is constituted by the alternation of these two periods and guarantees the gas exchange required by the organism. Respiratory muscles are responsible for ventilatory modulation, which is needed when oxygen demand changes.

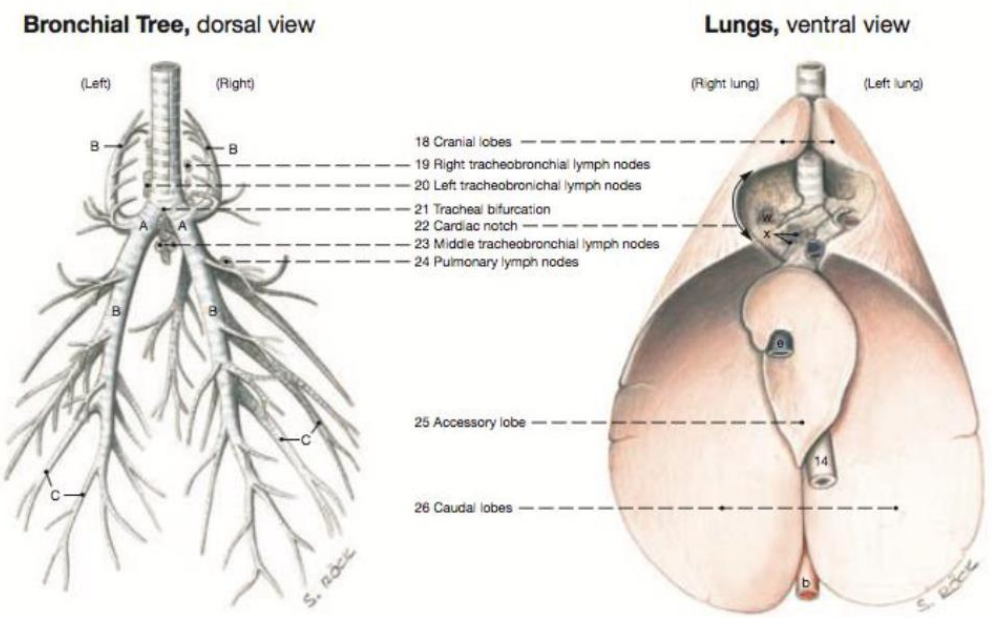

Figure 1.1 - Bronchial tree and Lung

Horse's respiratory system is divided into an upper and a lower airway. The former tract includes nostrils, pharynx, larynx down to the trachea, whereas the latter is composed by bronchi, bronchioles and lungs, including alveoli. Equine lungs reflect the shape of the thoracic cavity, usually depicted as a truncated cone shape where the organs are long and laterally compressed.

Total lung capacity in adult healthy subjects is 50/60 L, ventilation at rest is 80 L/min, derived form a respiratory frequency of 12-15 acts/min with a tidal volume of 5/6 L, whereas during exercise air flows reach 100L/s and breathing frequency increases up to 120 acts/min. A graph representing main volumes of interests is reported.

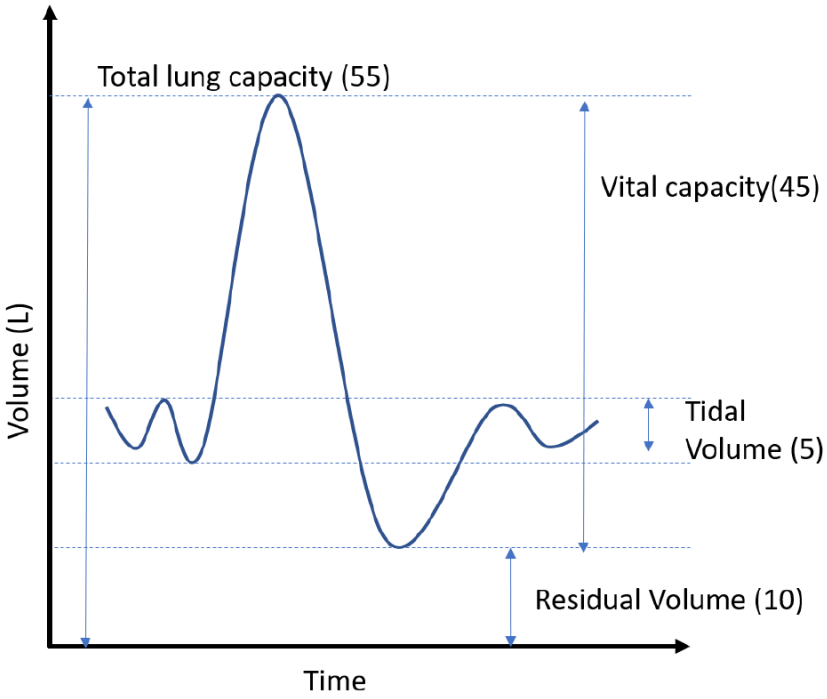

Figure 1.2 - Equine lung volumes

The mechanical equilibrium of main respiratory structures in horse is placed at the midpoint of the tidal volume [17], this implies that both inspiratory and expiratory phase are constituted by an initial passive phase and consequently by an active one to perform a breath. This particular way of breathing generates a characteristic biphasic pattern [18]. It is possible to separate the respiratory muscles into expiratory and inspiratory muscles, these are involved in the breathing act to generate the correct breathing cycle; in equine, as in many species, diaphragm is the main actor of the

inspiratory with the other principal pump being the abdominal muscles. In Figure 1.3 it is possible to notice the biphasic pattern during a normal breathing at rest condition.

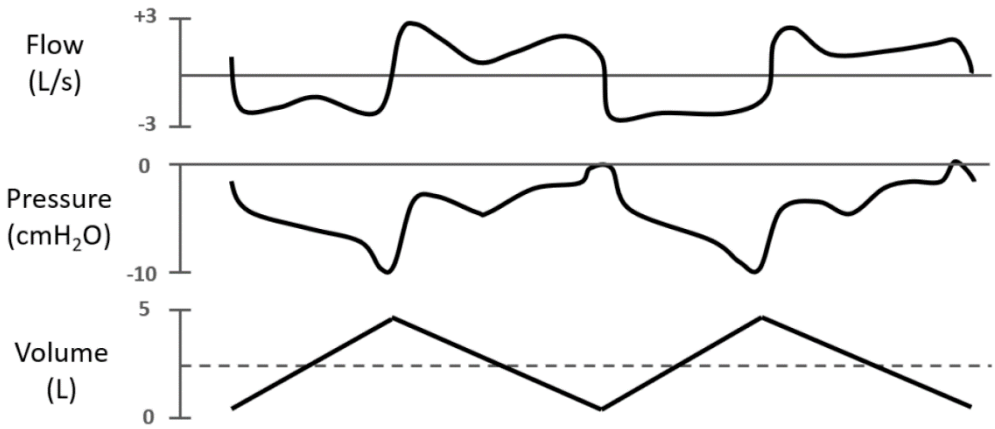

Figure 1.3 - Respiratory airflow, oesophageal pressure, tidal volume.

This breathing mechanism may be related to the low passive chest compliance and it may be a strategy to minimize the breathing elastic work [18]; furthermore the biphasic pattern is present also in donkey and mule [19].

Differently from most species, horses normally breathe around the relaxation volume, implying that the functional residual capacity (FRC) and end-expiratory lung volume (EELV) are not equal, as in humans, but EELV is always smaller than FRC, a graphical explanation is shown in Figure 1.4.

An interesting parameter is the so-called expired minute ventilation

$$\dot{V}_e = \dot{V}_a + \dot{V}_d$$

defining the first index V_a as the alveolar ventilation and V_d as the volume of the dead space which is the volume of air not taking part in the gas exchange [2]. The ratio between the physiologic dead space and tidal volume $\frac{V_d}{V_t}$ represents a parameter that indicate how much air is wasted during the breathing act. Its value in horses is almost double with respect to human's or dog's amount.

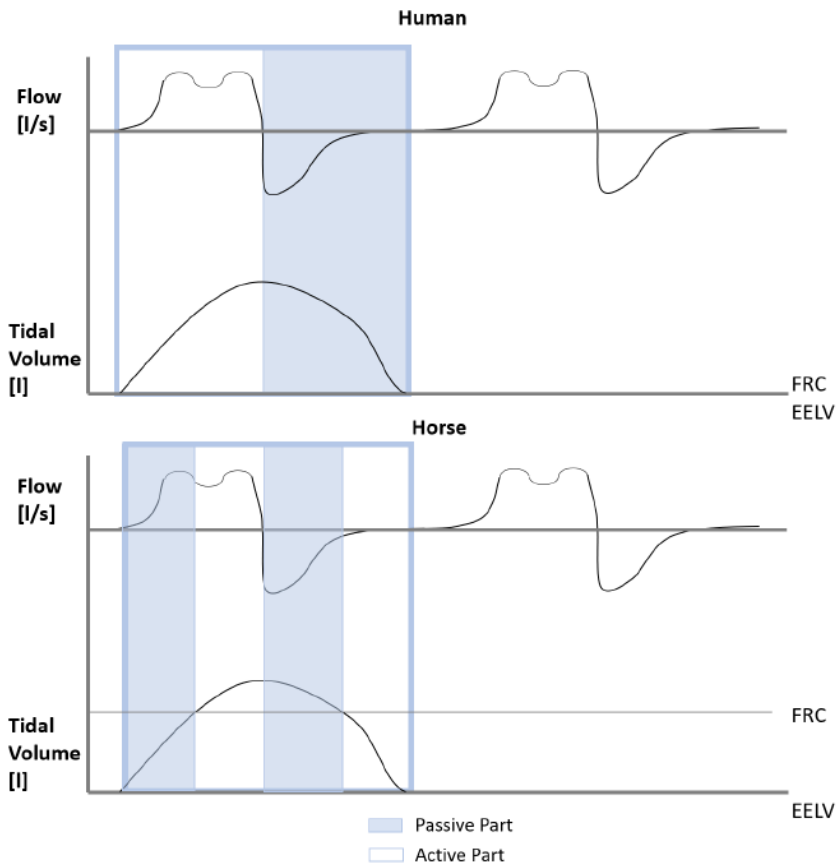

Figure 1.4 - Flow and Tidal Volume in human and horse.

The alveolar ventilation is the active part in the gas exchange, it is possible to extract the relationship between tidal volume and this parameter:

$$\dot{V}_a = f(V_t + V_d)$$

and remembering the minute ventilation's equation:

$$\dot{V}_e = \dot{V}_a + \dot{V}_d$$

it is noticeable that the ideal gas exchange occurs when the alveoli ventilation $\dot{V}_a$ is the highest which is correlated to the lowest value of the ratio $\frac{V_d}{V_t}$.

These two parameters modify their value as consequence of the physiologic requirements. During non-intensive exercise V_d does not change amplitude, whereas a notable increase of V_t results in an increase of the minute ventilation. If the exercise is protracted, breathing frequency and $\frac{V_d}{V_t}$ will increase, thus leading to a rise in $\dot{V}_d$ which causes a reduction of the efficiency. During high intensity exercise it is noticed a decrease of the ratio due to a drop in V_d. It is important to underline that the

anatomic dead space is not expected to change during exercise, so this drop in dead space volume is primary caused by a decrease in alveolar dead space dimension through the recruitment of under-perfused pulmonary capillary beds.

As in many mammals, horses are subject to a vertical gradient of pleural pressure caused by the gravitational force. This difference creates a trans-pulmonary pressure at FRC grater dorsally than ventrally as well as alveoli placed dorsally are more distended than the ventral ones.

Thorax shape, orientation of the respiratory muscle and position can modify the ventilation in specific areas creating difference between zones. These dissimilarities do not act as an important factor in gas exchange during the low frequency breathing at rest, but they are meaningful during exercise which increases the respiratory rate. Horses with recurrent airway obstruction (RAO) experience bigger inequalities, especially during activity [2] [20].

1.2 Model of lung

The respiratory system can be represented in mathematical terms with a mechanical model constituted by an elastance, representing the elastic properties of tissues, a resistance, which describes the hindrance of the airways to air flow and an inertance that accounts for the movements of the air mass inside the lung. The active and passive driving forces, generated by pulmonary muscles and tissues, create a pressure difference between atmosphere and alveoli. The resulting pressure gradient can be summarized as the sum of the three components described above:

$$\Delta P = P_{el} + P_R + P_{in}$$

The balance of forces considering the volume V, the flow $\dot{V}$, the pressure P, the acceleration $\ddot{V}$, compliance C (equal to the reciprocal of the elastance E), resistance R and inertance L of the system is given by:

$$\Delta P = \frac{1}{C} + R\dot{V} + L\ddot{V}$$

At rest, the inertial force can be considered negligible, thus the respiratory system can be simplified and modelled as an RC system described by elastic and resistive components only:

$$\Delta P = \frac{1}{C} V + R\dot{V}$$

The linear equation, describing pressure-flow relationship in case of laminar flow, turns to non-linear for turbulent flows; this is the case of high ventilation rates. In particular flow is now related quadratically to the resistive pressure component:

$$P_R = K_1\dot{V} + K_2\ddot{V}$$

1.2.1 **Airway Resistance**

The resistance of the respiratory system is composed by three main elements disposed in series: the tracheobronchial airway R_{aw}, the lung tissue R_{ti} and the chest wall resistance R_{cw}. The total resistance is therefore the sum of the three components:

$$R_{tot} = R_{aw} + R_{ti} + R_{cw}$$

Considering the system as a Newtonian model, the resistance can be obtained using the Hagen-Poiseiuille equation:

$$R = \frac{\Delta P}{\dot{V}} = 8\,\frac{\eta l}{\pi r^4}$$

In a healthy horse at rest, the component due to airway and lung tissue accounts for more than 80%; considering the sequential compartments of the upper airways the R_{tot} is given for 50% by the nasal passage, 30% by the remaining upper airways and 20% by the intrathoracic airway. Moreover horses cannot switch from nasal to oro-nasal breathing, causing an increase of each contribution to the R_{tot}. [2].

1.2.2 **Lung Elasticity**

The elastic properties of the lung are the sum of two major contributions: the elasticity of the tissues fibres and the tension generated by the air-water interface at alveolar level. Their contribution is summarized in a parameter which quantify the

stiffness of the lung; this is called compliance of the lung and it's proportional to the volume change per unit change in trans-pulmonary pressure gradient.

$$C = \frac{\Delta V}{\Delta P}$$

1.2.3 **Pulmonary Inertance**

Inertance is the measure which quantify the force needed to accelerate and decelerate air masses inside the respiratory system, according to its inertia. This contribution is given by the driving force divided by the change in air flow:

$$L = \frac{\Delta P}{\ddot{V}}$$

Inertance in resting horses is usually neglected as it represents only the 1.5% of the transpulmonary pressure gradient; on the contrary, during exercise, this value increases up to 50%, being one of the more important ones.

1.3 In Vitro Model

In 1981, Franken et al. [39] developed a theoretical model describing the exact aerodynamic characteristic of a cylindrical conduit; this model can be used to estimate impedance value of a system with high precision.

The model describes the propagation of oscillatory fluid waves through a cylindrical conduit. Two basic assumptions were introduced:

1. The fluid flow in a cylindrical conduit is treated as one-dimensional thus the vectorial velocity is reduced to its single axial component u.
2. At the entry of the tube, only small pressure swings are applied. Consequently, the density variations of the gas are small compared with the mean density value.

Considering an infinitesimal segment of the tube (length dz), the quantities of interest at a given radial position are the average fluid velocity u, average pressure p, average axial gradients of velocity $\frac{\delta u}{\delta z}$ and pressure $\frac{\delta p}{\delta z}$. It's then possible to distinguish two types of physical phenomena within this system:

1. The axial pressure gradient $\frac{\delta p}{\delta z}$ resulting from losses of potential energy within a fluid flow governed by the Navier-Stokes equations.
2. The axial velocity gradient $\frac{\delta u}{\delta z}$ due to gas compressibility, which obeys the internal energy and state equations of a perfect gas.

The description of these phenomena requires a solution which satisfies simultaneously the equations of axial fluid flow and gas compression; however further approximations allow to separate the phenomena splitting the system of equations into two subsets and yielding separate approximate relationships [39].

1.3.1 Axial Fluid Flow

Navier-Stokes equations are:

$$\rho \frac{\delta u}{\delta t} = -\frac{\delta p}{\delta z} + \frac{4\mu}{3}\frac{\delta^2 u}{\delta z^2} + \mu\left(\frac{\delta^2 u}{\delta r^2} + \frac{1}{r}\cdot\frac{\delta u}{r}\right)$$

$$-\frac{\delta p}{\delta r} + \frac{\mu}{3}\frac{\delta^2 u}{\delta r \delta z} = 0$$

As the amplitude of the signals is assumed to be small, the equations can be simplified to their linear form; assuming also the compressibility effects as small it's possible to reduce the expression neglecting velocity derivatives in the axial direction. At this point, the pressure can be regarded as uniform over the cross section, defining the boundary conditions.

$$u = 0 \qquad at\ \ r = R$$

$$p = p_0 \qquad at\ \ z = 0$$

Solving the system of equations yields a relationship between volume flow $\dot{V}$ and pressure gradient $\frac{\delta P}{\delta z}$:

$$\dot{V}(j\omega) = \frac{A}{j\omega\rho_0}\cdot\frac{\delta P(j\omega)}{\delta z}\cdot\left(\frac{2J_1\left(jR\sqrt{\frac{j\omega}{\nu_0}}\right)}{J_0\left(jR\sqrt{\frac{j\omega}{\nu_0}}\right)\cdot jR\sqrt{\frac{j\omega}{\nu_0}}} - 1\right) \qquad (A)$$

Where $\dot{V}(j\omega)$ and $P(j\omega)$ are Fourier transforms of volume flow and pressure, respectively, and J_0, J_1 are Bessel functions of the first kind.

1.3.2 Gas Compression

The previous development neglected the axial velocity gradient, which is responsible for fluid compression. The pressure gradient must satisfy the continuity equation (1), other than the energy equation (2) and the state equation of a gas (3).

$$\frac{\delta p}{\delta t} + \rho_0 \frac{\delta u}{\delta z} = 0 \qquad (1)$$

$$k\left(\frac{\delta^2 T}{\delta r^2} + \frac{1}{r}\frac{\delta T}{\delta r} + \frac{\delta^2 T}{\delta z^2}\right) - \rho_0 c_v \frac{\delta T}{\delta t} = p_0 \cdot \frac{\delta u}{\delta z} \qquad (2)$$

$$dp = \frac{Rg}{M}(\rho_0\, dT + T_0\, d\rho) \qquad (3)$$

The system of equations has been linearized as the signal considered is a small amplitude pressure swing. Moreover, if the radius of the conduct is small in comparison with the wavelength of the oscillations, then the temperature variation in the axial direction can be neglected with respect to in the energy equation. Combining the previous equation into one simplified expression yields:

$$\frac{\delta^2 T}{\delta r^2} + \frac{1}{r}\frac{\delta T}{\delta r} - \frac{\rho_0 c_p}{k} \cdot \frac{\delta T}{\delta t} = -\frac{1}{k}\frac{\delta p}{\delta t}$$

In addition to the previous equation, also the differential thermal equation (4) describing the thermal conduction of the tube inner surface needs to be solved.

$$\frac{\delta^2 T_w}{\delta r^2} + \frac{1}{r}\frac{\delta T_w}{\delta r} - \frac{\rho_w c_w}{k_w} \cdot \frac{\delta T_w}{\delta t} = 0 \qquad (4)$$

Solution of the whole system has been computed accounting for the following boundary conditions:

$$T\ finite \qquad at \qquad r = 0$$

$$T = T_w \qquad at \qquad r = R$$

$$T_w = T_0 \qquad at \quad r = R + d$$

$$T = T_0\,, \qquad T_w = T_0\,, \qquad p = p_0 \qquad at \quad t = 0$$

Once the system has been solved, the relationship between pressure and gas temperature is transformed into a relationship between flow gradient and pressure, and explicating all the terms the final equation relating pressure P to flow gradient $\frac{\delta \dot{V}}{\delta z}$ is reported:

$$\frac{\delta \dot{V}(j\omega)}{\delta z} = -\frac{j\omega\pi R^2 P(j\omega)}{\gamma p_0} \cdot \left(1 + \frac{2(\gamma - 1)}{\left(jR\sqrt{j\omega A g}\right)} \cdot \frac{J_1\left(jR\sqrt{j\omega A g}\right)}{J_0\left(jR\sqrt{j\omega A g}\right) - j\sqrt{\frac{\rho_0 c_p k}{\rho_w c_w k_w}} \cdot J_1\left(jR\sqrt{j\omega A g}\right)} \right) \quad (B)$$

1.3.3 Distributed Line Model

Equations (A) and (B), relating $\dot{V}(j\omega)$ and $\frac{\delta \dot{V}(j\omega)}{\delta z}$ to $\frac{\delta P(j\omega)}{\delta z}$ and $P(j\omega)$, respectively, allow to assimilate the system to an electrical transmission line, characterized by a series impedance and a shunt admittance per unit length. The series impedance per unit length $Z(j\omega)$ relates axial flow to the axial pressure gradient, while shunt admittance per unit length $Y(j\omega)$ describes gas compression.

$$Z(j\omega) = -\frac{\delta P(j\omega)/\delta z}{\dot{V}(j\omega)}$$

$$Y(j\omega) = -\frac{\delta \dot{V}(j\omega)/\delta z}{P(j\omega)}$$

Substituting expressions of it’s possible to obtain the final equation.

$$Z(j\omega) = \frac{\frac{j\omega\rho_0}{\pi R^2}}{1 - \frac{2J_1\left(jR\sqrt{j\omega/v_0}\right)}{J_0\left(jR\sqrt{j\omega/v_0}\right)\cdot\left(jR\sqrt{j\omega/v_0}\right)}}$$

$$Y(j\omega) = \frac{j\omega\pi R^2}{\gamma\rho_0} \cdot \left(1 + \frac{2(\gamma-1)}{\left(jR\sqrt{j\omega Ag}\right)} \cdot \frac{J_1\left(jR\sqrt{j\omega Ag}\right)}{J_0\left(jR\sqrt{j\omega Ag}\right) - j\sqrt{\frac{\rho_0 c_p k}{\rho_w c_w k_w}} \cdot J_1\left(jR\sqrt{j\omega Ag}\right)}\right)$$

Model validity was tested measuring velocity profiles of the airflow through a cylindrical tube submitted to oscillatory pressure at its entry. Harmonics from 2 Hz to 32 Hz were used. The experimental results corresponded closely to the predictions of the model. Moreover, the model was used to determine the values of known impedances and respiratory impedance of healthy subjects; results were within 5 % for the known impedances and 10% for subjects [39].

1.4 Pathologic Horse

Recurrent airway obstruction (RAO), or heaves, previously known as Chronic Obstructive pulmonary disease COPD [14] refers to a group of diseases that cause airflow blockage and breathing-related problems. It differs to human COPD, as in equines it can be compared to human severe asthma, being characterized by chronic coughing, increased mucus secretions at airway level, anomalous breathing sounds, intolerance to exercise, remodelling of the airway, increased respiratory effort to maintain constant the tidal volume and airway hyper-reactivity. When horses are exposed to dust derived from hay and bedding, clinical signs are intensified, worsening their conditions; for this reason, horses kept indoor during winter manifest more serious symptoms [2].

The incidence of heaves is estimate at 10-15 % of adult horses living in temperate climates [1], increasing for horses older than 7 years [2]; moreover an important factor is related to the breed they belong to, in fact some particular breeds are more

likely subject than others, for example Thoroughbred, American Trotter, Morgan, Arab are more predisposed to the disease [2].

The disease is usually related to dust or organic molds exposure and poor ventilated environments. Clinical signs can vary in a wide spectrum of possibilities dependently to the severity of the RAO. Bronchoconstriction is correlated to the severity of the obstructive disease, muscle tone of the airway is controlled by autonomic nervous system and circulating levels of receptor agonists and antagonists. Bronchoconstriction can be quickly inverted by means of cholinergic antagonists, adrenergic agonists and phosphodiesterase inhibitors.

Severity of the disease determines the degree of impairment in breathing, so that horses with mild airway obstruction usually show only intolerance to exercise as clinical sign hence the diagnosis can be complex, especially to differentiate it from inflammatory airway disease (IAD). On the contrary, horses suffering from severe RAO exhibits increased respiratory effort, nostril flaring, neck extension, abdominal muscle contraction during heaving, exaggerated rib excursion during inspiration; they also show decreased appetite and weight loss. With the progression of the disease, hypertrophy of external abdominal oblique muscle becomes more marked and as consequence the characteristic “heave line” appears on the thorax of the equine. Usually in horses with RAO breathing frequency increases as consequence of the effort of the animal to maintain the same ventilation in pathologic conditions; pathology can involve different clinical sign, such as small airway obstruction, inflammation, bronchospasm, excessive presence of mucus and thickening of the airway wall.

1.5 Diagnosis of Asthma and Pulmonary Test in Horses

In order to diagnose RAO the veterinary should perform a physical examination and an analysis of the clinical history of the horse; additional tests are often required to increase the level of confidence of the diagnosis.

Pulmonary Function Tests (PFT) are objective evaluations of the lung and airway conditions. Most common measurements are peak of flow and forced expiratory

volume in one second (FEV_1), due to their non-invasiveness, simplicity and accuracy [20].

PFT measurements include lung volumes, test of mechanical function and gas exchange; these measures can be affected by diurnal ventilation, head position, sedation and type of equipment, thus a single measurement is rarely meaningful. PFT is often linked to the evaluation of a disease along time using day by day analysis.

Sedation helps the equipment placement, it brings advantages regularizing breathing and allowing a standardization of the neck angle. On the contrary it increases the resistance of upper airways.

As said, the equipment is a factor to be considered. Facemasks are a basic apparatus, in fact they are needed to assess many tests. The mask has to satisfy different requirements:

• Rigidity prevents possible mechanic damages.

• It must have low dead space to maximize air change and minimize moisture and heat accumulation.

• The shape should optimize the trade-off between minimum air leakage and comfort.

1.6 Measurement of Mechanical Properties

Mechanical properties of the respiratory system are a valuable measure to assess the health state of a horse. PFTs are used to evaluate different parameters as volume of air breathed, effort realized, gas exchange, distribution of air in the lung and others.

An indicator of horse pathological state is the increase of energy necessary to maintain tidal volume constant; this incremented effort can be reflected measuring the pressure change in the pleural cavity $\Delta P_{PLmax.}$ The measurement is performed using an endotracheal tube connected to a pressure sensor which allows to obtain the pressure at airways level. When an external flowmeter measuring the flow Q at the airways opening, it's possible to compute the total pulmonary resistance R_L.

Total pulmonary resistance can be used to evaluate the severity of the airway obstruction, whereas the measurement of dynamic compliance C_{dyn} represents the elastic characteristic of the lung, therefore can be related to the degree of small peripheral airway obstruction. During a respiratory crisis the pleural pressure increases, this reflects in an increase of resistance and a decrease of compliance related to a narrowed airway [21]. The main disadvantage of this measurement is the invasiveness.

Resistance and compliance of the respiratory system are the most common pulmonary function measurements. As previously explained R_L is an indicator of the airway condition whereas compliance C_{dyn} reflects the elastic properties of the respiratory system, especially the lung. Pathology can alter their values, such as RAO increases resistance and decreases compliance.

Resistance and compliance of the respiratory system are the most common pulmonary function measurements. As previously explained R_L is an indicator of the airway condition whereas compliance C_{dyn} reflects the elastic properties of the respiratory system, especially the lung. Pathology can alter their values, such as RAO increases resistance and decreases compliance.

1.6.1 Forced expiration

Whereas in human medicine different parameters are extracted from the forced exhalation, this circumstance is prohibitive to be repeated spontaneously working with horses. First experiments of forced exhalation implied anesthetization of the hoses and the use of tracheostomy.

In more recent trials forced expirations have been performed using a nasotracheal tube on anesthetized horses. The animals are mechanically ventilated, inflating to the total lung capacity. The animal is connected to a vacuum tank, a Q-V curve is created using the resulting forced expiration, then forced vital capacity FEV_1, force expiratory flow at 75/95% exhaled vital capacity and peak expiratory flow are calculated.

1.6.2 End-expiratory lung volume

In human beings, end-expiratory lung volume (EELV) is identical to the fractional residual capacity (FRC), this is related to the mechanical equilibrium point of the humans.

In horses the equilibrium is in the midpoint between inspiration and expiration and this reflects the fact that EELV is below the FRC.

In humans, airway obstruction tends to elevate EELV whereas restrictive condition tends to decrease it.

1.6.3 Endoscopy

Endoscopy is the most used diagnostic method. A pathological condition implies the presence of mucus in airway, using endoscopy the evaluation of secretion becomes instantaneous, moreover horses with severe RAO present marked erythema or edema in the airways that are also visible through endoscopy. In addition, this method allows the acquisition of respiratory samples permitting the cytological evaluation [4].

1.6.4 Immunological Test

Various studies have been done to evaluate the presence of intradermal allergen in diagnostic approach to RAO. It has been demonstrated a relationship between frequency and magnitude of skin response in pathologic horses, with respect to control horses, following intradermal injections of stable dust, mould extracts and various allergens [5] [6]. But in conclusion results do not show univocally the difference between pathological and normal subject [7]. Consequently, the analysis through these methods should not have to be considered for diagnostic purpose.

1.6.5 Arterial blood analysis

Commonly arterial blood analysis is used as a method to evaluate respiratory status, evaluating the magnitude of PaO2. In fact, pathological subject may have lower value of PaO2 in blood due to ventilation perfusion mismatch [8].

Unfortunately arterial blood gas analysis cannot be used in case of RAO with mild or moderate intensity because of it lacks of sensitivity [9].

1.7 Forced Oscillation Technique (FOT)

In 1956 Dubois et al described the Forced Oscillation Technique (FOT): it's a simple, minimally invasive technique conceived to measure the mechanical properties of the respiratory system without interfere with the regular breathing pattern cycle [10].

FOT aims to measure flow and pressure at the airways opening while a small amplitude sinusoid of pressure is superimposed to the normal breathing pattern. The acquisition of pressure and flow permits to estimate the respiratory reactance and impedance [22]. Since the only requirement is to superimpose a pressure signal to the normal breathing pattern of the subject, this technique is suitable for all the cases where non-collaborative subjects have to be tested, like with new-borns, severely impaired subjects or animals.

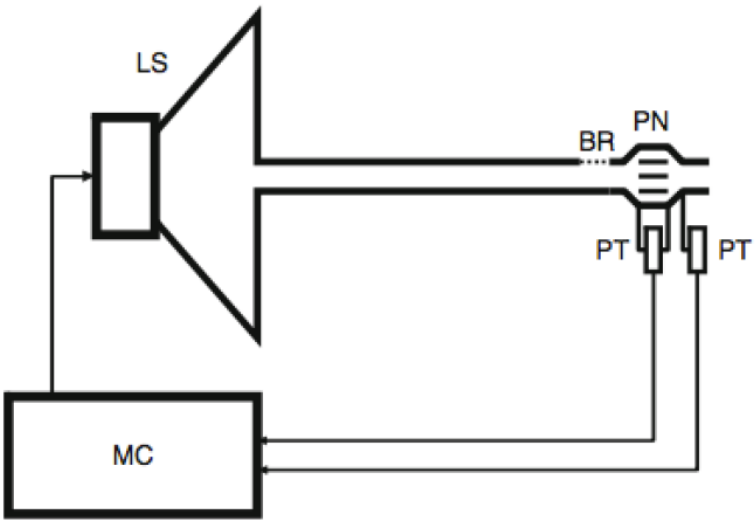

Figure 1.5 - FOT setup.

The set up for FOT is reported in figure 1.5 and it includes:

• A loudspeaker LS used to create and impose the sinusoidal pressure, transferred to the airways opening by means of a flexible hose

• A pneumotachograph PN to measure the air flow $\dot{V}$

• A differential pressure sensor PT to evaluate the change in pressure due either to the breathing baseline and the sinusoid superimposed

• A bias resistor BS, mounted between the pneumotachograph and the hose, to allow the spontaneous breathing of the patient and to avoid CO_2 rebreathing

• A microcontroller used to control the loudspeaker and sample the value of pressure P and flow $\dot{V}$.

The modulus of impedance Z is defined as the ratio between applied oscillatory pressure and the resulting oscillatory flow:

$$|Z| = \frac{P_0}{\dot{V}_0}$$

Amplitude and phase lag of the resulting flow depend on the mechanical load of the respiratory system, as the induced flow reduces if the mechanical load increases. Modulus and phase lag define respiratory impedance Z_{rs} which fully characterizes the oscillatory mechanics of the respiratory system at a given frequency. Z_{rs} is usually divided into its real and imaginary parts, respectively resistance R_{rs} and reactance X_{rs}: resistance describes the dissipative mechanical properties of the system, while reactance accounts for the energy storage capacity of the lungs.

Resistance can be computed as:

$$R_{rs} = \frac{P_R}{\dot{V}_0}$$

where PR is the pressure at maximum flow and zero oscillatory volume.

Reactance can be computed as:

$$X_{rs} = -\frac{P_x}{\dot{V}_0}$$

where PX is the pressure at zero flow and maximum oscillatory volume, thus accounting for the component of pressure out of phase with flow and in phase with volume. The values needed to compute resistance and reactance are shown in Figure 1.6 – Pressure and flow tracks recorded at the airway openings of an healthy subject during a 3Hz oscillation (top) and zoom of a 1s fragment of the two tracks obtained after digital filtering (bottom). Figure 1.6.

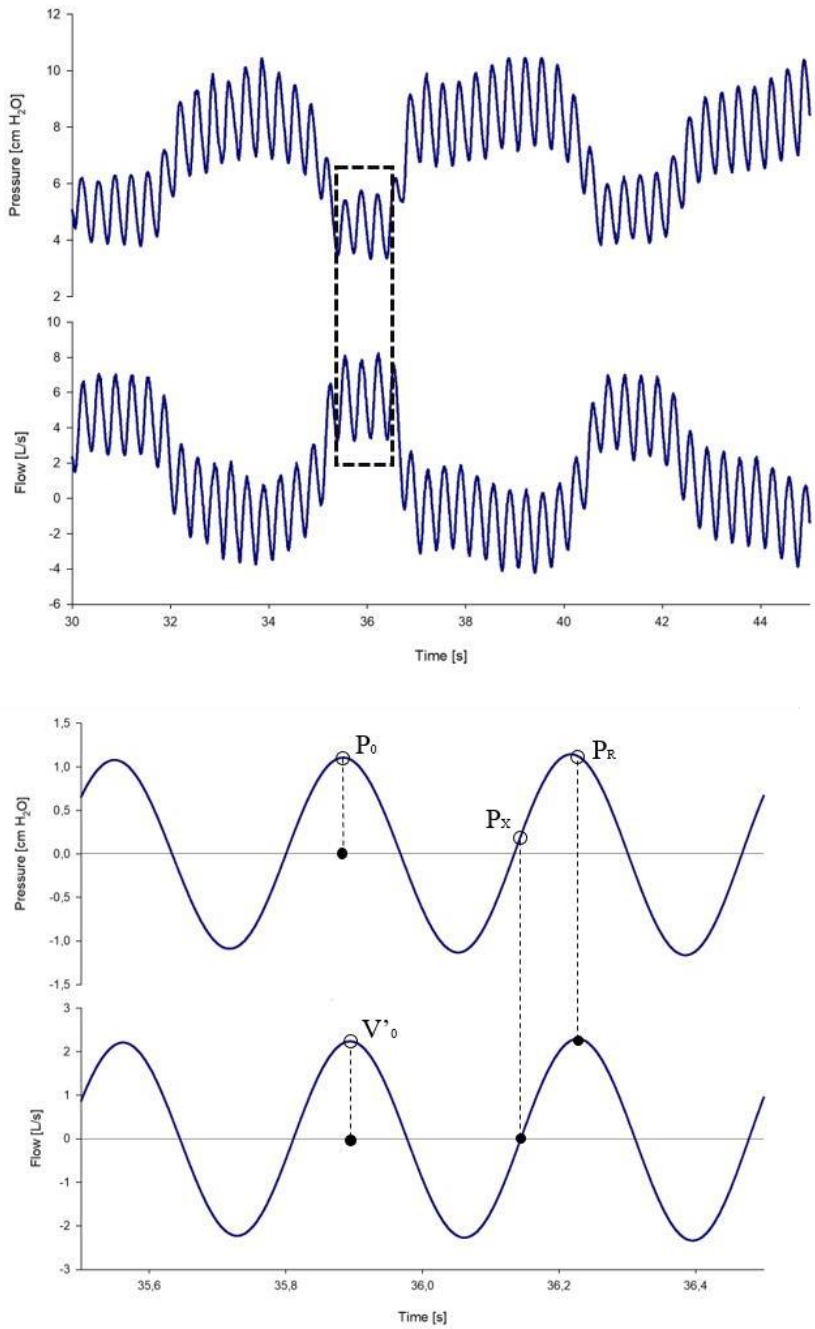

Figure 1.6 - Pressure and flow tracks recorded at the airway openings of an healthy subject during a 3Hz oscillation (top) and zoom of a 1s fragment of the two tracks obtained after digital filtering (bottom).

The amplitude of the oscillations should be small in order to avoid excessive lung volume changes and minimize the artifacts due to non-linearities of the system, but it should be enough to guarantee a sufficient signal to noise ratio. Also, wide amplitude pressure oscillation can cause discomfort in the subjects and may force their breath to synchronize with the oscillations.

For these reasons the amplitude is usually kept between 1 and 3 cmH2O, obtaining acceptable results [22].

The forcing frequency is chosen according to the part of the respiratory system that has to be investigated: low frequencies are representative of the mechanical properties of the peripheral airways while high frequencies are representative of the upper airways. That is because the respiratory system acts as a lowpass RC filter: the higher the forcing frequency, the more the amplitude of the oscillation will be reduced. Therefore, increasing the frequency of the forcing oscillations, information about the deeper parts of the respiratory system is gradually lost. The conventional frequency range for FOT measurements is therefore between 1 Hz and 30 Hz.

Tests made on healthy subjects show that resistance R_{rs} varies very little with frequency, while X_{rs} exhibits a marked frequency dependence, showing negative values at low frequencies and reaching positive values at frequencies higher than the resonance frequency as shown in Figure 1.7.

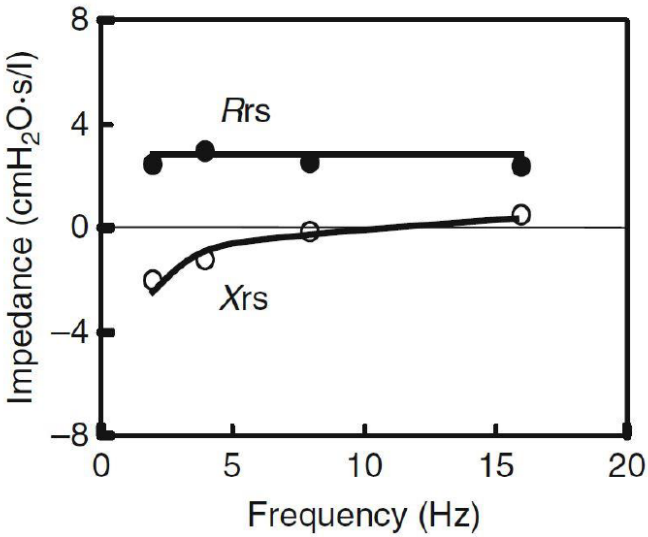

Figure 1.7 - Resistance and Reactance curves of a healthy subject.

Changes in Z_{rs} observed in patients vary accordingly to the position of the obstruction in the airways. Obstructions in upper or central airways lead to a parallel upward shift in R_{rs} and no changes in X_{rs}. Peripheral airway obstructions or nonhomogeneous time constant distribution of lung units, instead, result in an increase of R_{rs} more marked at low frequencies and in a decrease of the values of X_{rs} with a consequent higher value of the resonance frequency, the shift is graphically reported in Figure 1.8.

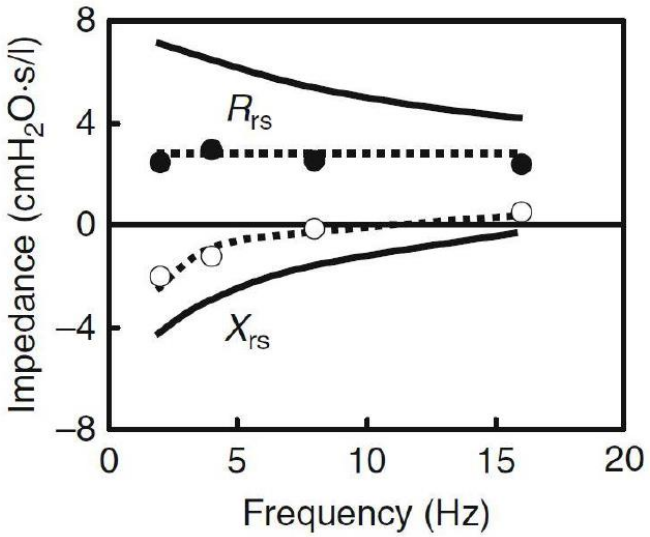

Figure 1.8 - Shift in resistance and reactance curves caused by a peripheral airway obstruction.

1.7.1 Impedance

It is useful to present an electrical equivalent of the respiratory system. Remembering the equation that explains the dynamic behaviour of the respiratory system

$$\Delta P = \frac{1}{C} V + R\dot{V} + L\ddot{V}$$

It is possible to extract the impedance Zrs of the system:

$$Z_{rs} = R_{rs} + j\left(-\frac{1}{\omega C_{rs}} + \omega L_{rs}\right) = R_{rs} + jX_{rs}$$

It is possible to notice two contributions in this equation. The first is the airflow resistance Rrs that is the real part of the parameter whereas Xrs represents the imaginary part called reactance which is related to the compliance and inertial components and depends on stimulation frequency.

At low frequency, the main component of Xrs is the compliance and the value of reactance becomes negative whereas at higher frequency the predominant element is the inertance and consequently Xrs assumes positive values. The zero-crossing point is the equilibrium between elastance and inertance and its frequency is called resonance frequency f_R.

In the RC model at low frequency at rest it is possible to ignore the inertance influence. In this model pressures and flows are represented as voltages and currents.

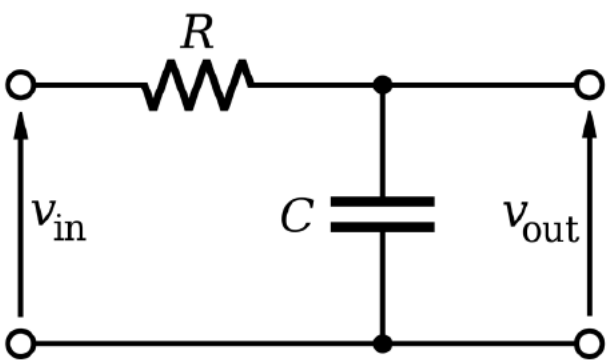

Figure 1.9 - RC model.

In the respiratory system, the airflow assumes different pathways; we can model the alveolar system as a bench of parallel RC. It is possible to calculate the total impedance of the system separating the different impedances:

$$\frac{1}{Z_{tot}} = \frac{1}{Z_c} + \frac{1}{Z_r}$$

where the value of Zr and Zc depends on the number of recruited alveoli during the breathing process.

Assuming time invariance of the linear system, it is possible to evaluate the transfer function of the system by stimulating with a sinusoidal pressure input and estimate the relationship between pressures and flow. Specifically, the sinusoidal input can be expressed as:

$$P_{rs} = P_{rs} e^{j\omega t}$$

Also the generated flow has to be sinusoidal, that is guaranteed by the frequency response theorem; hence the system gain is:

$$Z_{rs}(\omega) = \frac{P_{rs} e^{j\omega t}}{\dot{V}_{rs} e^{j\omega t + \varphi_{rs}}}$$

Where φ_{rs} represents the phase shift and its time constant is the product of the respiratory system resistance and the respiratory system compliance [23].

1.8 FOT on horses

Forced oscillation techniques can be applied to spontaneously breathing conscious animals imposing applied pressure signals via a rigid mask.

Young and Hall in 1989 performed tests on ponies with a specifically modified FOT set-up. They used a digitally generated pseudo-random signal to feed a power amplifier connected to two loudspeakers electrically in series, mounted facing a rigid, sealed cabinet with an outlet tube. This was connected to the measurement system by a 38 mm internal diameter, 1.5 m long tube. The animal breathed through a 32 mm internal diameter, 2.5 m long tube that acted as acoustic impedance. Horses wore a fitting rigid polypropylene mask, sealed to the face with bandage and

adhesive strapping. Mask pressure was measured with a differential air pressure transducer and respiratory gas flow was measured with a screen pneumotachograph. Frequencies measured ranged from 3 Hz to 40 Hz. The test signal contained a mixture of all those frequencies and the respiratory impedance was calculated at suitable intervals over the whole range [26].

Results showed a difference in the shape of the impedance-frequency curve with respect to human subjects, as the reactive component was found to be much smaller and usually positive in the whole range of frequency, suggesting that resonance frequency was below 3 Hz.

Further studies by Young and Tesarowski were later conducted on adult horses, first free from clinical signs of respiratory diseases [11], then also in horses with reversible allergic airway disease [12].

The forcing sinusoid was produced by means of a proportional pneumatic valve connected to a 400 kPa compressed air line, driven by a sinusoidal voltage waveform. This airflow was applied to the measurement system by means of a T shaped, 50 mm diameter, ABS plastic tube. To the side arm of the T piece, a 2 cmH2O·s/L resistance was attached to direct most of the oscillating airflow to the horse while allowing it to breathe relatively normally. The rest of the set-up is similar to the one used in the previous study.

In the study on healthy horses, measurements were made at 1, 2 and 3 Hz in random order. Signals were acquired and then band-pass filtered with a 12th order digital Butterworth filter with 0.2 Hz passband centred at the measurement frequency. Anyway, measures at 1 Hz resulted of poorer quality with respect to the ones at 2 and 3 Hz because of the greater level of interference from the natural respiratory pattern of the animals. From the results of this study Young and Tesarowski concluded that the equine impedance-frequency curve may be similar of that of humans but shifted down in frequency, because of the larger mass of the horse [11].

In the successive study on pathologic horses, respiratory impedance was measured at 1.5, 2, 3 and 5 Hz, using the same set-up descripted in the previous study. Measurements were taken with the horses in remission, then after acute antigenic challenge that produced clinical heaves, and then with heaves but after the administration of a bronchodilator (fenoterol) by inhalation. Results, reported in

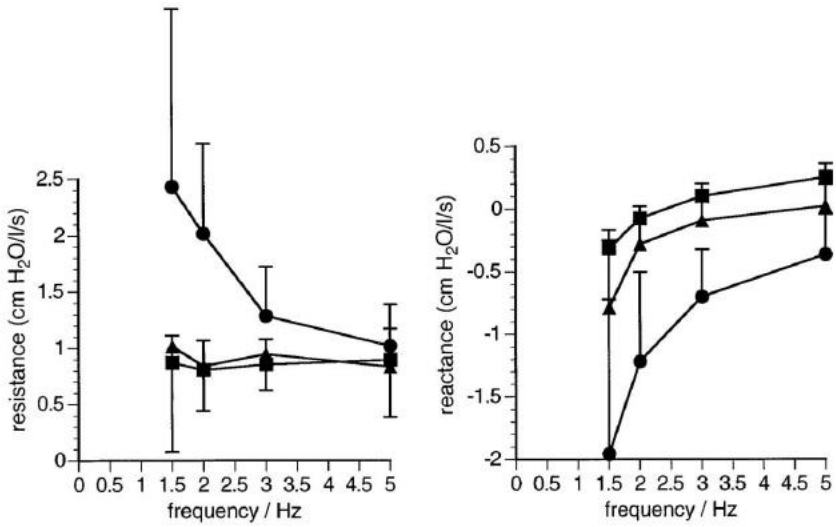

Figure 1.10 - Resistance and reactance values: squares, clinical remission; circles, acute exacerbation; triangles, after bronchodilation.

Figure 1.10, showed significant changes both in resistance and reactance with condition (remission, exacerbation, bronchodilation). Like what can be seen from results in human medicine, airway obstructions lead to an increase in low frequency resistance, in addition to an increased dependence from frequency. Regarding the reactance, it shows more negative low frequency values, thus increasing resonance frequency.

1.9 A new Approach

As previously described, Pulmonary Function Tests are the most common technique used by clinician in order to retrieve information about the condition of the subject. However, these methods are characterized by different drawbacks; these tests provide valuable information when day by day analysis is carried on, their main purpose is to monitor the physiological parameters during pathology course. Single acquisitions are subjected to large variability, thus results are often averaged after many measurements. This means long time is required to obtain a robust

measurement. Moreover, many techniques require the collaboration of the patient, which in many cases is not ensured, thus sedation is necessary. Use of instrumentation such as endotracheal tube may cause discomfort in the animal and increases the invasiveness of the measure. Many devices are bulky, their use results cumbersome and allow the acquisition only in controlled environment. Finally these methods are always evaluated in combination with the history of the subject, requiring a prior knowledge of the patient, meaning that a continuous monitoring of the animal would be required to obtain accurate results.

Successful results were obtained with a FOT-based approach applied on horses in studies comparing it with conventional oesophageal balloon method. The systems used in these studies are mostly derived from the setup used on humans. Limitations regarding complexity, expensiveness and encumbrance characterize the systems. Moreover, system structure increases the respiratory load and the dead space of to the animal [49].

A novel approach has been introduced in a recent work by TechRes Lab at Politecnico di Milano, where a different design for FOT, which was previously introduced on human subjects, has been implemented in a prototypal device for horses [49].

Starting from this work, the aim of this thesis is to develop a device based on the same FOT concept, with several improvements. The new device is characterized by major portability making it wireless, improving the simplicity of use and reducing the time needed for a measure. A more solid, organized structure are proposed, and a simpler, more intuitive user interface has been developed as a cross-platform desktop application. Finally the FOT measurement is based on a new control algorithm, increasing measurement reliability and robustness.

The development and validation process has been conducted at Politecnico di Milano and Università degli Studi di Milano (Lodi).

CHAPTER 2 A NEW DEVICE FOR PULMONARY ASSESSMENT IN HORSES

In the previous chapter current techniques used to evaluate respiratory functionality have been shown, underling their operation and their limits. The main problems are related to the invasiveness of the measurement and the need of a controlled environment, which forces the horse to be brought to a veterinary room.

With the aim to provide a less invasive technique which is based on a simpler measurement protocol and a major portability, this project proposes a new wireless device able to superimpose a sinusoidal pressure on the spontaneous breathing of the horse in order to evaluate the airway resistance and reactance of the subject exploiting the forced oscillation technique.

2.1 Requirements

Starting from the considerations listed above, the device has been developed according to some pivotal points. In particular, the device has to:

- Superimpose pressure oscillations to the normal breathing of the animal as desired
- Work without interfering with the normal breathing of the subject
- Correctly measure pressure and flow at the airways opening of the animal
- Compensate measurement for environmental factors
- Be simple to use
- Be portable, both in the structure and from the interface point of view
- Be solid to work even after abrupt movements of the subject
- Be modular in order to quickly change parts, if required
- Provide an intuitive and simple-to-use user interface

2.2 Architecture

The system is composed by different components which can be grouped as functional blocks. The main component is the air compression unit, composed by a motor coupled with a suitable propeller, which is responsible for pressure gradient and flow generation. Two sensors are used to acquire information about flow and pressure at subject airways opening. In order to control the delivery of the oscillating pressure pattern to be superimposed to the subject breathing, a microcontroller processes pressure and flow data and regulates motor behaviour through an electronic speed controller (ESC). A monitoring unit provides information about environmental parameters, so that collected data can be compensated for ambient temperature, humidity and pressure variations. The microcontroller computes parameters of interest, which are then sent to the laptop in order to be processed and visualized. The microcontroller is also responsible for wireless communication with

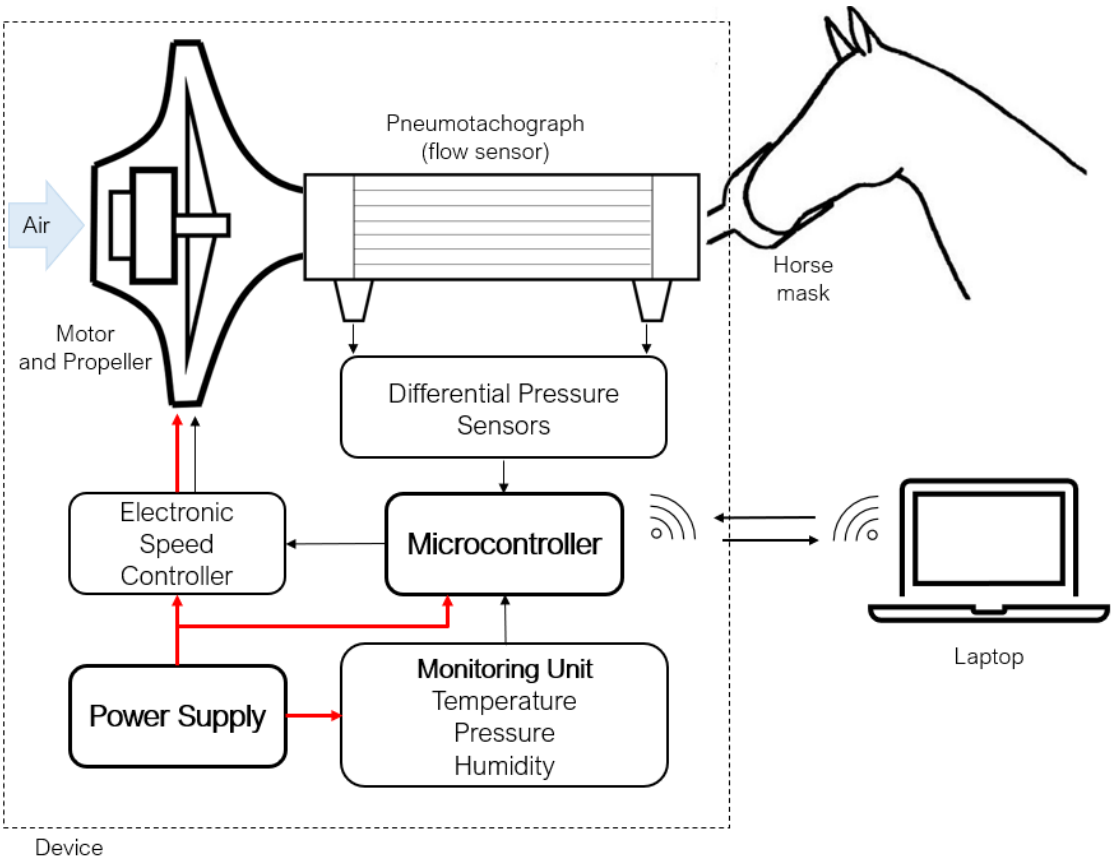

Figure 2.1 - Device Architecture Scheme.

the laptop. The whole system is organized as a modular structure which composes the horse mask. The mask hosts a LiPo battery, which provides the power supply for the hardware. A scheme of the system architecture is reported in figure 2.1.

2.3 Esp-32 Microcontroller

The core of the system is the microcontroller ESP32 developed by Espressif, which is responsible for the low-level control of the device and the wireless data transmission between the system and a laptop. The microcontroller characteristics are reported:

- Dual Core: 2 x Tensilica Xtensa 32-bit LX6 microprocessor
- Clock frequency: up to 240 MHz
- Performance: up to 600 DMIPS
- Ultra low power co-processor.
- Wi-Fi: 802.11 b/g/n/e/i (802.11n @ 2.4 GHz up to 150 Mbit/s)
- Bluetooth: v4.2 BR/EDR and Bluetooth Low Energy (BLE)
- ROM: 448 KiB.
- SRAM: 520 KiB
- RTC fast SRAM: 8 KiB
- RTC slow SRAM: 8 KiB
- eFuse: 1 Kibit
- Embedded flash:
- Up to 16 MiB of external flash are memory-mapped onto the CPU code space, supporting 8-bit, 16-bit and 32-bit access. Code execution is supported.
- Up to 8 MiB of external flash/SRAM memory are mapped onto the CPU data space, supporting 8-bit, 16-bit and 32-bit access. Data-read is supported on the flash and SRAM. Data-write is supported on the SRAM.
- Peripheral input/output: Rich peripheral interface with DMA that includes capacitive touch, ADCs (analog-to-digital converter), DACs (digital-to-analog converter), I²C (Inter-Integrated Circuit), UART (universal asynchronous receiver/transmitter), CAN 2.0 (Controller Area Network), SPI

(Serial Peripheral Interface), I²S (Integrated Inter-IC Sound), RMII (Reduced Media-Independent Interface), PWM (pulse width modulation), and more.

The microcontroller is based on a real-time operating system named Free RTOS. The APIs provided by the operating system allow to manage both cores in a flexible way, increasing the interpretability of the code, while also improving system performances. Firmware was written exploiting Espressif's official development environment ESP-IDF.

Printed Circuit Board

A printed circuit board (PCB) has been developed in order to embeds the electronics into the 3D printed device. The main requirements were compactness and area optimization; for these reasons a double layer PCB was designed.

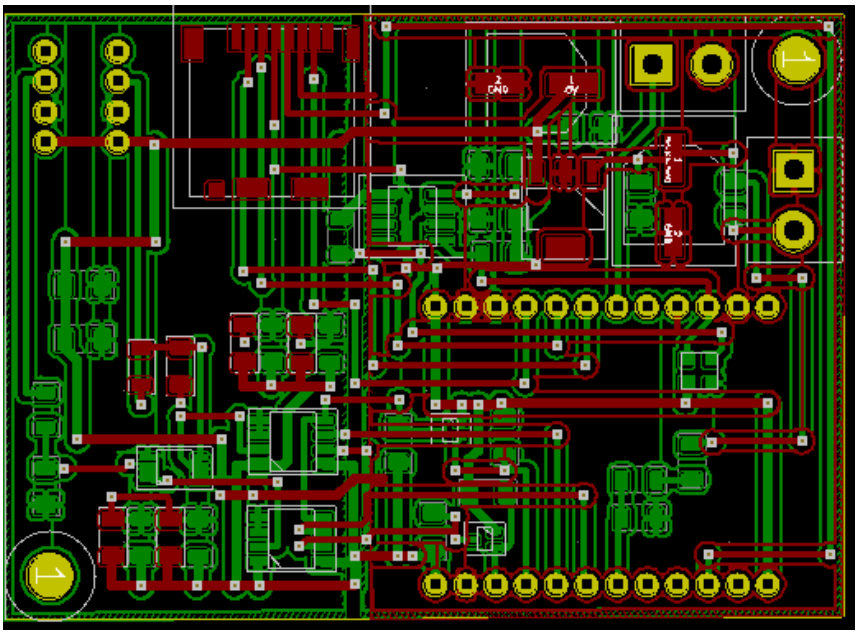

Figure 2.2 PCB scheme

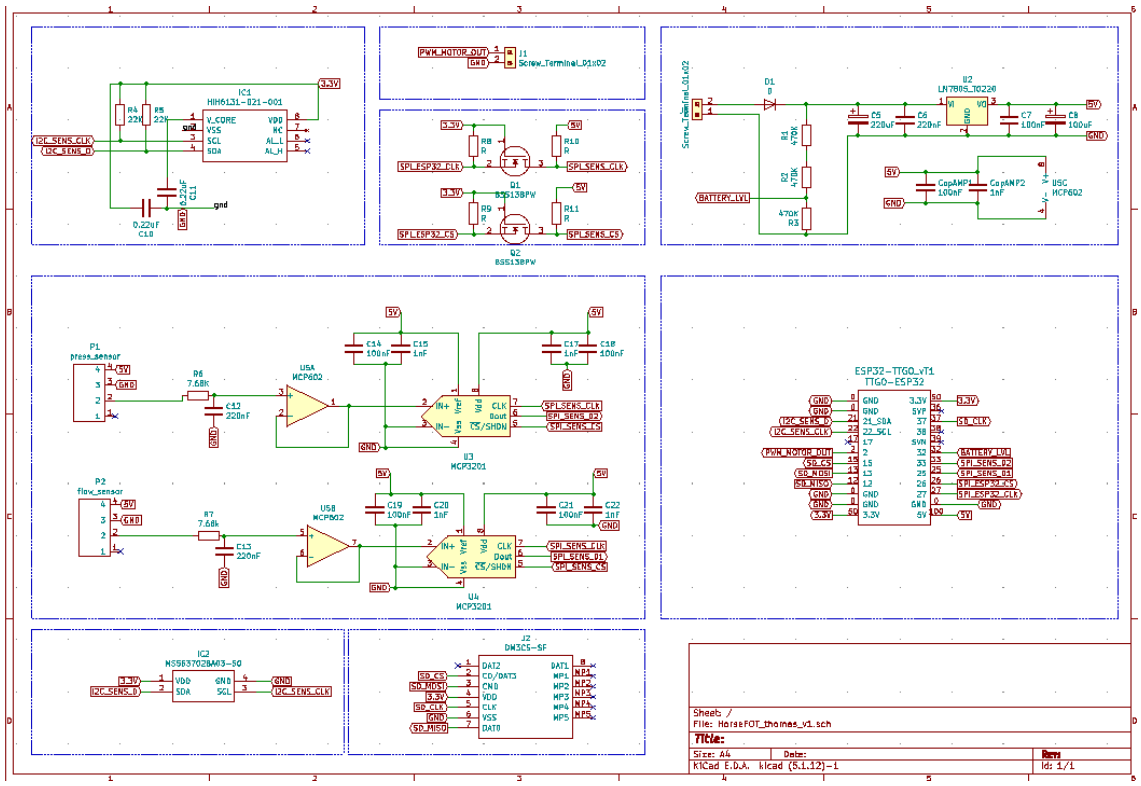

Figure 2.3 Device Schematic

2.4 Motor Unit

One of the more important modules composing the device is the motor. It is responsible for pressure wave generation, which are at the bases of the FOT. The motor chosen for this project is a brushless DC (BLDC) motor. Despite the more complex control logic, this type of motor was preferred with respect a brushed motor mainly due to lower weight, inertia and lack of friction, which ensures higher power efficiency [30]. In the next paragraphs a comparison between the two types of motor and their control logic is reported.

2.4.1 Brushed

The brushed direct current (BDC) motors are made with a stator, rotor brushes and a commutator. They are not expensive, easy to drive and they can have many different shapes and sizes; these characteristics allow many different applications.

The stator generates a magnetic field thanks to a permanent magnets or electromagnetic windings; this field surrounds the rotor which is made up of one or more windings. When energized, these windings produce another magnetic field hence poles appear on the rotor. The total effect is the rotor poles attraction by the stator poles of opposite polarity. As the rotor moves, the magnetic field switches in the rotor windings due to a different energization of the rotor. This is called commutation and prevent the rotor magnetic poles for overrunning the poles in the stator [31].

BDC motors do not need a controller in order to switch the windings current. This action is accomplished mechanically by the commutator placed inside the BDC. It is made by segmented copper sleeve and placed on the axle of the BDC motor. The other elements required for commutation are the carbon brushes, which allow the contact with the commutator in order to let the current flow.

It is crucial to underline the fact that BDC motors, specifically the brushes, are prone to wear because they slide on the commutator. This event implies that BDC motors, usually, have a shorter life than other type of motor, such as BLDC, in which there are no parts in contact during the movement. Hence brushed motors are not indicated in long term application.

2.4.2 BLDC

Brushless Direct Current (BLDC) motors are synchronous actuator, this means that the rotation frequency of the magnetic field generated by the stator is equal to the one generated by the rotor [32]. BLDC motors are classified by the number of windings which determines also the number of phases; the three phases motors are the most common actuators; they are constituted by three windings.

The device is constituted by two main parts: one stator and one rotor. The stator is constituted by a staked steel lamination with windings placed in slots axially cut along the inner periphery.

The rotor is characterized by a permanent magnet; it has a fixed number of pairs, alternating North (N) and South (S) polarization. Ferrite magnets and rare earth alloys are the most common materials used; ferrite is preferred thanks to its low price, but it has the drawback of low flux density for a given volume whereas the rare-earth alloys have higher magnetic density per volume allowing the rotor to reach the same torque with rotor of smaller dimension. Furthermore, rare-earth alloys magnets increase the size to weight ratio, allowing to reach higher torque e smaller inertia comparing to ferrite magnets of same dimension. Neodymium (Nd), Samarium Cobalt (SmCo) and the alloy of Neodymium, Ferrite and Boron (NdFeB) are some examples of rare earth alloy magnets.

In order to commutate the phases with the proper timing, different techniques are used to evaluate the position of the rotor which is critical to guarantee a proper rotation of the motor. For this reason, it is possible to divide the control strategy into two classes based on the presence or absence of position sensor in the actuator.

Sensored

The first class of BLDC motor is the sensored, this means that onto the motor are placed sensor for position detection. There are two main type of sensors: Hall sensor and optical encoder.

Hall Sensor

In 1879 Edwin Herbert Hall discover the so-called Hall effect which states that if an electric current carrying conductor is kept in a magnetic field, the magnetic field exerts a transverse force on the moving charge carriers which tends to push them to one side of the conductor. A build-up of charge at the sides of the conductors will balance this magnetic influence, producing a measurable voltage between the two sides of the conductor. The Hall sensor are used to evaluate position exploiting the Hall effect.

To detect the position of the rotor, a three phases BLDC motor requires three hall sensors. There are two types of outputs, related to the position of the sensor: 60° and 120° phase shift. Each Hall sensor gives a high or low response signal when a N or S magnetic pole of the rotor passes close to it. Arranging these three signals it is possible to estimate the required commutation sequence to move the rotor in a proper way.

Digital Encoder

Another technique for position detection is by means of optical encoder placed onto the motor. It gives two signals, shifted in phase by 90°, through which speed and direction of rotation can be estimated. Frequently a third signal is present, related to pulse per revolution (PPR), used for positioning application.

Sensor less

If there is not any position sensor in a brushless motor, this is defined sensor less. This absence implies that different strategies are required for position detection. In case of this type of motor, the Back Electromotive Force (BEMF) is used for this purpose. This BEMF is generated by each winding, the consequence of this effect is a potential difference of opposite polarity to the voltage supplied to the windings; this voltage is measurable in order to estimate the position.

A three phase BLDC works energizing two branches while the third open winding is sensed to measure the back electromotive force; by detecting the zero-crossing of the BEMF on the open winding it is possible to determine the proper winding commutation sequence.

There are three main factors on BEMF:

- Angular velocity of the rotor
- Magnetic field generated by rotor magnets
- The number of turns in the stator windings

$$BEMF = (E)\ aNlrB\omega$$

N is the number of winding per phase, l is the length of the rotor, r is the internal radius of the rotor, B is the rotor magnetic field density and ω is the motor's angular velocity, this implies that there is a minimum speed to achieve a sufficient estimation of the speed [33].

Sensored vs Sensorless approach

Analysing the signals from Hall sensors and the BEMF evaluation, as in Figure 2.3, it is possible to notice the time correlation between the change of polarity of Hall sensor and the zero-crossing of the Back Electromotive Force. This assures that the BEMF zero-crossing provides a sufficiently precise position information.

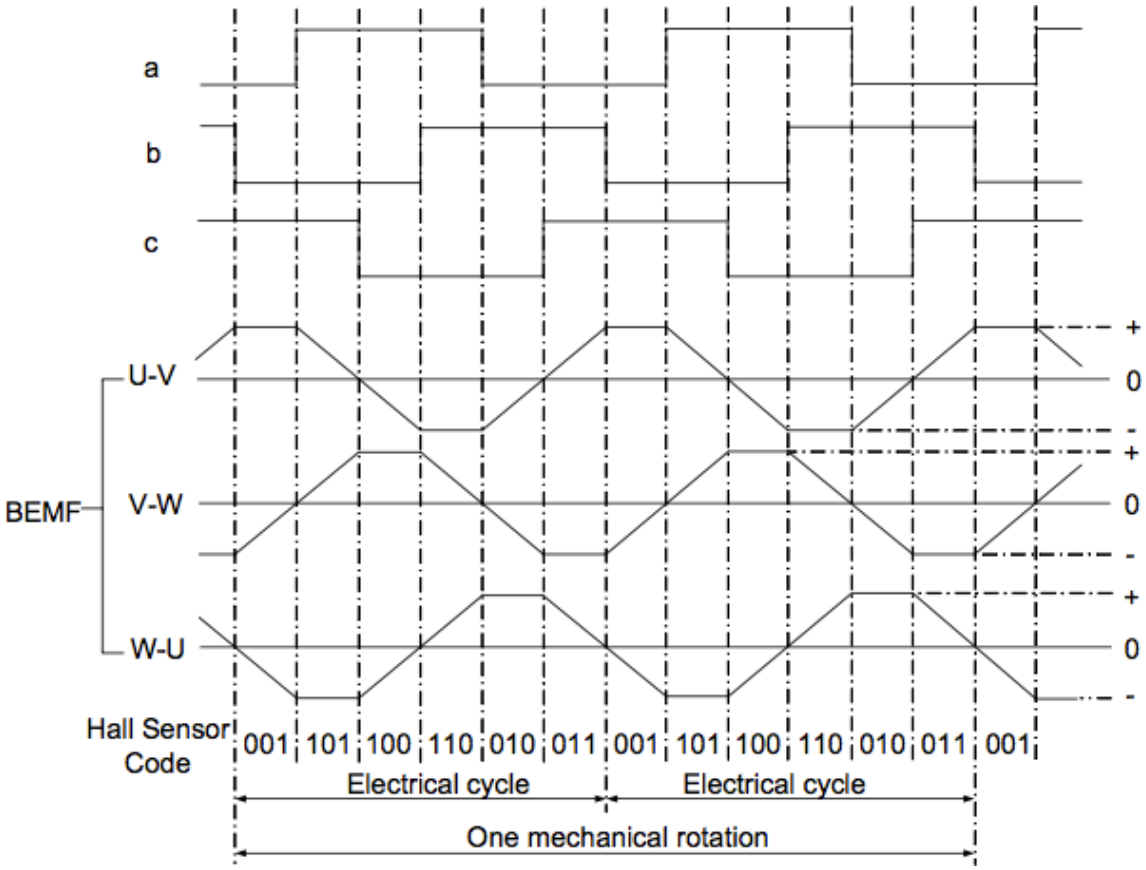

Figure 2.4 - Hall sensor and BEMF response.

The absence of sensors implies a lower cost and maintenance but, in contrast, the use of BEMF to pilot the motor is sensitive to noise and artefacts. Moreover, an initial open-loop control is required in the sensorless approach in order to receive BEMF values sufficiently high to be used. Oppositely, using sensored motor the

initialization is not needed because the position is acquired though the Hall sensor signals. The drawback of the sensored approach is related to the higher cost and maintenance, which can be critical in the medical field.

The motor chosen for this application is the model LS2207 from EMAX, shown in Figure 2.3. It is a three phase, sensorless, BLDC motor, it is quite small (diameter: 27.5 mm; length: 31.2 mm), light (weight: 30 g) and cheap. It is designed to be mounted on drones and to be powered by a 3-5s LIPO battery, which corresponds to a 18.5 V, and its ratio between RPM and applied voltage (KV) is 2550.

Figure 2.5 - Emax LS2207.

2.4.3 Control strategy

In order to energize three branches, a 3-phases H-bridge is used, the configuration of the bridge shown in Figure 2.6. Each transistor is driven by a Pulse Width Modulation (PWM) signal, which consist in a high frequency square wave applied to the MOSFET gate in order to let the current flow properly, following the correct activation sequence of the phases [30]. The transistors work as switches, allowing or not the correct current flow; thus one phase of the motor is connected to the positive voltage, the second phase discharges the energy to the negative (or ground), while the third is an open circuit through which BEMF is sensed.

It is fundamental to prevent the simultaneous activation of two lines to avoid short-circuiting the positive voltage to the negative one. The gate of each transistor is directly connected to the microcontroller which governs the gates. Typically, one diode per each transistor is placed between drain (collector) and source (emitter) in order to deny the return current.

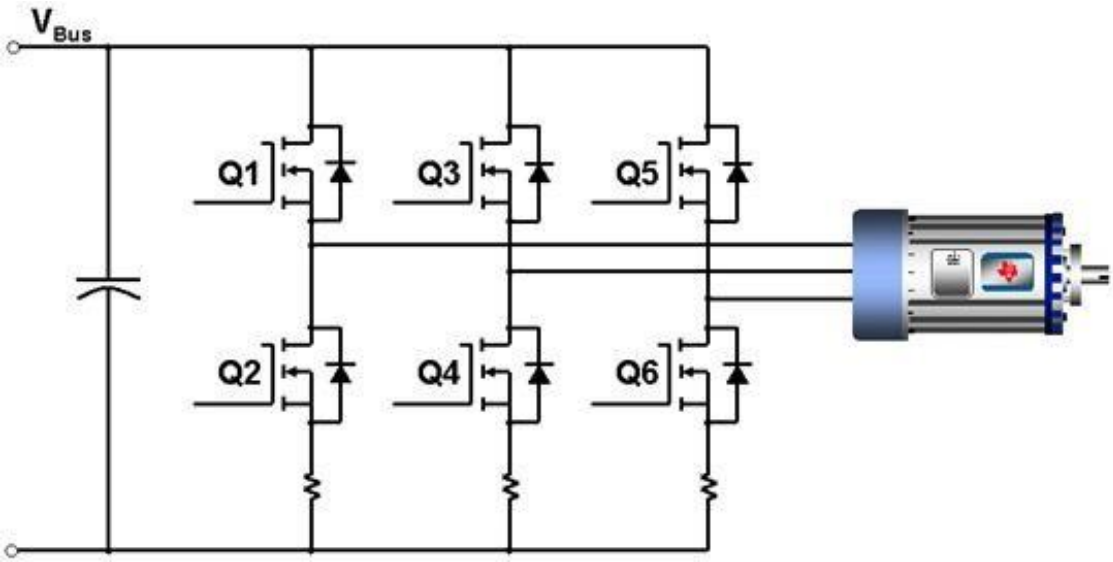

Figure 2.6 - Three Phase H-Bridge.

There are two different approaches to control a BLDC motor: 2-Quadrants or 4-Quadrants which differ in the type of deceleration. The first method is based on passive breaking exploiting the inertia of the motor or dynamic braking by short-circuiting the 3 phases. The 4-Q method is active and it is possible thanks to the use of a specific PWM technique called “complementary mode”. It consists in applying the PWM signal of opposite polarity on the two transistors of the same phase line. Hence, it allows to brake the rotor dynamically and have higher precision than 2-Q technique. The four-quadrants approach is preferable for high performance system and for rapid deceleration [34].

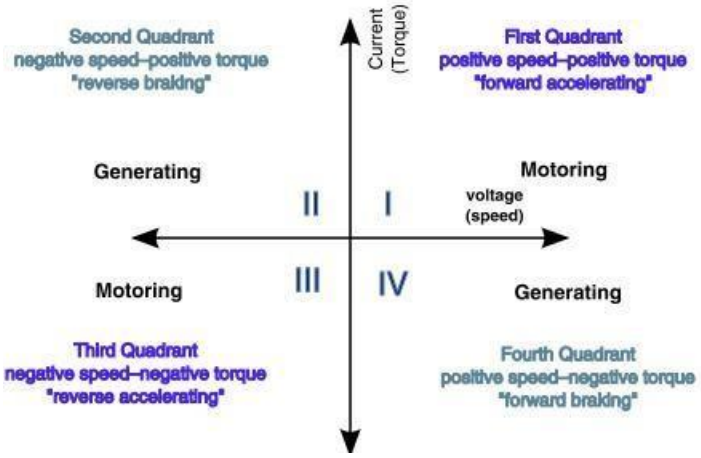

Figure 2.7 - Quadrants and motor operation.

2.4.4 ESC

The Electronic Speed Controller (ESC) is a compact printed circuit board (PCB) designed specifically for BLDC motor controlling. Typically, ESC is designed for hobby application, such as drones or RC cars, hence it is inexpensive and have small sizes.

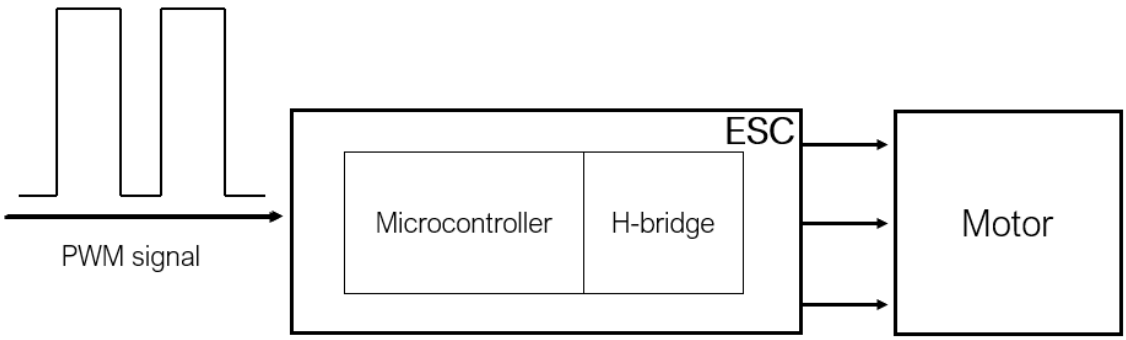

Figure 2.8 - ESC architecture.

Its task is to drive the motor through the power devices, in particular a three phase H-bridge is present in the board, so it has a strong dynamic response, and it is capable of delivering high current to the actuator. It lightens the main microcontroller load, demanding only a signal related to the target speed of the motor. To allow the BEMF sensing, an embedded OpAmp circuit is present. Then, this amplified signal is sampled by the microcontroller in order to evaluate the back electromagnetic force value.

Usually it requires a DC voltage supply in the range of 14-22V, this is used to control the motor. Since the embedded microcontroller needs a lower voltage, usually 3.3 or 5V, ESC has a DC/DC voltage regulator.

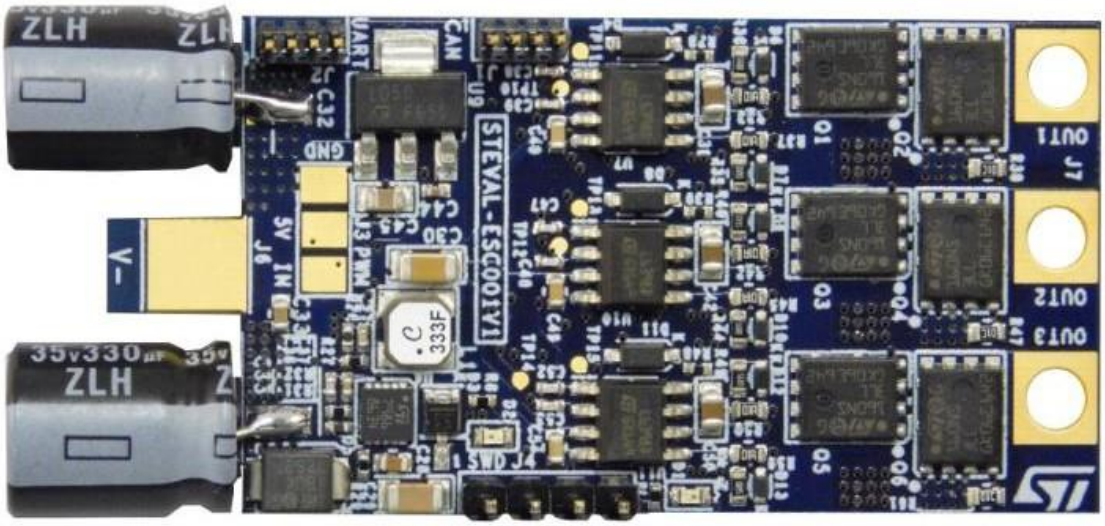

Figure 2.9 - Example of ESC circuit.

2.5 Air Compression Unit

The objective of the motor unit is to produce a pressure at the airways openings and create the sinusoidal oscillations required for the FOT. To do so, the motor has been coupled with an adequate propeller and placed in a specifically 3D printed plastic housing, that encapsulates the unit, helping to compress the air and direct the flow through the flowmeter and into the mask.

2.5.1 Motor Housing

As previously mentioned, the motor unit is inserted in a specifically 3D printed housing that channels the air to the flowmeter and the mask, thus helping to generate the required pressure.

The housing is composed by two matching pieces that enclose tightly the motor unit,

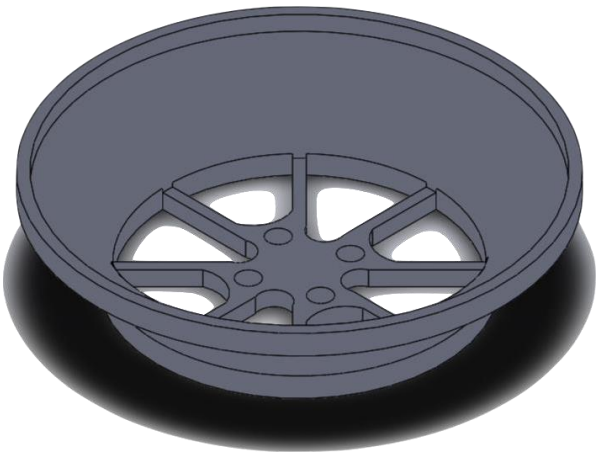

Figure 2.11 - Motor Housing Inferior Part

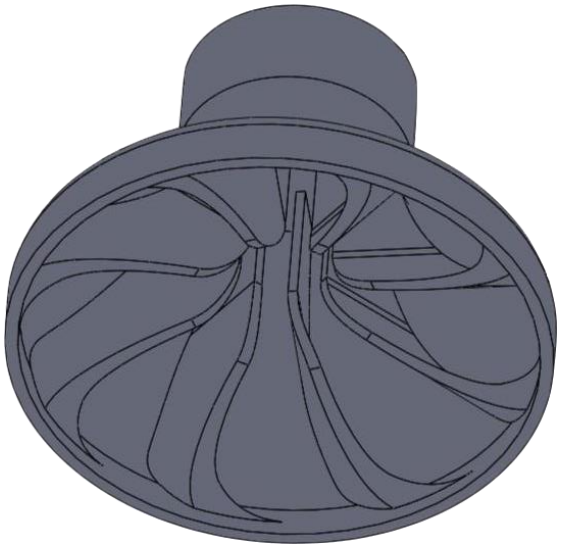

Figure 2.10- Motor Housing Superior Part.

an inferior part and a superior part. The inferior part offers a support on which is possible to screw the motor while simultaneously allowing the air to enter the housing. The dimension of the base is reduced to expose the motor itself to the airflow as it warms up significantly with the use and it needs to be cooled down.

The superior part is shaped to exactly match the dimension of the inferior part at the level of the propeller, then the section is gradually reduced to accelerate the airflow and channel it into the flowmeter and the mask. Some septa are present in the internal surface of this part to eliminate the rotational component of the airflow and prevent the air to bounce back in the wrong direction, thus drastically reducing turbulences and substantially improving motor efficiency.

2.6 Sensor Unit

The device embeds different sensors with the aim to collect data both regarding the subject breathing parameters and the surrounding environment.

The main sensors are those responsible for the measurement of parameters at the subject airways opening; these are two differential pressure sensors: the first one measures the pressure difference between ambient pressure and the one at horse

airways opening, while the second collects a pressure drop across a resistance, which is then converted into a flow measure.

A second pair of sensors is used to measure ambient parameters such as absolute pressure, temperature and humidity. These data will be used to compensate the measurement of the first pair of sensors according to the surrounding conditions, allowing a correct measurement in many different environments.

2.6.1 Differential pressure sensors

Both pressure and flow sensors are built over a differential pressure sensor. This kind of sensor is constituted by two chambers separated by a semi-rigid membrane over which a deformation is applied. The deformation due to the pressure difference in the two chambers is measured and converted into a voltage variation through a calibration. Sensors used are part of the ELVR series from All Sensors, and are designed to provide a linear output proportional to the applied pressure, reducing offsets due to changes in temperature, warm-up, common mode errors, long period drifts and effects of position. The sensor is equivalent to a full Wheatstone bridge, whose voltage is:

$$VG = VS \cdot G \cdot \varepsilon$$

where VS is the supply voltage, G the Gauge factor and ε is the strain caused by the pressure difference. The analog output of the sensor is ratiometric to the supply voltage which is set to 5V by means of a linear voltage rectifier (LM7805 Microchip Technology, Chandler, USA) and proportional to the applied differential pressure. Sensor readout circuit is composed by a low pass RC filter, whose output is buffered to a 12-bit Analog to Digital Converter (ADC).

The sensor used for pressure measurement is the model ELVR-L10D that provides a linear P/V relationship between -25 and 25 mbar (about -25,5 and 25,5 cmH2O). Flow is measured by means of a pneumotachograph, a device which relates flow of a fluid with a differential pressure measured across a hydraulic resistance:

$$Flow = \frac{P}{R}$$

The sensor used to measure this pressure drop is the pressure range of ±2.5 mbar (ELVR-L01D).

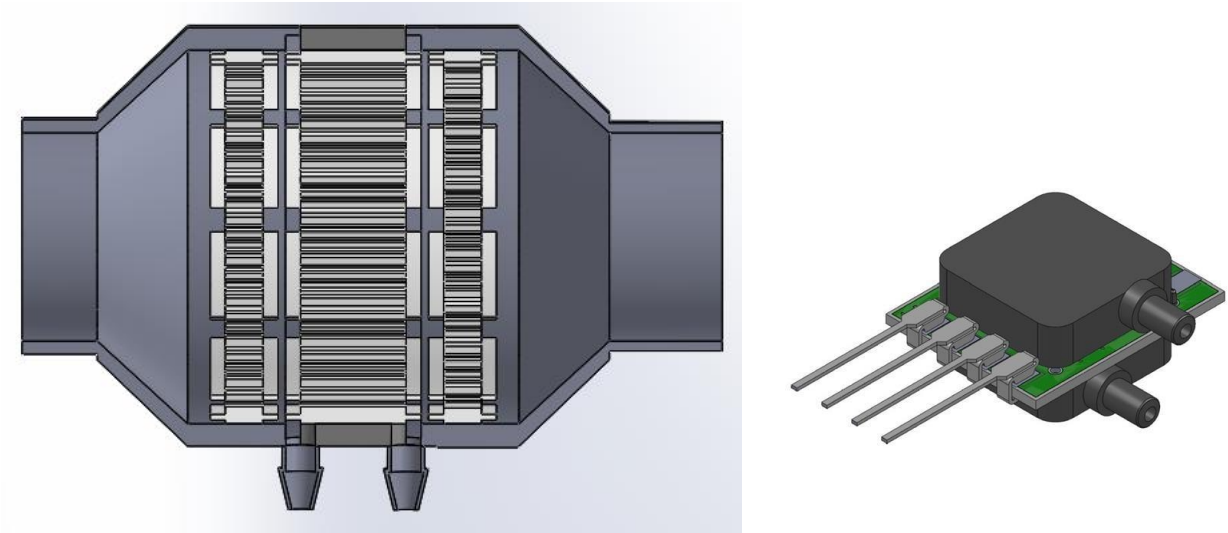

Figure 2.12 - Pneumotachograph section (on the left). Differential pressure sensor (on the right).

2.6.2 Pneumotachograph

The pneumotachograph measures flow rate by sensing the pressure change across a small but laminar resistance. The design ensures that the differential manometer senses the true lateral pressure exerted by the gas on each side of the resistance element.

In this project a custom pneumotachograph has been designed in order to measure a large flow typical of equines. The instrument is composed by a single element embedding a mesh of the same material as the conduct. In order to obtain the desired shape and material, the pneumotachograph has been 3D printed with polymeric resins. A longitudinal section is reported in Figure 2.10.

The core element is the central mesh, which allows to estimate the airflow by measuring differential pressure at its poles and dividing it by the hydraulic resistance of the central mesh itself, according to Poiseuille law.

In order to use Poiseuille equation a laminar flow should be considered; for this purpose, two thin meshes are added at the sides of the central mesh. The three meshes are composed by thin layers arranged to form squares of 1.5 mm side length. Another design choice is the void circular crown placed next to the central mesh at both sides. This shape avoids turbulences due to side lodgings necessary to measure differential pressures. Another important element is the symmetry of the instrument, which should be maximized to obtain a reliable measurement for flows of air in both directions.

The benefits of the polymeric resin are manyfold: it allows to design a customized pneumotachograph with a fine resolution, reduces moisture accumulation during measurement and reduces damage risk due to its plastic mechanic properties, ensuring a good compromise between rigidity and elasticity.

Calibration

Flow and pressure sensors are each connected to a 12-bit analog to digital converter (MCP3201, Microchip Technology, Chandler, USA) that needs an appropriate calibration procedure to rescale the logic values sampled into the correct analog values.

Pressure sensor can be calibrated by acquiring data at known pressure values. To do so, a U-type liquid manometer has been used. One of the two entries of the manometer has been left at ambient pressure while the other one has been connected in series with one of the two inputs of the pressure sensor. A syringe has been used as a pressure generator and has been connected in parallel to the connected inputs of the manometer and the sensor. During the calibration process the syringe was used to change with small steps the pressure values read from the manometer and acquired with the sensor. Pressure voltage sensors are linear, so obtained data were processed in MATLAB by fitting them on the equation:

$$P = m * D + q$$

where P is the pressure value for each step and D is the digital value from the ADC.

To calibrate the flow sensor, a volume-based calibration process has been used. In fact, as volume is the integral over time of flow, a known volume can be used to produce a flow exploited to calibrate the sensor. To do so, a calibration syringe with a known volume was connected in series to the pneumotachograph and its piston was moved to generate the flow. To obtain a good reliability 5 consecutive strokes were made. Raw data were recorded and processed with MATLAB.

Flow data were integrated, after the offset suppression, to obtain a volume displacement. The slope of the calibration curve is obtained by the ratio between the real volume [L] and the one obtained from the integration [digits · second], while the intercept can be obtained considering the offset.

2.6.3 Monitoring Unit

The device should be highly portable, allowing the measurement of respiratory system properties in different environments, extending its usage from clinical room to houses or farms. Measurements of pressure and flow are subjected to sensors' sensitivity change when exposed to environmental changes, such as altitude, temperature and humidity. These factors influence air properties, such as density or composition. A compensation strategy can be developed in order to obtain correct measurements in different environmental conditions, allowing the usage of the device in different scenarios and with higher robustness and reliability.

Absolute pressure sensor

The first compensation to be taken into account is the absolute pressure, which may vary with altitude or due to whether condition. Changes in absolute pressure may affect the measurement of pressure at subject airways opening, which is computed as differential measure with the external pressure.

The sensor (reported in figure 2.11) used in this project is the MS5637-02BA03, which features very small dimensions (3 x 3 x 0.9 mm), low voltage supply and low cost. The sensor is based on MEMS technology which allows to fabricate in a small chip a piezo-resistive sensor and a sensor interface integrated circuit. A temperature sensor is also embedded in the chip, allowing a compensated measurement.

The sensor is connected to the microcontroller through the I2C interface, in this way only two pins of the microcontroller are necessary to communicate with all the peripherals connected to the I2C bus.

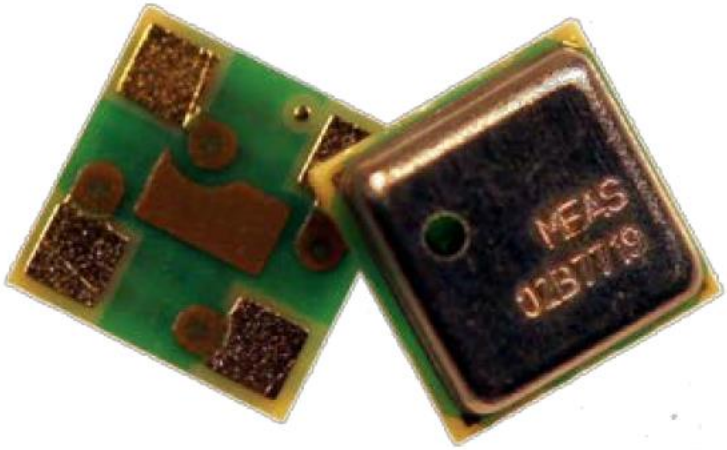

Figure 2.13 - Absolute Pressure Sensors MS5637.

Temperature and Humidity sensor

In order to compensate the measurement for temperature and humidity changes a Humidity/Temperature sensor (Honeywell HumidIcon Digital HIH6100 Series) has been integrated in the system. These are digital output-type relative humidity (RH) and temperature sensors combined in the same package. The sensor provides an accuracy level of ±4.0 %RH and a temperature accuracy level of ±0.5 °C.

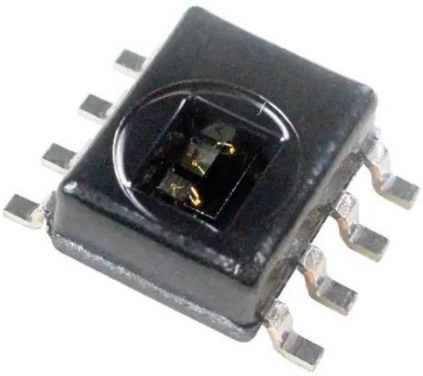

Figure 2.14 - Temperature and Humidity Sensor HIH6130.

HIH6130/6131 Series sensors use a laser trimmed, thermoset polymer capacitive

sensing element, which combined to a multilayer structure ensure robust performances against moisture or dust.

This sensor is interfaced via I2C protocol to the microcontroller, which can read a measurement any time it's needed, sharing the data and clock line with the absolute pressure sensor. Its output is digital and already calibrated, thanks to a small integrated circuit embedded in the sensor. The package chosen for this project is reported in figure 2.12.

2.7 Power Supply

The components of the device work at different voltages, for this reason different sources are obtained from the same power supply.

The first one is required to drive the motor, through the ESC. This power supply must deliver high current to guarantee the sufficient energy to the motor, a voltage of 12 V is provided with the main power supply.

The second source provides energy to the microcontroller and consequentially to the sensors and other peripherals, which work at 3.3 V or 5 V; in the first case the supply is provided by the 3.3V pin of the microcontroller, while the 5V is established using a voltage regulator LM7805 which control the transition between 12 V of the main source to the 5V needed for this circuit. A schematic representation of power supply distribution is reported in Figure 2.13.

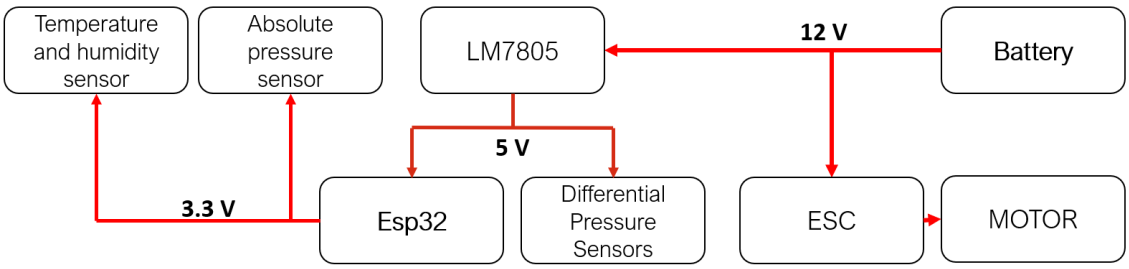

Figure 2.15 - Power Supply scheme.

The choice of the power supply for this project has been sought among portable batteries. They have the advantage of being portable and it allows to acquire data even outside, which is important considering that the subjects are animals. The

battery used for the project is a Lithium-ion Polymer battery (LiPo). It is composed by lithium-ion and polymer electrolytes, instead of liquid electrolytes.

It has the advantage of being rechargeable, of having small dimensions making it easily transportable and the capability to produce the high current required by the motor. Moreover, due to the high request of the hobby market related to RC cars and drones, LiPo batteries can be easily acquired and they are produced with many different characteristics, allowing to choose the best fitting power supply for the project. Each battery is composed by one or more Li-polymer cells in series; each cell creates a voltage difference of 3.7V, the standard nomenclature of the LiPo battery contains the number of cells in series followed by "S" – for example 4S means 4 cells in series – and considering that each cell produces 3.7V this nomenclature explicits the potential difference of the battery. Also the maximum discharge current rate is a crucial parameter, it is defined by the C letter

$$Capacity * discharging\ rate = current\ supplied$$

The main problem of the LiPo batteries is related to the duration of one single charge. In fact, they are not suitable for long period acquisition due to their short life, which depends on the current supplied.

Since the need of a small, light and easily available battery was the main requirement for the power supply choice, LiPo were chosen as appropriate battery. The possibility to have more than one battery available during the measurement allows to possibly change a low battery with a charged one, while the first one can be recharged.

Damage Prevention

Considering the high current flowing, its necessary to protect both the device and the power supply from the current flow-back and overvoltage. Transient Voltage Suppression Diode are used for this purpose.

Diodes are placed between the positive pole of the power supply and the positive input of the ESC in order to prevent current to flow back to the power supply. Exploiting these elements, voltage shoots are avoided but there is the need to dissipate this excess of charge. For this reason, transils are used; they shunt the excess current when the induced voltage is higher than their avalanche breakdown

potential. Transils suppress the voltages above their breakdown voltage, working as a resistor and consuming the transient energy.

2.8 Control Unit

The system has to carry out different tasks during its functioning, being able to switch settings runtime and provide data also in real time to the user. The control of such a device results complex, thus it has been divided in two classes:

- Low Level Control responsible for hardware management.
- High Level Control related to device settings and acquisition modality.

The first one is implemented in the microcontroller firmware, with the aim of acquire data from pressure sensors, process them and correctly update PWM signal to drive the motor. The communication between microcontroller and laptop has to be synchronized and controlled by the Esp32.

The latter is implemented as user interface on the user laptop; the user can act on the device tuning measurement settings, processing data, saving them locally or on a micro-SD card and display them real time or offline.

2.9 Communication

The microcontroller manages the data transmission between peripherals. More in

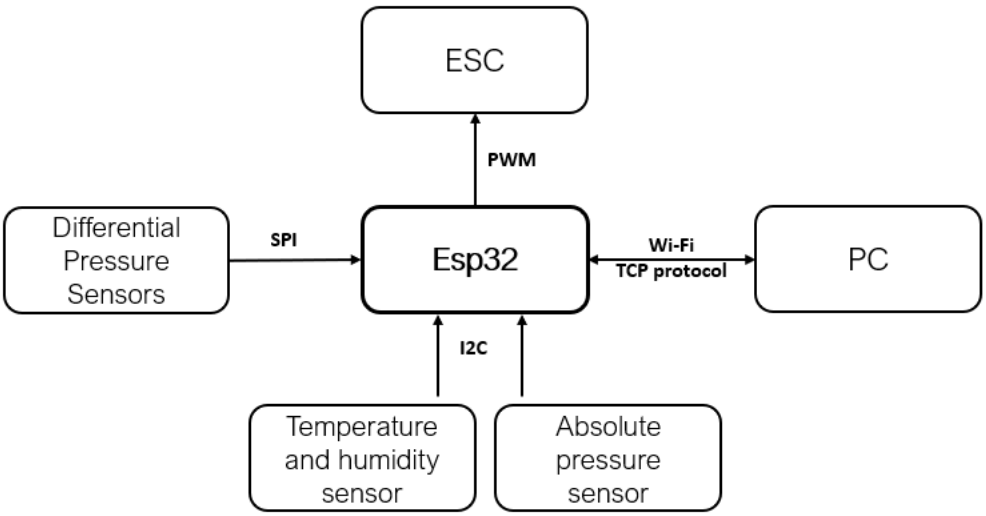

Figure 2.16 - Communication hierarchy scheme.

detail, data are collected from sensors, then motor speed is corrected accordingly, so the microcontroller has to set duty cycle via ESC. Finally, the system functioning can be controlled and monitored from a laptop, which exchange information with the microcontroller. A scheme reporting relationships between peripherals is shown in Figure 2.14. Data transmission is carried out in different ways according to the peripheral of interest.

2.9.1 Wireless Transmission

One of the more important features of the device is the portability. The best way to ensure a portable and handy system is to make it wireless, especially in the contest of non-collaborative subjects as animals are.

For this reason, the microcontroller chosen for this project embeds a radio frequency module which allows to establish a wireless communication. More in detail, the Esp32 microcontroller is equipped with hardware and software which allow Bluetooth and Wi-Fi services.

Bluetooth

The Bluetooth Classic radio is a low power radio that streams data over 79 channels in the 2.4GHz unlicensed industrial, scientific, and medical (ISM) frequency band. The technology is based on a point-to-point device communication; it's mainly used to enable wireless audio streaming and has become the standard radio protocol

behind wireless speakers, headphones, and in-car entertainment systems.

Another option is the so-called Bluetooth Low Energy (BLE) which is designed for very low power operations. It transmits data over 40 channels in the same radio band as Classic Bluetooth. Differently from Classic, BLE supports multiple communication topologies, such as broadcast and mesh, enabling Bluetooth technology to support the creation of large-scale device networks. A table reporting main specifications for both technologies is depicted below.

Feature	Bluetooth Low Energy (BLE)	Bluetooth Classic
Frequency Band	2.4GHz ISM Band	2.4GHz ISM Band

Channels	40 channels with 2 MHz spacing (3 advertising channels/37 data channels)	79 channels with 1 MHz spacing
Modulation	GFSK	GFSK, π/4 DQPSK, 8DPSK
Data rate	Up to 2 Mb/s	Up to 3 Mb/s
Communication Topologies	Point-to-Point, Broadcast, Mesh	Point-to-Point

Table 1 - Bluetooth and BLE characteristics

Wi-Fi

When electrons move, they create electromagnetic waves that can propagate through space, even in a vacuum. When an antenna of the appropriate size is attached to an electrical circuit, the electromagnetic waves can be broadcast efficiently and received by a receiver some distance away. All wireless communication is based on this principle [41].

Wi-Fi technology is based on the Institute of Electrical and Electronics Engineers (IEEE) wireless communication standard 802.11 released in 1997. This standard defines the lower two level of the seven described in the ISO/OSI convention; Physical Layer (PHY) and Data Link Layer (DLL) are further subdivided in Logical Link Control (LLC) and Medium Access Control (MAC) respectively. MAC sublayer determines how the channel is allocated, that is, who gets to transmit next. Above it is the LLC (Logical Link Control) sublayer, whose job it is to hide the differences between the different 802 variants and make them indistinguishable as far as the network layer is concerned.

The signal is physically transmitted by the mean of radiofrequency in the bands 2.4 GHz and 5 GHz and, 6 GHz. From that time on, it has continually improved, up to the sixth generation of Wi-Fi. Specifications regarding different standards are reported in table.

Generation	IEEE Standard	Maximum Linkrate	Radio Frequency
Wi-Fi 6E	802.11ax	600 to 9608 Mbit/s	6 GHz
Wi-Fi 6	802.11ax	600 to 9608 Mbit/s	2.4/5 GHz
Wi-Fi 5	802.11ac	433 to 6933 Mbit/s	5 GHz
Wi-Fi 4	802.11n	72 to 600 Mbit/s	2.5/5 GHz

Table 2 - Wi Fi characteristics

All of the transmission methods also define multiple rates. The idea is that different rates can be used depending on the current conditions. If the wireless signal is weak, a low rate can be used. If the signal is clear, the highest rate can be used. This adjustment is called rate adaptation. Since the rates vary by a factor of 10 or more, good rate adaptation is important for good performance [41].

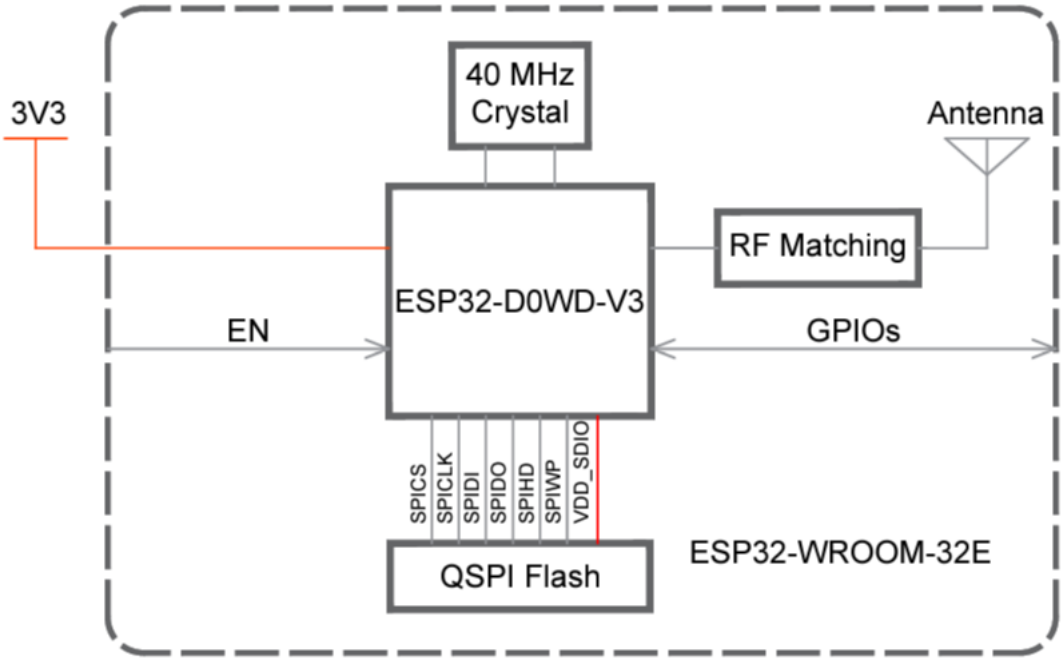

Figure 2.17 - ESP32-D0WD-V3 block diagram.

This technology allows exchanging data without a physical mean, exploiting modulation of electromagnetic waves. The microcontroller chosen for this project embeds the ESP32-D0WD-V3 module, figure 2.15 reports a block diagram.

The two technologies are equivalent under many aspects. They are both based on the same physical principle, they both exploit ISM frequency bands subdivided in channels and are characterized by a speed of transmission and range of functioning. For this project the choice of Wi-Fi over Bluetooth was motivated by a main reason.

Wi-Fi technology allows the implementation of a wireless connection that can either be limited to a local area (LAN) or extended to internet access. This could be useful to implement further functionalities that may require internet access, such as cloud support for data repository or the software extension to a website.

As previously said, the strategy used in this project was based on Wi-Fi technology. Each device capable of establishing Wi-Fi communication is called a station. Each station can either share its own network, working as an access point, or access another network as a node. For this project, the microcontroller promotes its own network, waiting for a host device to connect. When the host connects to the access point, ESP32 provides a new local IP address to the host machine. From this time on data can be transferred between the two devices via Wi-Fi.

2.9.2 TCP protocol

In order to implement information exchange using wireless transmission, a higher-level protocol is needed to guarantee data exchange occurs according to defined rules.

TCP is a connection-oriented, end-to-end reliable protocol that allows a byte stream originating on one machine to be delivered without error on any other machine. It segments the incoming byte stream into discrete messages and passes each one on to the internet layer. At the destination, the receiving TCP process reassembles the received messages into the output stream. The TCP provides reliable inter-process communication between pairs of processes in host computers attached to distinct but interconnected computer communication networks [41].

The interface between TCP and lower-level protocol is essentially unspecified except that it is assumed there is a mechanism whereby the two levels can asynchronously pass information to each other. Typically, one expects the lower-level protocol to specify this interface. TCP is designed to work in a very general environment of interconnected networks.

The TCP must recover from data that is damaged, lost, duplicated, or delivered out of order by the internet communication system. This is achieved by assigning a sequence number to each octet transmitted and requiring a positive acknowledgment (ACK) from the receiving TCP. The sequence numbers are used at the receiver to correctly order segments that may be received out of order and to eliminate duplicates. Damage is handled by adding a checksum to each segment transmitted, checking it at the receiver, and discarding damaged segments. [41]

When two processes wish to communicate, their TCP's must first establish a connection (initialize the status information on each side). Since connections must be established between unreliable hosts and over the unreliable internet communication system, a handshake mechanism with clock-based sequence numbers is used to avoid erroneous initialization of connections.

To allow for many processes within a single Host to use TCP communication facilities simultaneously, the TCP provides a set of addresses or ports within each host. A single device will be provided with multiple ports, allowing establishing more than one connection channel. When their communication is complete, the connection is terminated or closed to free the resources for other uses.

2.9.3 I2C protocol

The Integrated to Integrated Circuit (I2C) is a synchronous serial communication protocol used to exchange data. Synchronous means that there is the necessity of a clock line used to keep in synch the different peripherals. This protocol is based on the Master - Slave architecture and the connection between the two devices is depicted in Figure 2.16.

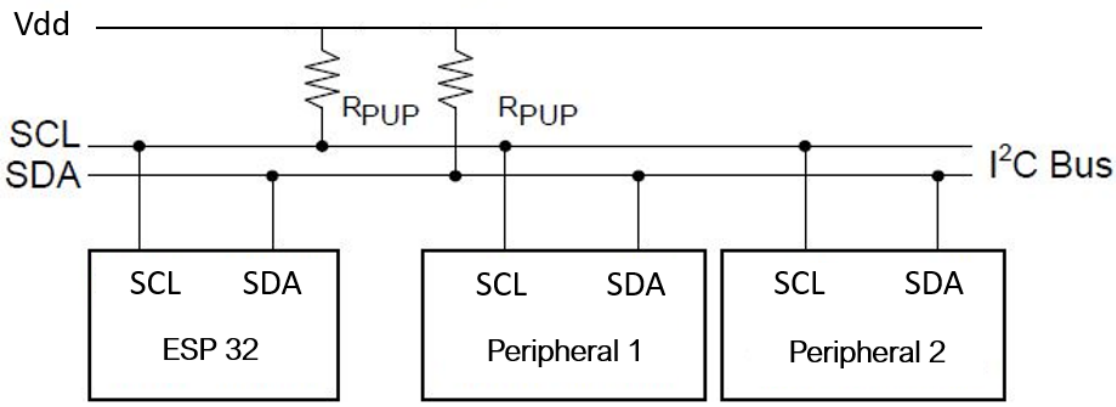

Figure 2.18 - I2C connection scheme.

The I2C bus uses two wires: serial data (SDA) and serial clock (SCL). All I2C master and slave devices are connected with only those two wires. Each device can be a transmitter, a receiver, or both. The master generates a bus clock and initiates communication on the bus. Other devices are slaves and respond to the commands on the bus. In order to communicate with a specific device, each slave must have an address that is unique on the bus [40].

Each I2C command initiated by the master device starts with a START condition and ends with a STOP condition. For both conditions, SCL has to be high. A high to low

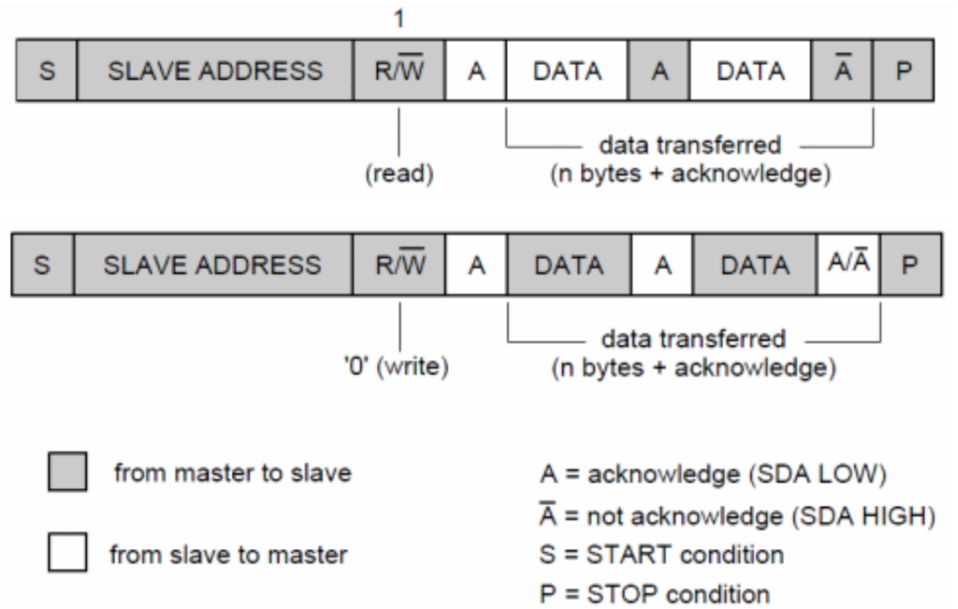

Figure 2.19 - I2C istruction example.

transition of SDA is considered as a START and a low to high transition as STOP. Data on the I2C bus is transferred in 8-bit packets. There is no limitation on the number of bytes; however, each byte must be followed by an Acknowledge bit. This bit signals whether the device is ready to proceed with the next byte. The master must generate clock pulses for all data bits, including the Acknowledge bit. An example of data exchange for the read and write instructions is reported in Figure 2.17.

The communication starts with the Start condition, followed by the 7-bit slave address and the data direction bit. If this bit is 0, the master will write to the slave device. Otherwise, if the data direction bit is 1, the master will read from the slave device. After the slave address and the data direction is sent, the master can continue with reading or writing. The communication is ended with the Stop condition, which also signals that the I2C bus is free.

In this project, both the absolute pressure sensor and the temperature and humidity sensor are based on the I2C protocol; Esp32 initiates a communication as master, require data from the sensors which are slave devices.

2.9.4 SPI protocol

The Serial Peripheral Interface (SPI) is a synchronous serial communication protocol, similarly to I2C, it's based on the Master - Slave architecture. Connections are different from the I2C case, in particular the presence of two data lines allow the bidirectionality of data exchange. Connections between the two devices is reported in Figure 2.18.

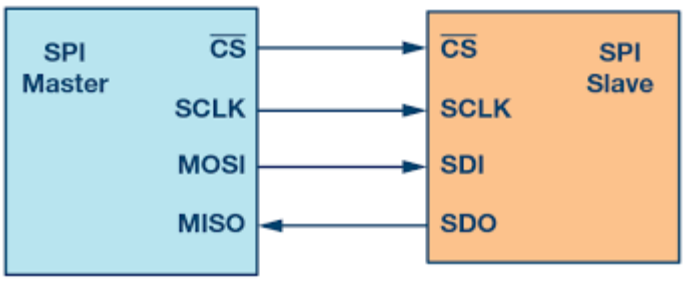

Figure 2.20 - SPI connection scheme.

As previously said, the SPI protocol is bidirectional, both master and slave can transmit data simultaneously. The interface master-slave can be developed either with three or four wires.

- Clock CLK
- Chip Select CS
- Master Out Slave In MOSI
- Master In Slave Out MISO

The device which generates the clock is the Master. The clock signal is used to synchronize the different peripherals, whereas the Chip Select is required to select which slave peripheral has to receive the data. The exchange of data occurs through the MOSI and MISO lines, each one has a preferred direction hence having two lines the bidirectional transmission is obtained [37].

In this project the differential pressure sensors exploit the SPI communication protocol; more in detail, the sensor analogue output is converted to a digital value by an external ADC, which is then read by the microcontroller. The ADC is configured using the SPI protocol.

2.9.5 ESC

The electronic speed controller interprets the input signal in order to regulate the speed of the motor; it is not able to produce signal if not governed, hence it requires a PWM as input. The signal is provided by the microcontroller, which generates the square waves through the PWM peripheral embedded on the chip.

The communication between the microcontroller and the ESC occurs through the Pulse Width Modulation, in particular the square wave has duration of 2ms. Regulating the duty cycle of the PWM, the ESC decodes the duration of the duty cycle in order to establish the target speed. Constrains on the minimum duration of the duty cycle are present, in fact the accepted range is between 1ms and 2ms which means from 50% to 100%, the speed increases linearly with the duty cycle.

2.10 Horse Mask

The device structure has been thought to be modular and compact. The need for a modular design arises from different considerations.

Moisture and mucus may accumulate especially through the PNT mesh, where the section of the conducts reach 1.5 mm^2. One should be able to disassemble the system in order to polish the single components individually and reassemble them in a simple way.

Moreover, recalling that the subjects of measurement are horses, it's necessary to take into account the possibility of system damage due to abrupt motions or impact with objects. The need to rapidly replace single components due to localized damage also requires the systematic subdivision in modules. Finally, due to the high level of components customization, the 3D printer is a valid method to ensure quick and low-cost components.

The system integrates all its components into a unique structure which can be easily assembled; the main moduli are:

- Motor housing and pneumotachograph.
- Horse mask.
- Electronic PCB.
- LiPo battery.
- Mask seal.

Design of the whole device is reported in figure 2.21, enhancing subdivision of different submodules.

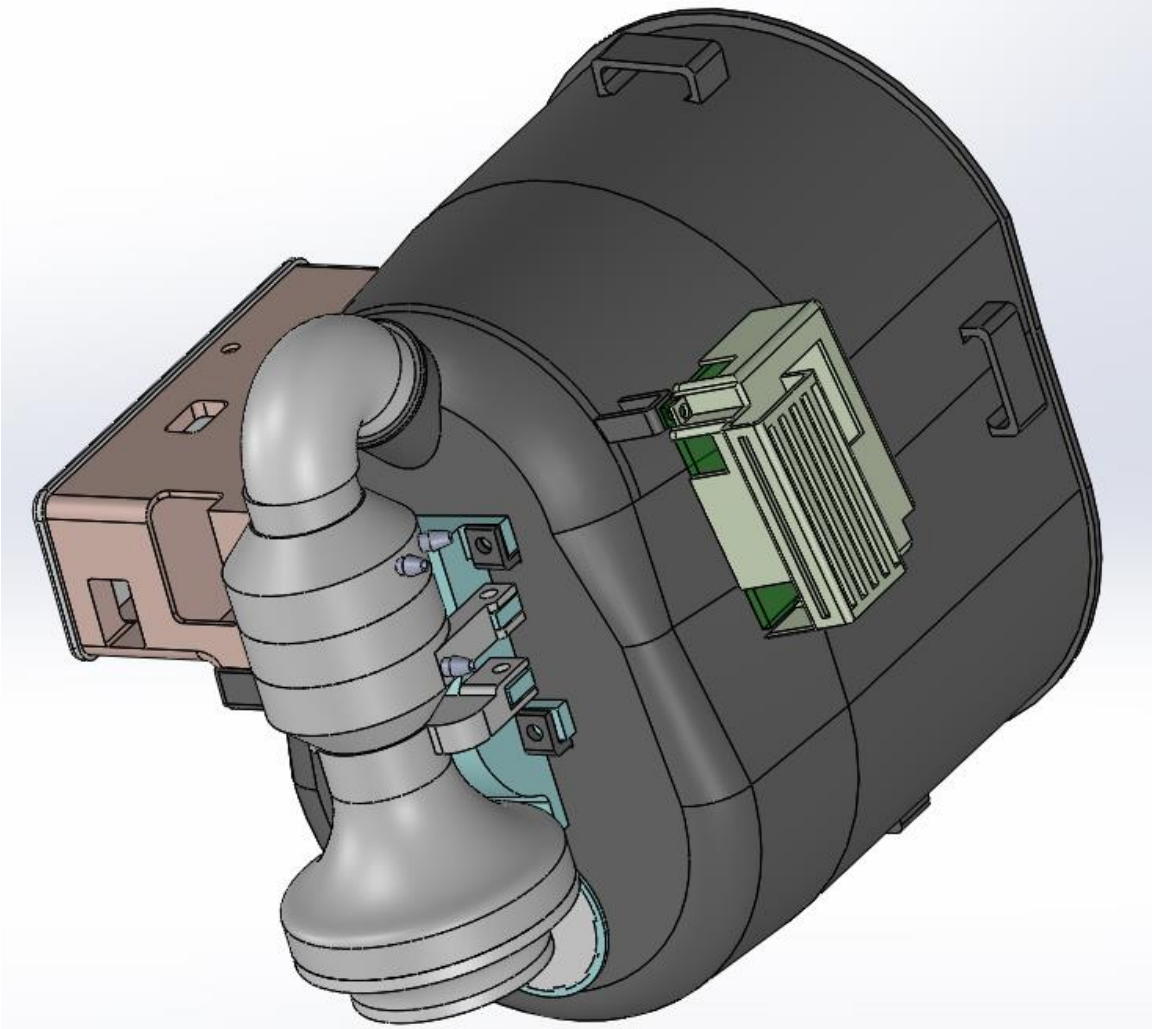

Figure 2.21 - Horse mask design. Different colours identify different moduli: black for mask, green for PCB housing, red for power supply housing, grey and light blue for PNT and Motor module.

The most important structure is composed of the horse mask, which was built from a standard horse mask for respiratory measurement. The peculiarity of this component is the possibility to attach the other components in a secure and straightforward way, using screws. Motor and pneumotachograph constitute the crucial module for pressure oscillation generation, while LiPo battery and PCB are submodules embedded in their own case, designed to embeds the necessary electronics. Finally mask seal was designed starting from standard seals, with the precise aim to seal the mask, obtaining a system without leaks.

The whole device (omitting power supply and electronic components) was realized starting from 3D printed materials. In this project, the use of 3D printing allowed to test different designs of the device, reducing time and costs during the development phase. According to the system module, the final choice of materials and printing methods consists of two types of printing materials and techniques, plus the use of silicone for soft and flexible components.

2.10.1 3D-printing Process

Polymer printing is advantageous because it enables printing low-cost functional parts with various properties and capabilities. Suitable polymer printing processes include extrusion, resin, and powder 3D printing, which will allow directed material deposition for the design of advantageous and customized architectures [42]. The horse mask has been printed in Nylon PA with powder 3D printing technique. Other components were designed to have different mechanical properties; resin 3D printing was employed for these modules.

Powder 3D printing relies on fusing powders of a selected material using lasers in selective laser sintering or by chemical means in binder jetting. In these processes, a powder bed is solidified and replenished layer by layer to form a part [42]. Nylon PA is based on the need for a rigid, mechanically resistant structure, other than high accuracy for details during the printing process. Moreover, the material is biocompatible and waterproof, both features are important for medical applications.

Resin 3D printing relies on applying ultraviolet light in specified patterns to form a part layer by layer by curing deposited liquid resin, which is commonly used for stereolithography printing [42]. Different types of resin were employed for two sub-modules.

ABS-like resin is a grey-opaque photopolymer, characterized by sturdiness, and high stress and strain resistance. It has been employed as material for PNT and motor housing, other than battery and PCB housing.

Translucent resin was the material used to realize plates for silicone components. This type of resin was chosen for its high accuracy that ensures smooth walls, while the typical fragility is not problematic for the use of the components restricted to laboratory.

2.10.2 Silicon components from moulds

Soft but flexible components were necessary in this project mainly for interface between materials. This is the case of the component used as vibration dumper, but also the mask seal, which is placed among the mask and the horse itself; the seal should therefore be soft enough to adapt its shape for different horses, but flexible enough to maintain its natural form at rest. These features correspond to the one of silicone; moreover the production of components starting form a 3D-printed moulds result highly repeatable, low cost and simple.

Silicon based object production process require the design of a mould which is often obtained from the subtraction between a solid and the desired object shape. The silicone is then poured into the mould until it becomes solid. A crucial step consists of air removal from the silicon, to ensure no air bubbles will be present in the final object. This result can be achieved by submit the silicon to low pressures in a close environment using a vacuum pump.

Mould for mask seal is reported in figures 2.22, 2.23.

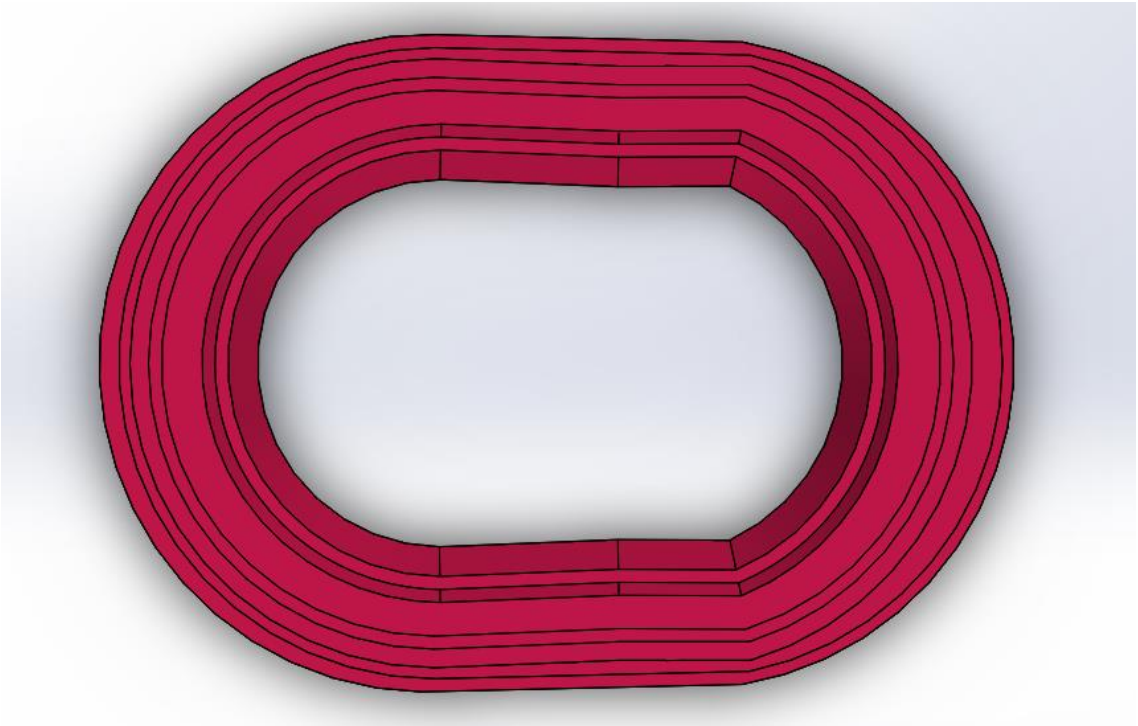

Figure 2.23 - Mask seal stamp, front view.

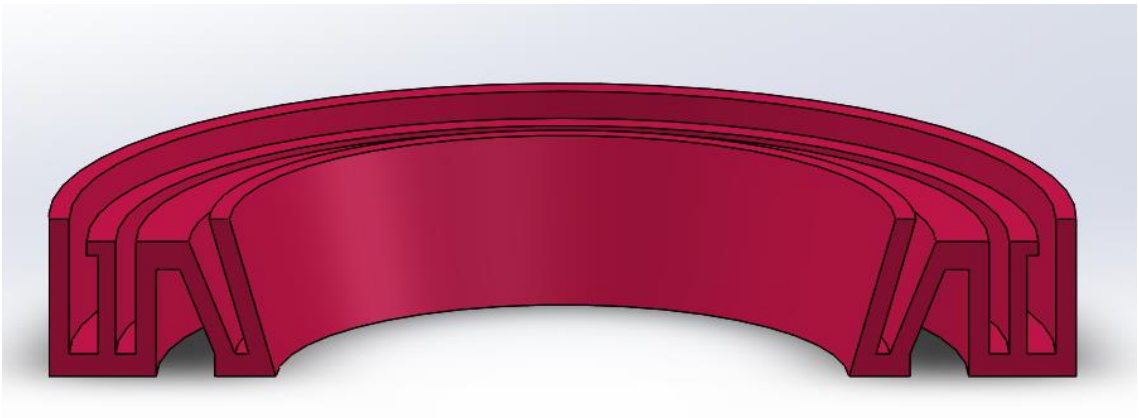

Figure 2.22 - Mask seal stamp, section.

CHAPTER 3 FIRMWARE AND CONTROL STRATEGY

A device should be governed by an efficient control strategy that ensures the system's correct functioning. The user can access the system with the graphic interface running on its laptop to adjust parameters, start and stop the measure or even look at measurement result. This can be defined as a high-level control and will be explained in detail in the next chapter.

When the device executes a task and accomplish a measurement, the peripheral control is managed by the microcontroller. This is the core of the system, establishing the device behavior at a lower-level.

3.1 Low-Level Control

As already said, the device working algorithm which controls sensors and actuators works according to the user directives, and it is depicted in this work as Low-Level Control; it is responsible for the correct functioning of the actuators at every step of the measurement, ensuring that a FOT measurement session is performed correctly.

In this work, the actuator to be controlled is the brushless motor; in particular, its speed is related to the pressure developed at the animal airways opening. This implies that in order to obtain a correct pressure modulation, the control of motor speed is necessary. The electronic signal which controls the motor speed is the PWM signal. The variable responsible for PWM signal modulation is the duty cycle (DC) of the square wave. The low-level control will thus be responsible for correctly assigning the DC value at the PWM signal driving the motor to obtain the desired pressure value at the subject’s airways opening.

There are two classes of control loop: open-loop control and closed-loop control, also called feedback control. In an open-loop controller strategy, the control action of the controller is independent from the variable of interest: usually, it is fast and computationally light, but obviously, it requires supervision from the user, as manual corrections should be performed to compensate for deviations from the ideal

situation. In a closed-loop controller, the control action is instead dependent on the controlled variable: this variable, therefore, has to be sensed and compared to a target value so that the controller is capable of automatically correcting its own control actions to maintain the variable as close as possible to the target value.

3.1.1 Open loop

In this control strategy, the pressure at the airways' openings does not affect the control action of the controller. This means that the actual pressure obtained is not compared with a target setpoint, therefore, input variables should be manually changed to reach and maintain the desired pressure values.

The two variables that can be manually changed are the offset and the sinusoid amplitude in the duty cycle formula seen above. Anyway, as the load is generally not known in advance, it is impossible to define a priori velocity of the motor that will result in the desired pressure.

Other disadvantages of this approach are the lack of safety controls in case of unwanted pressure values and the impossibility to anticipate the system's behavior, as errors or drifts in pressure are not compensated by the controller. On the other hand, it is easy to implement, and therefore it has been used during the preliminary tests with the device.

3.1.2 Closed Loop

This kind of control logic is used to automatically change some parameters to maintain the system's output at a chosen set point, which is the controller's input. It is based on the computation of an error defined as the difference between the target setpoint and the measured process variable. The controller's task is to minimize this error in the output by varying the process control inputs.

The Proportional-Integral-Derivative controller, or PID controller, is one of the most widely used closed-loop control techniques, and it is based on the combination of three different parameters computed starting from the measured error.

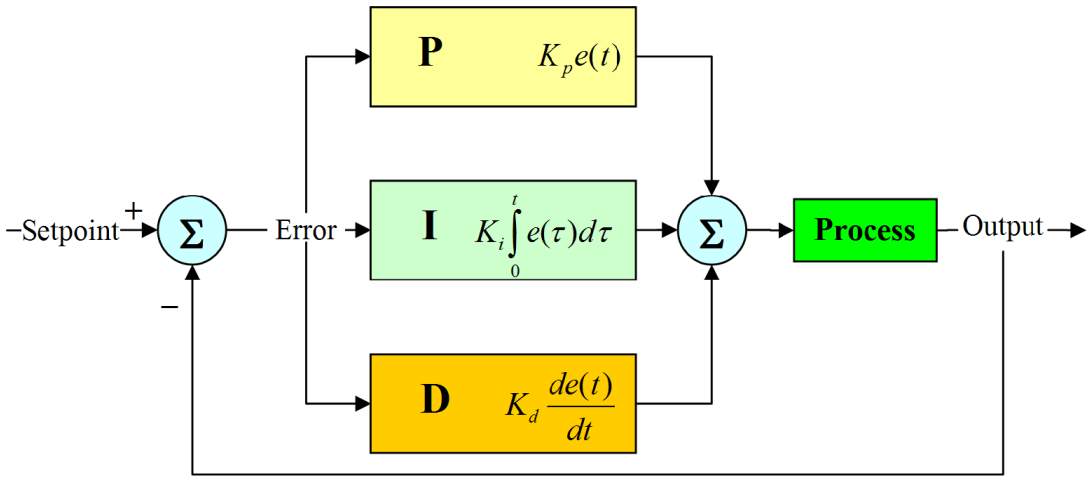

Figure 3.1- Example of PID controller scheme

The first parameter is the Proportional term, computed by multiplying the current error value with a constant K_p to obtain an output proportional to the error value:

$$P_{out} = K_p \cdot e(t)$$

The second parameter is the Integral term, which is based on the accumulation of the past error. It considers the previous values of the error and integrates them over time, then multiplies the result by the integral gain K_i to produce an output dependent both on the magnitude of the error and on its duration:

$$I_{out} = K_i \cdot \int_0^t e(T) dT$$

This term is used to eliminate the residual steady-state error and to accelerate the convergence to the target setpoint. However, since this term depends on errors accumulated in the past, it can cause overshooting over the target setpoint.

The third parameter is the Derivative term, which estimates future errors based on the current rate of change. It is computed by multiplying the time derivative of the error by the derivative gain K_d:

$$D_{out} = K_d \cdot \frac{de(t)}{dt}$$

This term is used to predict the system's behaviour and improve its stability.

The system output will then be the sum of the three terms and can be expressed with its Laplacian transform as:

$$U(s) = \left(K_p + \frac{K_i}{s} + K_d s\right) e(s)$$

PID controllers must be properly tuned to ensure the required properties of the system, such as stability, precision, and robustness. This is done by adjusting the values of the three parameters $K_p,\ K_i,\ K_d$. These parameters have been tuned manually, observing the effects on the system's behaviour.

There are different approaches to estimate an optimal set of values for a specific system, some of which require the presence of a model describing the system. In other cases, such as this one, in which a model of the system is not available, the three parameters can be tuned manually by observing the effect of the variation of their values over the system's behaviour.

3.2 Custom Control Strategy

As mentioned before in the thesis, the measurement of the mechanical properties using the FOT consists of a session of data acquisition while a sinusoidal pressure waveform is applied at the subject's airways opening superimposed to normal breathing. The measurement is repeated one time for each sinusoid frequency from 7 to 1 Hz.

With the aim of obtaining an automatic measurement process that untrained operators can use, three key points in the control strategy were identified:

- The device should reach the predefined pressure offset in a comfortable time for the subject, accounting for spontaneous respiration (Offset Control).
- The device should be able to deliver sinusoidal waves at the correct frequency and amplitude during the normal breathing of the subject (Sinusoidal Amplitude Control).
- During the FOT measurements, a small but constant, positive pressure should be maintained at the airways' openings in order to keep the average pressure

at the same value during the transitions between inspiratory and expiratory phases (Intra-breath Baseline Compensation).

Moreover, the waveform of the sinusoids with low frequencies is comparable to the horse's respiration one, suggesting that the same control algorithm wouldn't work for high frequencies and lower ones.

3.2.1 Offset Control

The main concern of the offset control is to ensure that the device is able to reach a target pressure offset autonomously, independently on the load, represented by the subject respiratory system.

A straightforward solution could be to map the PWM signal needed to generate a pressure at the airways opening of an average horse represented by an average load; in this way, an open-loop control would be easily used to reach the desired pressure offset. Unfortunately, since each animal has its own peculiarities in physiological structures, depending on the pathophysiological state of its respiratory system, it's not possible to assume an average load value sufficiently robust to be used as a reference.

Therefore, the offset control was based on a simple closed-loop algorithm that senses the pressure at the subject's airways opening, averages the collected values over a window, and compares the obtained average with the desired pressure offset. The parameters for such a controller were chosen to ensure the controller's high stability and a long rising time of the pressure to reach the target, necessary to ease the animal during the transition to the positive pressure.

Due to the necessity of a long rising time and a large window that averages the respiration waveform, this controller is not suitable to stabilize the pressure baseline during the following phases, as a faster control will be required.

3.2.2 Sinusoidal Amplitude Control

The sinusoidal shape of the pressure can be achieved by modulating the motor speed with a sinusoidal DC of the PWM signal. With the aim of obtaining different

sinusoid frequencies, a period of the sinusoidal function has been sampled at 1 Hz. The desired frequency N is obtained under sampling of N times the original sinusoid.

The best and probably most complex type of control is a closed loop control that compares the values of the sampled pressure signal with an ideal sinusoid to obtain a point-to-point control of the motor speed modulating the pressure at the airways opening. Unfortunately, this solution was proven to be highly unstable in this application, other than highly frequency-dependent; for this reason, a different controller was developed.

The amplitude of the pressure sinusoid is a crucial parameter that should be kept constant during the whole measurement. To do so, the strategy chosen is the implementation of a PID controller, which senses the pressure at the opening of the airway and corrects the PWM signal to reach the correct pressure amplitude. The PID compares the target sinusoid's amplitude with the one measured at the opening of the airway over a single period. The measured amplitude is computed by real-time search of the maximum and minimum of the pressure. Moreover, the pressure signal is first de-trended with a least-square method to eliminate the slow pressure variations due to the animal breathing activity.

It has been empirically acknowledged that this type of control works for frequencies above 3 Hz. In contrast, for lower frequencies, the computation of local maxima and minima of the signal is corrupted by the subject breathing act, which cannot be efficiently deleted with the de-trend algorithm. For this reason, the PID output value used for 4 Hz oscillation is kept and corrected according to a calibration coefficient to deliver lower frequency pressure sinusoid in an open-loop fashion.

3.2.3 Intra-breath Baseline Compensation

The last concern is to keep a constant positive pressure at the subject airways' opening to reduce the pressure variability during the inspiration and expiration phase. For this reason, one last PID controller was developed to rapidly contrast pressure changes at airways opening, which are typically present during breathing. The controller is based on a moving average measure over a sinusoidal period to be

compared, at each sampling instant, with the desired baseline value, which is the same as the initial pressure offset.

The response of the PID controller needs to be fast and stable, correcting rapid pressure changes due to changes between expiration and inspiration and vice versa.

A table reporting controllers' parameters is depicted below. All the PID values were adjusted by empirical tests using a simulator that resembles the mechanical properties of the horse's lungs.

Table 3 - PID controllers coefficients

PID Type	Kp	Ki	Kd
OFFSET	0	0.15	0
AMPLITUDE	0.25	0.75	0
BASELINE	1	0.01	0.5

3.3 Firmware

The firmware of the Esp32 was developed using the ESP-IDF framework and Eclipse IDE. The first is a set of tools necessary to correctly configure the microcontroller from laptop, other than containing the set of libraries that define the required APIs for a higher-level interpretation of peripheral control. The Eclipse IDE is one of the most known programming environments, which facilitates code developers with different features regarding interpretability, debugging, and code editing.

The microcontroller is a dual-core system on chip embedding a Wi-Fi and Bluetooth module. These features allow multitasking execution, meaning that the microcontroller can execute more than one task. The microcontroller can be programmed with the integration of an open-source Real-Time Operating System (FreeRTOS). This set of APIs allows the management of different tasks to be executed over one or the other core, timing, and context switching, other than microcontroller memory access since the two cores share the same memory.

More in detail, FreeRTOS operates by tasks execution. Each task is executed at a specific frequency; tasks are managed by the core only when they are *available*, ensuring the correct timing for that code section. The *scheduler* runs the task with the highest priority among the available ones. The operating system allows to write the firmware according to some fundamental rules:

- A task cannot run in a loop without any break, as the scheduler should have the time necessary to execute and manage tasks.
- The scheduler runs at 1000 Hz within a system interrupt. Thus, tasks can be temporized at a lower frequency. Temporization is obtained by the mean of delays expressed in milliseconds where the task cannot be executed.
- The highest priority task is always executed when available.
- Interrupts are always executed on top of tasks, meaning they have a higher execution priority.
- The operating system manages memory access, task execution hierarchy, availability, and choice of the core of execution.

The firmware has been developed taking into account the capability of the system and the device requirements, enhancing the attention for data transfer using wireless

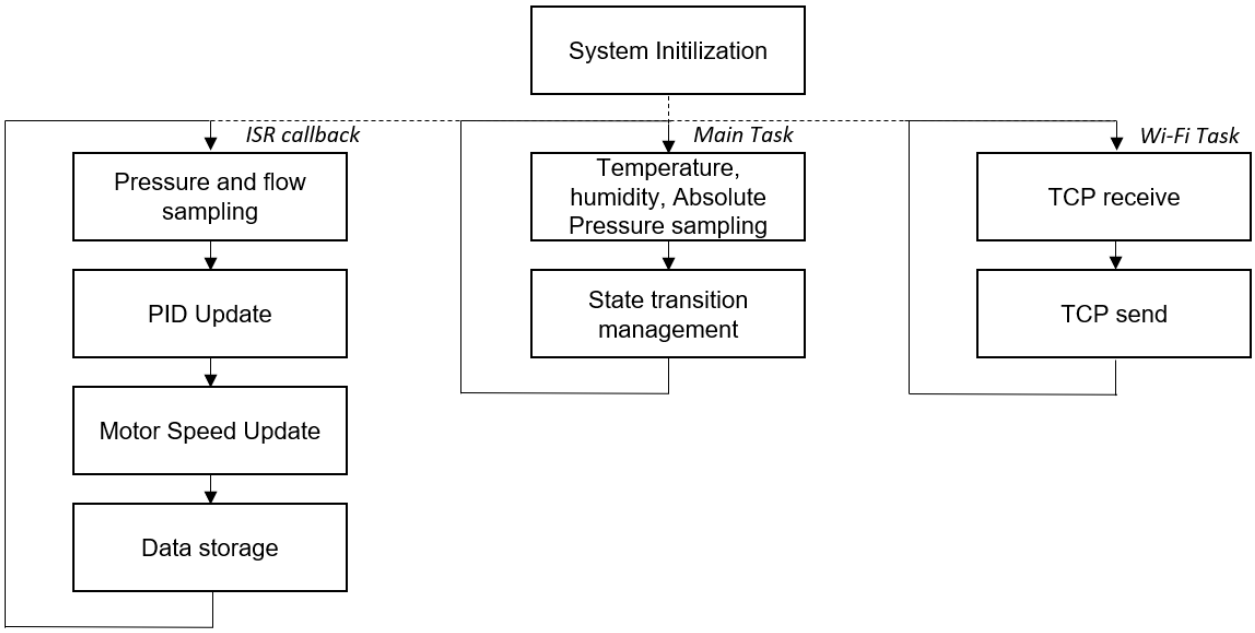

Figure 3.2 - ESP32 algorithm flowchart

technology and the correctness of the control algorithm. A scheme of the main tasks is reported in figure 3.2.

The firmware was developed according to a state machine paradigm. This means that depending on the value of a specific variable, defining the state of the system, the microcontroller will execute the corresponding portion of code. Particular events trigger conditions that are responsible for state transitions.

As reported by the previous figure, firmware is divided into three main sections:

- The Main task, executed on core n. 1, responsible for state management and monitoring unit readout.
- Communication task, executed on the core 0, responsible for Wi-Fi communication with the laptop.
- Interrupt Service Routine running at 500 Hz, responsible for pressure and flow sampling and motor control management.

3.3.1 Main Task

The Main task is executed with a frequency of 2 Hz. It is responsible for state management, meaning that conditions for state transitions are mostly contained in this code section. The states available are the following:

- *STOP*: during this state, the device keeps the motor off, waiting for instructions. The transition to the next state is triggered by a command received from the user interface.
- *STARTED:* this state enables the motor control (handled in the ISR) to perform the first FOT measurement and commences the wi-fi transmission of pressure and flow data.
- *TRANSITION*: this state handles the transitions between the different frequencies of FOT measurements. When the measure of a single FOT frequency ends, the motor duty cycle is gradually brought to the value associated with the desired pressure offset without any oscillation.
- *STOPPING*: The device enters this state when the whole FOT measure ends or when the user decides to stop the current measure. It ensures a smooth

transition toward the null speed of the motor from the current one, bringing back the state to *STOP*.

The main task is also responsible for environmental data acquisition from temperature, humidity, and absolute pressure sensors, which are collected once every five seconds.

3.3.2 Motor Control

The control of motor behaviour is a crucial task of the firmware, as it defines the quality of the delivery of sinusoidal pressure waves to the subject. The pressure at the airways opening depends on the motor speed, which is controlled by the Pulse Width Modulated (PWM) signal provided to the Electronic Speed Controller. The sinusoidal pressure oscillations are obtained by modulating the duty cycle with a sinusoidal function of time. With the employed ESC, the velocity varies proportionally from 0 to its maximum values, with DC values between 50 and 100 %.

An interrupt triggered by the timer counter register overflow at 500 Hz allows executing an ISR (Interrupt Service Routine).

The motor control is entirely implemented in the ISR when the system's state is set to *STARTED*.

When an FOT measure starts, the motor is gradually accelerated to reach the desired pressure. During this phase, the control scheme is the one previously described as *Offset Control*. At each instant, a new pressure sample is acquired and stored in an array. The last *N* samples are used to compute the average value, which is fed to the controller. When the error between the average value of pressure and the desired pressure offset is sufficiently low for 10 consecutive times, the PID output is saved, the control scheme changes to *Sinusoidal Amplitude Control*, and FOT oscillations start.

When the *Sinusoidal Amplitude Control* is active, the spontaneous breathing of the animal might interfere with the computation of the oscillations' amplitude. Spontaneous breathing occurs at lower frequencies compared to the FOT ones. However, they introduce a trend over which the oscillations are superimposed. This

effect can be subtracted from the signal by estimating a linear trend that employs a least square method for each sinusoidal period to estimate the breathing trend's slope. The maximum and minimum of each sinusoid are then computed. The sinusoid amplitude is calculated as the difference between the first and the latter, and then it is fed to the PID controller.

When the pressure amplitude is stable or ten seconds elapsed, the control strategy changes to *Intra-breath Baseline Compensation.* The amplitude control is still active during this phase, but it operates in synergy with a controller that maintains the average pressure stable during the intra-breath phases (inspiration, expiration). This controller calculates the moving average of the pressure signal over a sinusoidal period and regulates the mean value of the DC.

After 20 seconds, the FOT measurement at the current stimulation frequency is concluded. The STATE variable is changed to *TRANSITION* where the motor speed is brought to the steady value computed with the *Offset Control* controller. When the value is reached, the FOT frequency for the next measure is updated, and the control strategy restarts from the *Sinusoidal Amplitude Control*.

As previously said, lower FOT oscillation frequencies are comparable with horse ventilatory acts. For this reason, a feedback control doesn’t work appropriately. The implemented solution consists of an *OPEN LOOP* controller for frequencies of 3, 2, and 1 Hz that uses the previously saved respiratory parameters to compute the desired pressure signal.

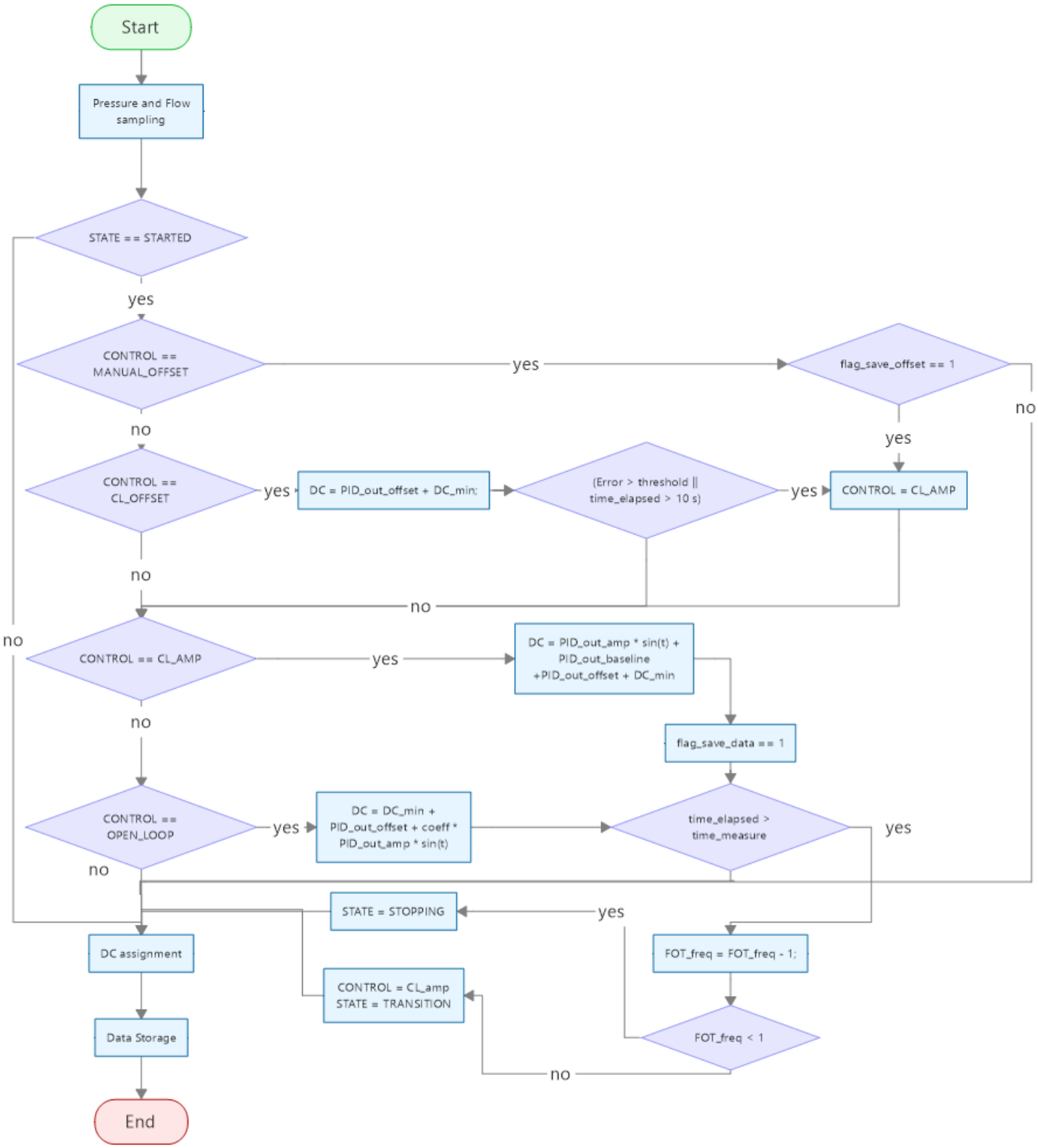

Figure 3.3 - Motor control algorithm flowchart

3.3.3 Communication Management

Communication is initiated in the main, during the system initialization phase, executed once the system is turned on. As previously mentioned, the communication exploits the ESP Wi-Fi module to establish a wireless connection with the host. During the initialization phase, the ESP32 initiates its own LAN; the user is required to join the network with his device. The microcontroller and laptop will then start TCP/IP connection, establishing a socket, a channel associated with a pair of IP addresses, and PORTS, describing the connection between the two devices.

Once the device finishes the initialization phase, the communication is managed in the *wifi_task* executed every 100 milliseconds. The task controls if data are present on the socket, meaning that the laptop has sent commands. If the commands are available, then a switch case executes a code portion according to the content of the command. Examples of commands are setting of measurement parameters, measurement start, end, and transition toward another frequency.

If the system's state is either *STARTED*, *TRANSITION*, or *STOPPING* (those for which the motor is on), then data are sent to the laptop. Data are organized according to a custom communication protocol:

1. 2 Bytes are used as header, defining data content type.
2. 76 Bytes are used to store data content.

Message integrity and packets order are ensured by TCP protocol.

CHAPTER 4 SOFTWARE AND USER INTERFACE

Several tools and programming languages designed to create Graphical User Interfaces (GUI) are available. However, starting from scratch usually requires a lot of time resources. Therefore, specialized software tools, such as frameworks, have been created to ease the programmer's burden [64].

Information Technology defines a framework as a support structure in which other software applications can be organized and developed. Frameworks may include support programs, code libraries, a scripting language, standard services, interfaces, or other software packages/utilities to help create and glue together the different components of a software application [65].

Typically, a desktop application is created for a specific operating system (OS) using each operating system's specific native application framework [66, 67]. In this thesis project, a graphic user interface was developed as a cross-platform desktop application, which can run on devices hosting an operating system like Windows, MacOS or Linux.

Building an application that runs on multiple operating systems is always challenging, as developing one for each platform needs a lot of effort and technical knowledge in each platform [66]. The desktop application was implemented using the *Electron framework*, which allows the development of cross-platform applications quickly.

4.1 Electron Framework

Electron is an open-source framework developed by GitHub for creating native applications with web technologies such as JavaScript, HTML, and CSS. These applications can be packaged to run directly on macOS, Windows, or Linux [5]. Chromium, created by Google, is the open-source library used by Google's browser Chrome.

Node.js (or Node) is a tool for writing JavaScript programs on servers, accessing file-systems, and networks. An API (Application Program Interface) describes the set of functions available to use a library. Electron works by combining the Chromium content framework and Node.js in a single framework with a set of custom APIs for native operating system functions like open file dialogues, notifications, icons, and more [67, 5].

The development of desktop applications usually requires different development tools for other operating systems, resulting in multiple versions of source code, each of which is associated with an individual operating system. Whereas the desktop applications built with Electron would ensure more maintainability by using one set of source code, also reducing the cost and time of development [68].

4.2 Application Architecture

Electron consists of three main pillars:

- Chromium for displaying web content
- Node.js for working with the local filesystem and the operating system
- Custom APIs for working with often-needed OS native functions

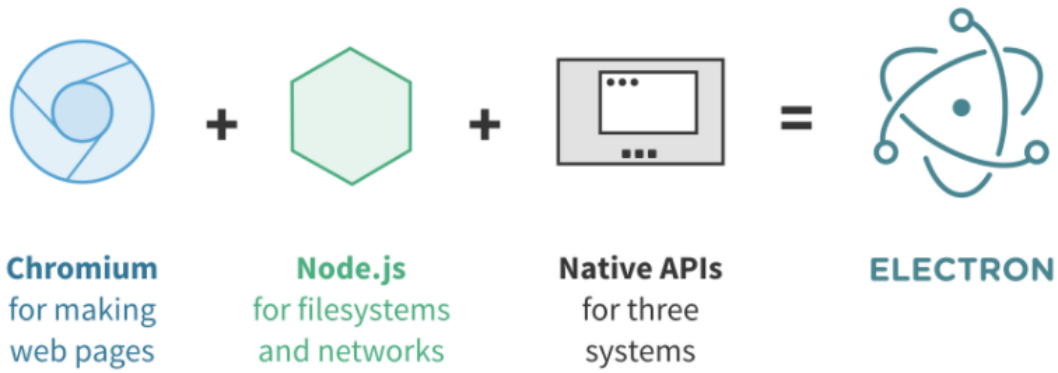

Figure 4.1 - Electron Framework Architecture.

Developing an application with Electron is like building a Node.js app with a web interface or building web pages with seamless Node.js integration [5]. Chromium handles the front-end, while Node.js manages the back-end. Traditional web applications are more limited in terms of native operating system API access. Web applications are distributed over servers while the client's browsers render the web

pages in separate processes that do not have access to the native OS resources and APIs.

For a desktop application, it is essential to access native operating system APIs, but in Chrome, each tab is rendered on its own process. The chromium sandbox model encapsulates processes inside a very restrictive environment. This architecture restricts the processes from accessing the native APIs. To provide native access, the Electron team modified chromium as well as Node.js built-in and third-party modules. In Electron, the chromium sandbox protection can be disabled so that any application running inside Electron is given unfiltered access to the operating system. Electron provides unlimited and direct access to Node.js APIs as well as Node Package Manager (NPM) modules from web pages inside the application. Unlike standard web pages, the entire Node.js runtime is available inside the application, enabling one to use custom node modules and third-party modules without any additional effort. Also, compiled Node.js native modules, usually written in C or C++, can be used [66].

Two types of processes are managed in an Electron application: Main and Renderer.

- The Main process, commonly a file named "main.js", is the entry point to every Electron app. It controls the application's life, from the opening to the closing. It also calls the native elements (resource-intensive interactions, doing it in the main will leave the renderer uninterrupted) and creates each new renderer process in the application. The Main process creates web pages by creating *BrowserWindow* instances. Each *BrowserWindow* instance runs the web page in its Renderer process. The Main process also manages all the created web pages and their corresponding Renderer processes.
- The Renderer process manages only the corresponding web page. Unlike the Main process, there can be multiple renderers, and each one is independent, so that a crash in one Renderer process does not affect the others. Also, a renderer process can be hidden and used to execute code in the background. Calling native GUI-related APIs from the Renderer process is restricted due to security concerns and potential resource leakage.

The two types of processes communicate via Inter-Process Communication (IPC) to perform GUI operations on a web page. The communication between processes is possible via IPC modules: *ipcMain* and *ipcRenderer*, utilized in the Main and Renderer process respectively. Electron APIs are assigned based on the process type, meaning that some modules can be used from either the main or renderer process, and some from both. Electron's API documentation indicates which module can be used by each process. Electron also exposes full access to Node.js API and its modules both in the Main and Renderer processes [5].

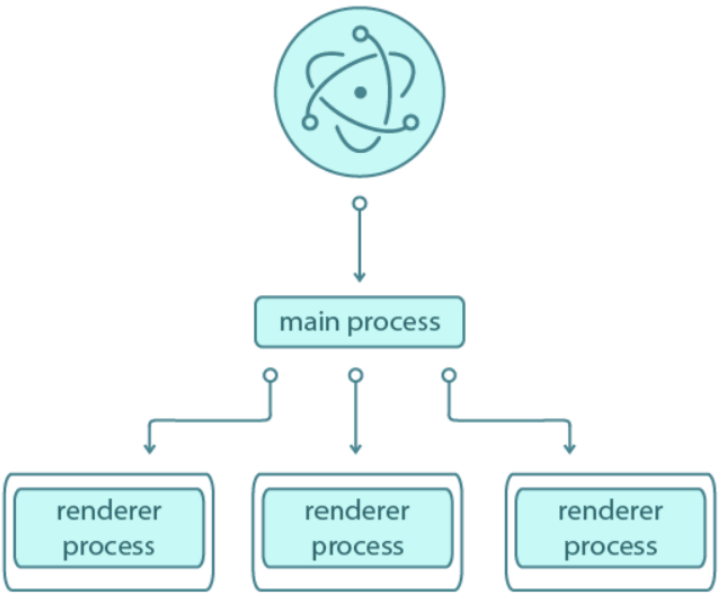

Figure 4.2 - Processes hierarchy.

4.3 High-Level Control

Software running on the user laptop is crucial for user-device interaction. For this reason the way in which the device will operate depends on the choice of the user when interacting with the graphic interface. For this reason, the software is responsible for the high-level control of the device.

The whole system is designed to be used in a practical way, allowing the user to interact with the system through an effective user interface on its own machine. A user can decide to start the system as a *Developer* or *Physician* according to different modalities. Though both modalities share the same low-level control algorithm, they differ in high-level control. A scheme reporting modalities working method is presented in figure 4.3.

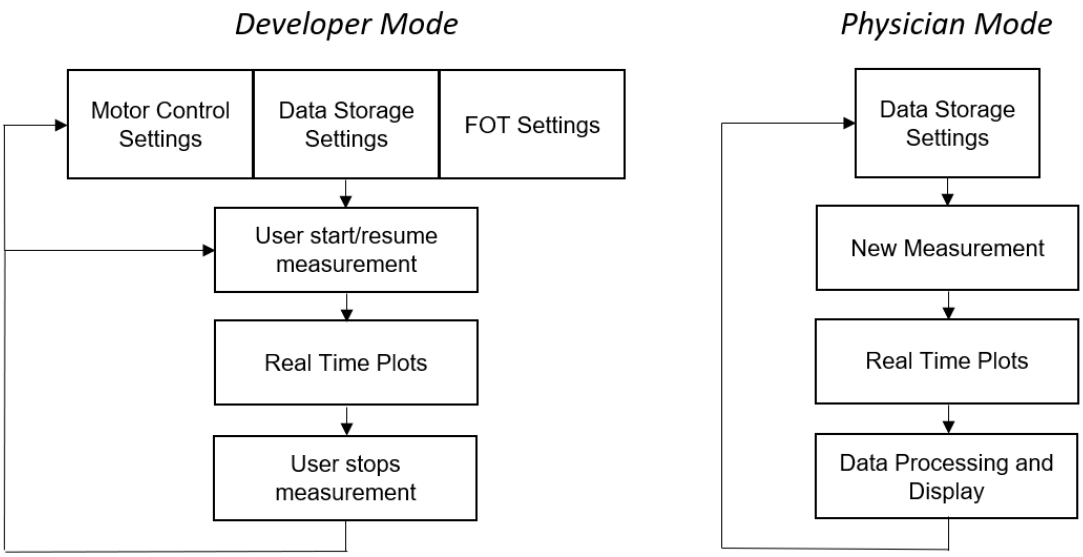

Figure 4.3 - High level control scheme. Left: Developer mode. Right: Physician mode.

The *Developer Mode* allows the user to fully control the device functioning, decide control parameters, FOT settings, visualize real-time data, and choose when to start or stop the measurement and data recording. This modality is necessary for device development, update, or bug fixes and guarantees a total freedom in terms of performance recording and testing. The user must know how the device is supposed to perform in different conditions to explore and understand the device's behavior under different test conditions.

The *Physician Mode* was thought to be based on a solid, simple interface that implements a complete measurement cycle automatically. The steps of the measurement are controlled by the firmware, reducing the user role to start the measurement and decide where to store collected data. In this way, no knowledge of the control strategy and FOT settings values are required to the user, increasing the simplicity of the measurement.

4.4 Software Organization

The main.js file is the entry point of the application. It runs in background, controls the application's life, and creates all the other renderer processes, which are `menu.html, plots.html, settings.html, and dataProcessing.html,` together with their corresponding JavaScript scripts `menu.js, plots.js, settings.js,` and `dataProcessing.js`. The `styles.css` is the CSS file that defines all the adopted styling techniques.

Each HTML file defines the components of the corresponding renderer using HTML elements. The <head> element requires the CSS file, the <body> element encapsulates all the components visualized in the window. It can contain , <table>, <section>, <input>, <button> elements, depending on what has to be displayed. For example, if a button has to be on the screen, the element in the HTML file will be of type <button>. Each of these elements is identified by the *id attribute*, by which they can be recognized in the CSS and in the respective JavaScript files and used there as variables. Elements with common styling features are also identified by the same <class>. Elements belonging to the same <class> are equally coded in the CSS file (e.g., buttons). The <body> also contains the <script> element, always requiring the JavaScript script, in which the dynamic behavior and styling of the window are handled.

As mentioned above, the Main process is the application's entry point, and it is the only process that can access native APIs. For this reason, the Main process is responsible for application organization, other than renderers management, while each renderer process is, in some measure, responsible for a specific task.

4.4.1 Main Process

The Main process is the most critical process in the application. When the application is launched, the initializations necessary for renderer processes to be created and displayed are performed, together with esp32 communication initialization. After the application starts, it is responsible for wireless communication management, data storage, and renderer processes management with an inter-process communication module. A scheme reporting the most important tasks is depicted in figure .

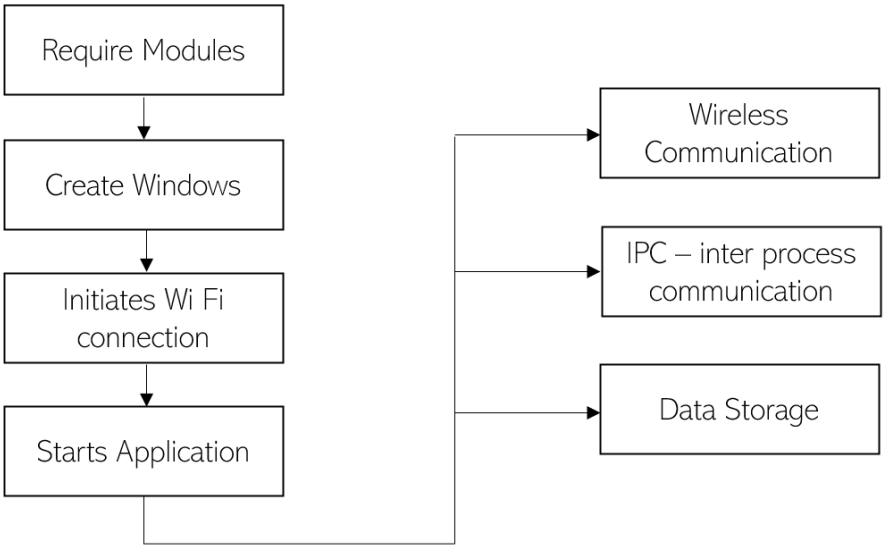

Figure 4.4 - Main process logic chart.

Windows Creation

The required renderer processes and related browser windows are then created. Each window is loaded to its local HTML file using the path and URL modules. The menu window is displayed full screen, while other windows are displayed over it, with a 100% width and a 90% heigh, showing the upper navigation bar of the menu window.

Once Electron has finished initializing the application, it emits the "ready" event.app object and windows are created. Only the "MENU" renderer window is shown, as the first choice is whether to access the application as a user or developer. Other windows will be shown only when requested.

Similarly, when the electron app emits the *"windows-all-closed"* event, the application is quit, i.e., closing all windows will terminate the application.

Communication with ESP32

The Node net.js library is used to perform the communication with esp32. The socket object is constructed by specifying the server IP address and port. When the socket is created, the connection between the two devices is established, and the 'connected' event is emitted.

In order to receive data packets, the 'readable' event is activated each time a data buffer is available on the socket. In order to read the correct number of bytes, the data buffer is read and thus deleted from the data line only when its length is equal to 77, which is the chosen length for the custom protocol used by esp32. The Main is responsible for different actions in response to different incoming messages.

Function *.send* is used to buffer data on the socket, so the microcontroller then receives that. In this case, packets are composed of an 8 bytes string. One byte indicates the type of command, and the remaining ones indicate a numerical value expressed as char variables.

File Saving

Folders for file saving are created through the *fs* module if they do not already exist. A new folder is created when a new measurement is started. The folder name will default be "*FOT_session_mm/dd/yyyy*" where *mm* corresponds to months, *dd* to days, and *yyyy* to years. The user can also decide on another name for the folder, for example, specifying the subject ID or the type of measurement.

Inter-Process Communication (IPC)

All the listener functions and channels needed for the Inter-Process Communication are initialized in the Main Process. Listeners' functions are executed when an event is fired on the corresponding channel. These functions are fundamentals for the correct application execution; examples of the essential IPC handlers are reported:

- Data received from esp32 are transmitted to the *PLOT* window via IPC communication; the IPC handler updates the plot content every time new data are available.
- Parameters inserted by the user in the *SETTINGS* window are sent via IPC to the Main process in order to transmit them to the microcontroller.
- Pressure and Flow data received from the microcontroller by the Main process are sent to the *DATA PROCESSING* window via IPC communication.
- Information regarding the STOP and START button is communicated to the main process via IPC to be sent to the microcontroller.

4.4.2 **Renderer – menu.html**

This renderer process is mainly responsible for navigation through different windows or measurement phases. It is the first window to be displayed, in order to guide the user toward one of the two possible modalities: *developer* or *physician* mode. The choice between these two modalities will determine the content of the following window to be displayed.

Figure 4.5 - Application Strating Window.

The *developer* access will display the *settings.html* file, while the *menu.html* will change its appearance with a navigation toolbar represented by buttons. During a developer session, the user can change parameters in settings.html and visualize pressure and flow signals in *plots.html*. Changes between the two windows are allowed by the menu.html window.

The *physician* access will instead change the appearance of menu.html only, displaying a window in which the user can choose the name of the folder which will contain the stored data and access the settings.html window using a button. For the measure to start, another button has to be pressed, which will again change the menu.html appearance to a screen showing information on the ongoing measure.

Figure 4.6 - "Start a new session" window.

The window will provide information on the current measurement stage, informing the user of the current oscillating frequency. A button allows showing the *plots.html* window so that the user can also decide to see the real-time pressure and flow signals. When the measure stops, the *dataProcessing.html* window is displayed.

4.4.3 **Renderer – settings.html**

In order to allow the modification of parameters before the measurement starts, this renderer process is displayed on request. It shows a window containing settings that the user can change. According to the chosen modality, the window will display a set of parameters:

1) When the modality is the *physician mode*, the available parameters are:

a) FOT parameters such as pressure offset at airways opening, sinusoid amplitude expressed in cmH_2O, and measurement duration.

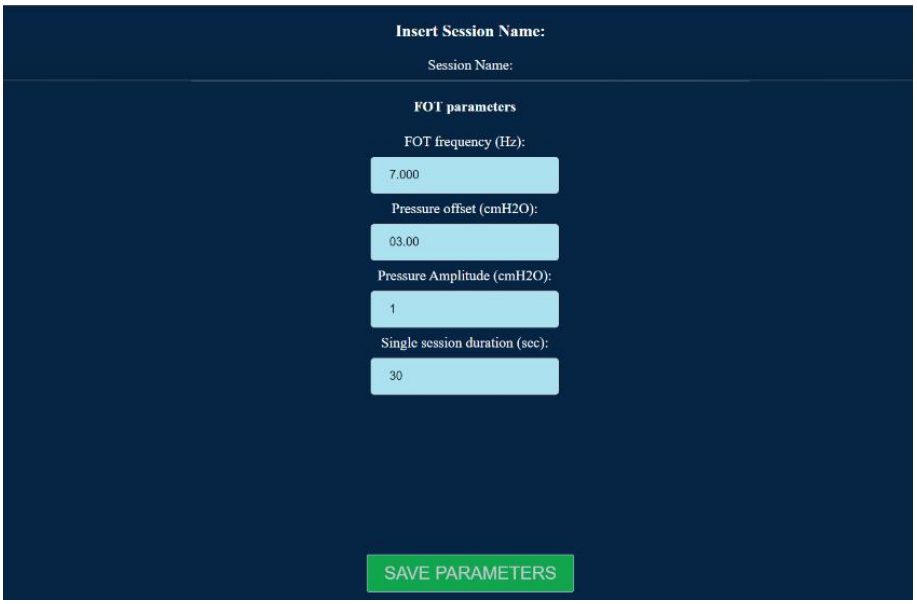

Figure 4.7 - Settings Window – Physichian Mode.

2) When the modality is *developer mode*:
   a) FOT parameters as pressure offset at airways opening, sinusoid amplitude and frequency, measurement duration.
   b) PID controllers' parameters such as PID constants (proportional, integral, and derivative) and window length of measured signal for OFFSET control.
   c) Complete control of motor settings, meaning that the user can set motor speed deciding the duty cycle of PWM signal and type of controller to be activated.

Figure 4.8 - Settings Window – Developer Mode.

4.4.4 **Renderer – plots.html**

This rendering process is responsible for data visualization. It can be shown to the user while the measurement is performed and consists of four main screen divisions. Two smaller divisions are displayed on the right and left sides as columns host data values such as average pressure and flow values, environmental parameters, measurement duration, battery level, and current oscillation frequency. The other two divisions are used to display pressure and flow signals during the measurement.

Graphs are represented using *plotly.js* module, allowing data to be represented as time series while optimizing the computational load required for plot refresh. Data

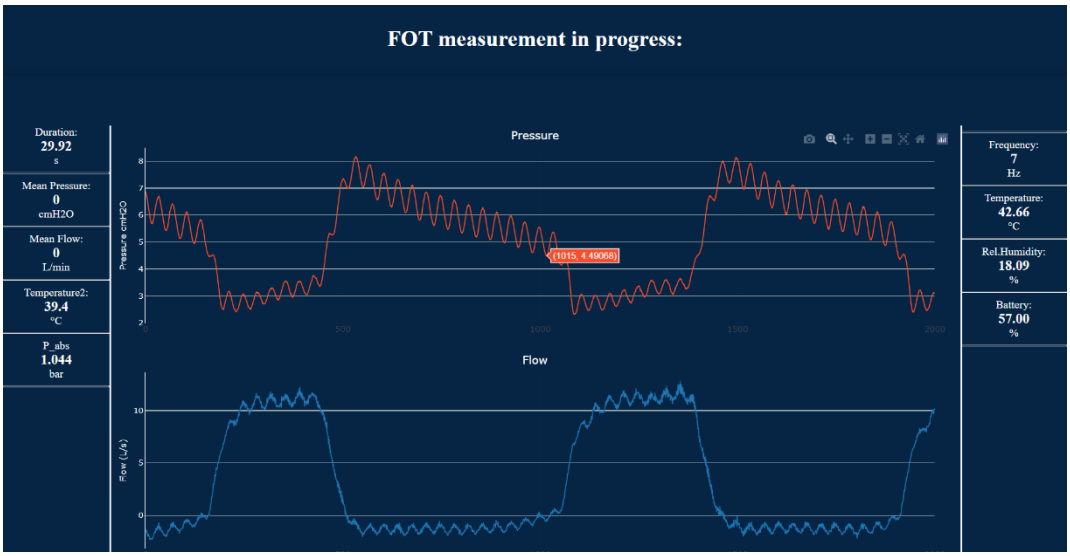

Figure 4.9 - Plots Window: example of pressure and flow tracks during measurement.

are added in packets of 50 samples with a refresh rate of 20 Hz. 20 Hz is the refresh rate of the human eye, meaning that images refreshing at a higher rate are perceived as fluid. This choice results from a trade-off between graph fluidity and low computational cost, proportional to the refresh rate.

4.4.5 **Renderer – dataProcessing.html**

The most important task is the data processing; after the measurement has been completed, a renderer process called *dataProcessing.js* receives pressure and flow data relative to each frequency FOT session.

In order to compute the impedances from pressure and flow data, which have been stored during the measurement, an algorithm for data processing and impedance computation has been developed. The algorithm is executed at the end of the measure.

Impedance calculation algorithm

The algorithm exploits a least square method to estimate the sinusoidal coefficient comparing a window with the length of a stimulus period comparing it to an ideal sinusoid represented by the following equation:

$$S(t) = r(t) + a_0 + a_i \cos(2\pi f t) - b_i sin(2\pi f t) = r(t) + a_0 + \Re[(a + jb)e^{j2\pi f t}]$$

The weights a_i and b_i play a key role, they represent the rate of coherency between the ideal signal and the signal analyzed. Furthermore, $r(t)$ indicates the noise superimposed and a_0 the stimulus offset. Moreover, it is possible to rewrite the equation in matrix form, sampling the window and hence working in discrete time.

$$S = AX + R$$

In the equation, the desired signal is explained by the S value, while A is called *system* matrix, X matrix represents the parameter to be estimated, and R is the noise. To solve the least square problem, the equation has to be inverted, explicating the X

$$X = B * S$$

$$B = (A^T A)^{-1} A^T$$

Where B is the pseudo-inverse matrix that does not change when varying the window. In addition, B depends only on the stimulus frequency. Hence, if the sinusoidal frequency does not change, the matrix B can be computed only at the first iteration. Instead, the X vector is computed either for the pressure and flow, taking into account a window with dimension equal to an entire period of the sinusoid at the current frequency.

The impedance can be computed as the ratio between the pressure and the flow:

$$Z_{rs} = \frac{P}{V} - \frac{a_{P,1}(l) + jb_{P,1}(l)}{a_{V,1}(l) + jb_{V,1}(l)}$$

This equation makes it possible to notice two parts, the real and the imaginary part of the impedance. They explain the resistance and the reactance, respectively.

$$R_{rs}(l) \ = \ \Re e(Z_{rs}(l))$$

$$X_{rs}(l) \ = \ \Im m(Z_{rs}(l))$$

The algorithm proceeds iteratively, shifting the window by one sample per time and calculating the new value of impedance, resistance and reactance until the interval is covered.

Data processing

In order to compute impedances, both pressure and flow signals are filtered with a digital bandpass 2nd order Butterworth filter with a cut-off frequency of $f_{FOT} \pm 0.5\ Hz$. Impedance computation is performed starting from filtered pressure and flow signals with the algorithm presented above for each frequency. Resistance is obtained considering the real part of the computed impedance, while reactance consists of the imaginary part.

Due to the subject spontaneous breathing, both resistance and reactance signals are subjected to abrupt changes in correspondence of end of inspiration and expiration. For this reason, each breathing phase has been divided into three equal time intervals, and impedance is computed as the average of the values corresponding to the selected intervals.

To compute the volume signal, the raw flow signal is filtered with a low-pass 4th order Butterworth filter with a cut-off frequency of 0.5 Hz to delete high-frequency components such as noise and FOT signal. Flow is integrated to obtain a volume trace, which is then corrected for drift with a least-square detrending algorithm. The obtained trace represents the tidal volume of the animal's breathing process. Computation of local maxima and minima of volume signal is necessary in order to localize in time end of inspiration and expiration, respectively.

With the information obtained with the procedure reported above, it is possible to estimate the resistance and reactance, reflecting the mechanical properties of the subject's respiratory system. A scheme reporting complete data processing steps is reported in figure 4.10.

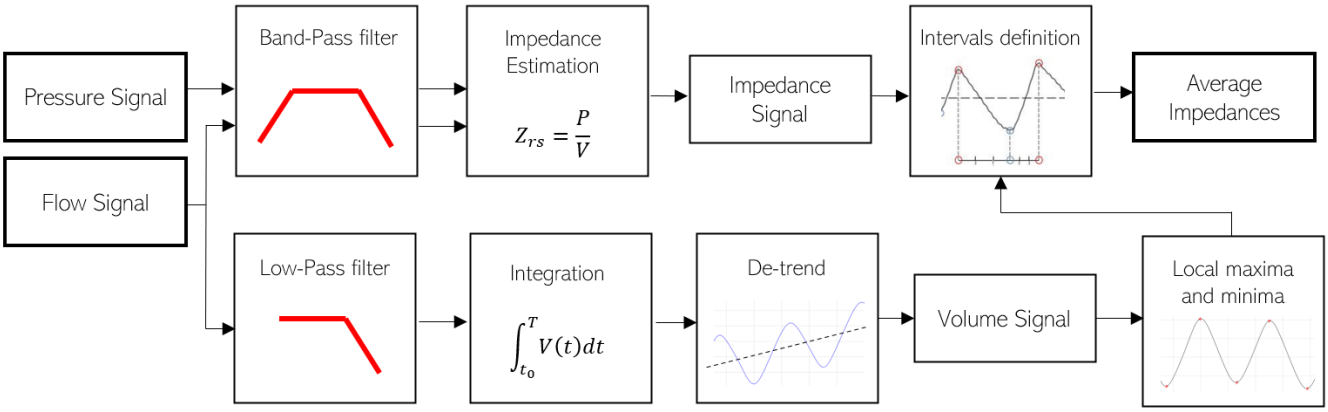

Figure 4.10 - Data Processing Scheme.

Results Visualization

When impedances have been computed as the averages of the instantaneous values during the second interval in inspiration and expiration, data are reported on a scatterplot, using one of the functionalities of *plotly js* module. The window represents two scatterplots, one for resistance and the other one for reactance. In both scatterplots, two traces are reported, one for inspiration and the other one for expiration.

Data Repository and Visualization

The *Developer mode* provides additional functionality to the application, which is unavailable in *Physician mode*. A developer should be able to quickly look at data

that have been recorded during past sessions, as data collected during different trials or laboratory tests can be precious to improve the device's performance.

For this reason, the DATA PROCESSING window supports the possibility to allow the user to browse the computer repository using the *file system* module. The user selects the file of interest, which is then opened by the program with the possibility to display recorded signals. Users can also zoom or change the trace to be plotted with a sliding, multiple-choice bar.

CHAPTER 5 VALIDATION

Device validation is necessary to evaluate the device's performance in different conditions objectively. The device presented in the previous chapters has been validated using in-vitro setups that resemble the horses' respiratory system. Then a few in-vivo measurements were performed on well-characterized horses at the veterinary hospital of *Università di Milano* (Lodi).

5.1 In-Vitro Validation

The device was tested at *Techres Lab* at *Politecnico di Milano*, evaluating whether it satisfies the following requirements:

1. Sinusoidal pressure wave generation at the animal airways opening.
2. Quantitative evaluation of the flowmeter characteristics.
3. Assessment of the mechanical properties (impedances) of a test lung through the forced oscillation technique.

5.1.1 **Sine Generation**

The first requirement that was evaluated was the pressure sine-wave generation at different frequencies. In order to obtain a sinusoidal pressure wave, the duty cycle of the motor was modulated to obtain a sinusoidal velocity. However, the non-linearities of the compressor could modify the pressure and flow sinusoidal shape. To assess the quality of the sinusoidal shape, it is possible to compare the shape of an ideal sinusoid with the measured data. The quality assessment is based on the measurement of Pressure and Flow waveform by the mean of the Pressure Shape Index (PSI) and Flow Shape Index (FSI) [49]. Shape Index is defined for each point of the recording, considering a window of N samples covering an entire period of the sinusoid, as:

$$SI = \frac{\sum_i^N |(a_0 \cos(x_i) + b_0 \sin(x_i)) - recorded\ signal_i|}{\sum_i^N |recorded\ signal_i|}$$

The measurements were performed using the device connected to a test lung with the following mechanical properties:

- Resistance: 2.57 cmH2O·s/L;
- Compliance of 0.0385 L/cmH2O;
- Inertance value equal to 0.0274 cmH2O·s²/L.

The experimental setup is described in detail in section 4.1.3.

Tests were repeated for FOT frequencies from 1 to 7 Hz with a peak-to-peak amplitude of 0.75 cmH_2O. An example of Pressure, Flow and Duty Cycle is reported in figure 5.1.

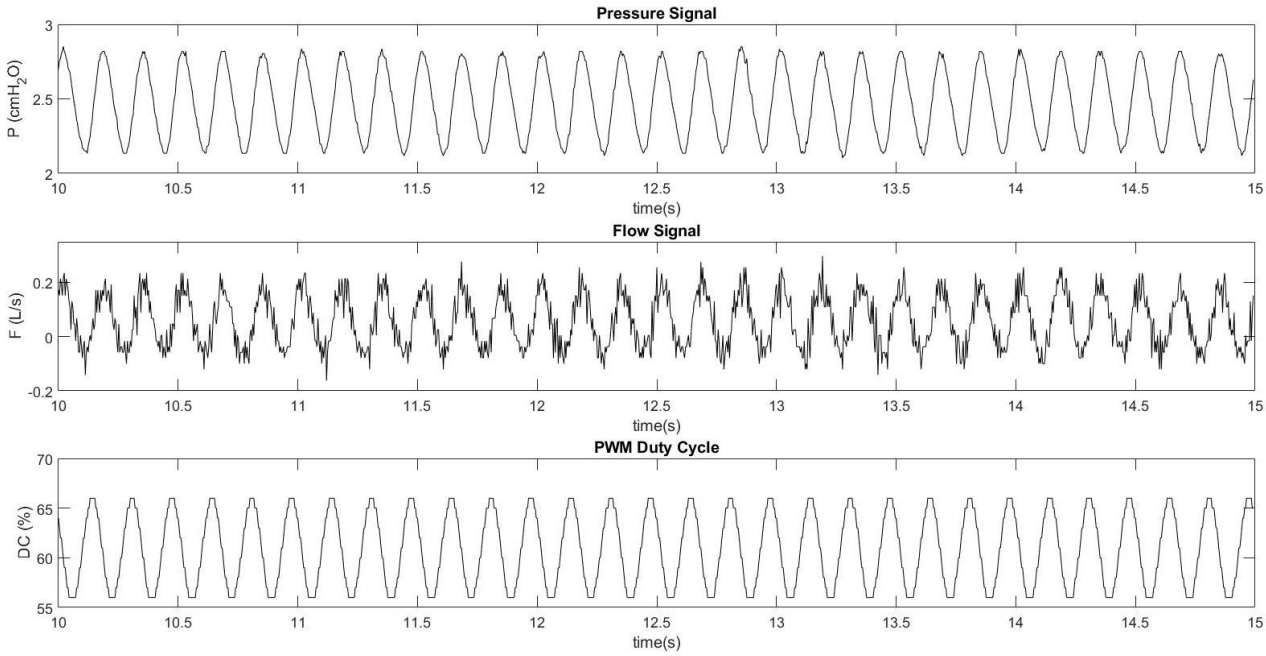

Figure 5.1 - Sinusoidal waveforms. From top to bottom: pressure, flow and PWM duty cycle.

For every measurement the Fourier power spectrum, the PSI, and the FSI were computed. The Fourier power spectrum was calculated for each frequency, from 0 to 125 Hz, with the sampling frequency of 250 Hz. The plots are reported in figure 5.2, enhancing the peaks at each FOT frequency.

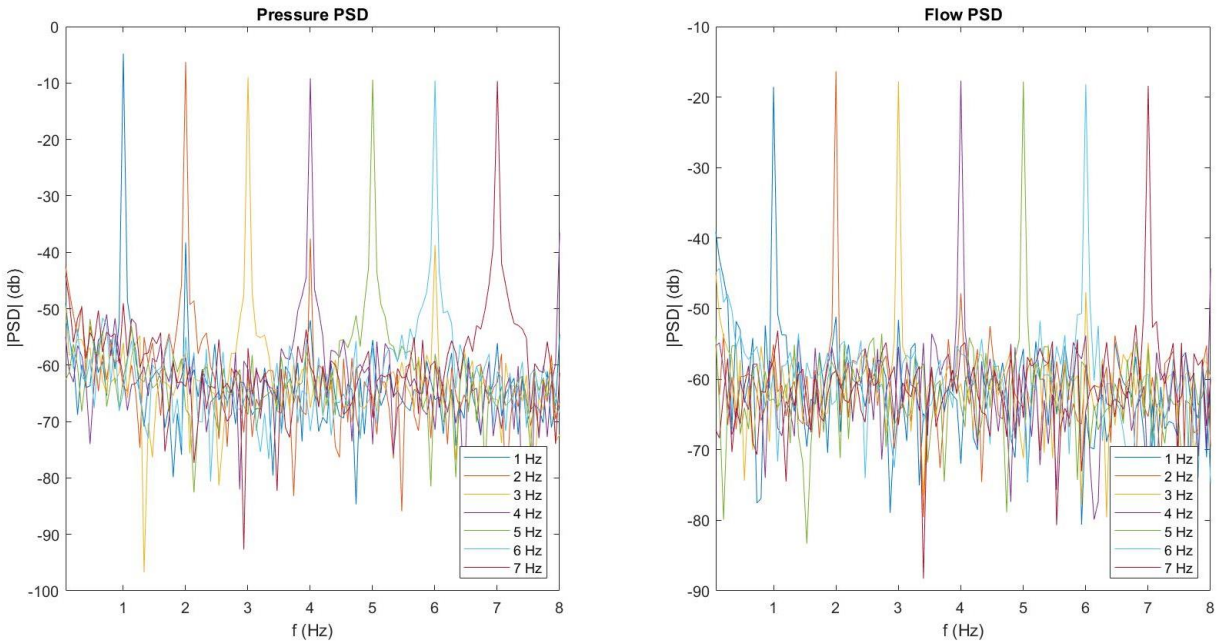

Figure 5.2 - Pressure (left) and flow (right) periodgram for different sinusoid frequency.

The PSI and FSI are reported in table 4. The more the value of PSI is closer to 0, the more the oscillation acquired is close to a perfect sine. The guidelines suggest that an accurate value of PSI is below 0.1 [22].

Table 4 – PSI for FOT frequency range

	1 Hz	2 Hz	3 Hz	4 Hz	5Hz	6Hz	7Hz
PSI	0.0748	0.0532	0.0520	0.0519	0.0575	0.0688	0.1076

As noticeable in Table 4, all the measurements showed PSI and FSI below or around 0.1. Hence the sinusoids are created correctly, and they can be used for impedance estimation by means of FOT.

5.1.2 **Symmetry and Linearity of Pneumotachograph**

The linearity of the pneumotachograph ensures that pressure drop across the resistance and air flow passing through it are related by a linear relationship. This requirement is crucial when it comes to PNT calibration. To assess the linearity of the pneumotachograph, pressure and flow have been measured with no loads (only

PNT resistance); different motor speeds have been used to obtain the range of flows that are most often encountered in this project.

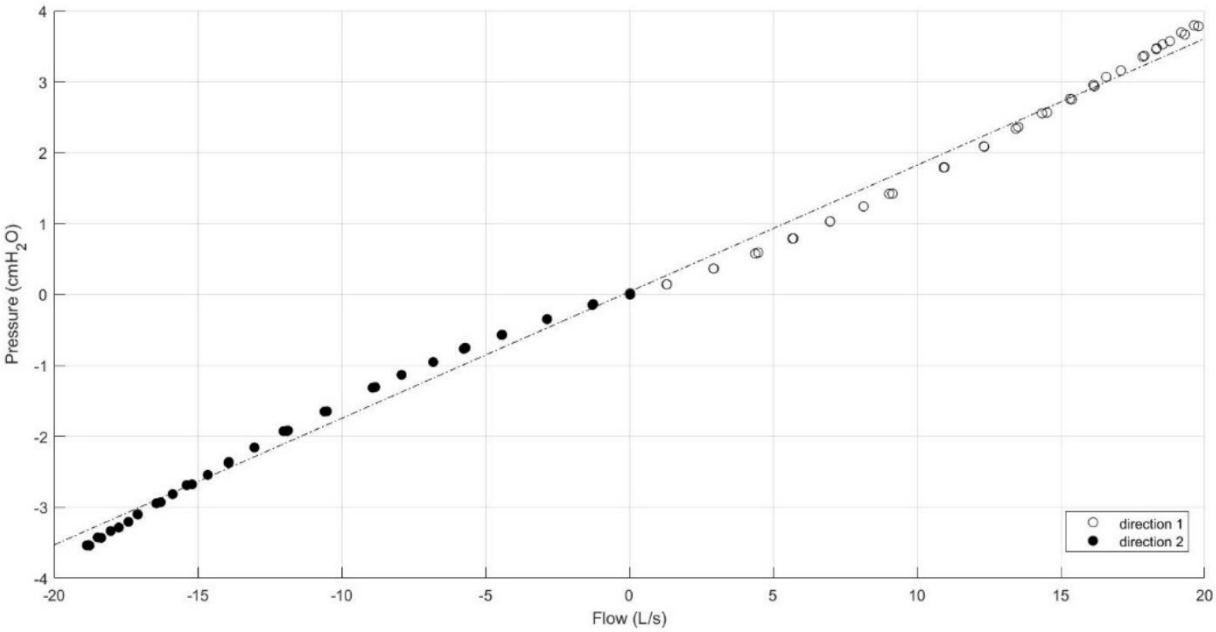

Figure 5.3 - Pneumotachograph Linearity. Data in white have been collected in flow's direction 1; Data in black have been collected in the opposite direction.

The mean resistance of the pneumotachograph was computed by averaging the ratio between pressure and flow tracks, resulting from being 0.178 cmH2O·s/L, which is an acceptable value in order to not add an excessive resistance to the subject. In this way, the horse can breathe spontaneously, and it is not required an extra effort that can be particularly problematic in asthmatic subjects. The estimated regression line approximates data distribution with an R-square value of 0.994.

The symmetry of the pneumotachograph is another crucial requirement for FOT measurements as it means that the sampled value is consistent for both directions of air flow. In order to evaluate the symmetry, a test was performed where the PNT and motor were left without a load so that when the motor speed increases, the air flow is restricted by the PNT resistance only. Pressure and flow measurements were collected for different motor speeds at constant steps without oscillations in both directions. The equations of the regression lines of the flow measurements in both directions were compared as reported in figure 5.4.

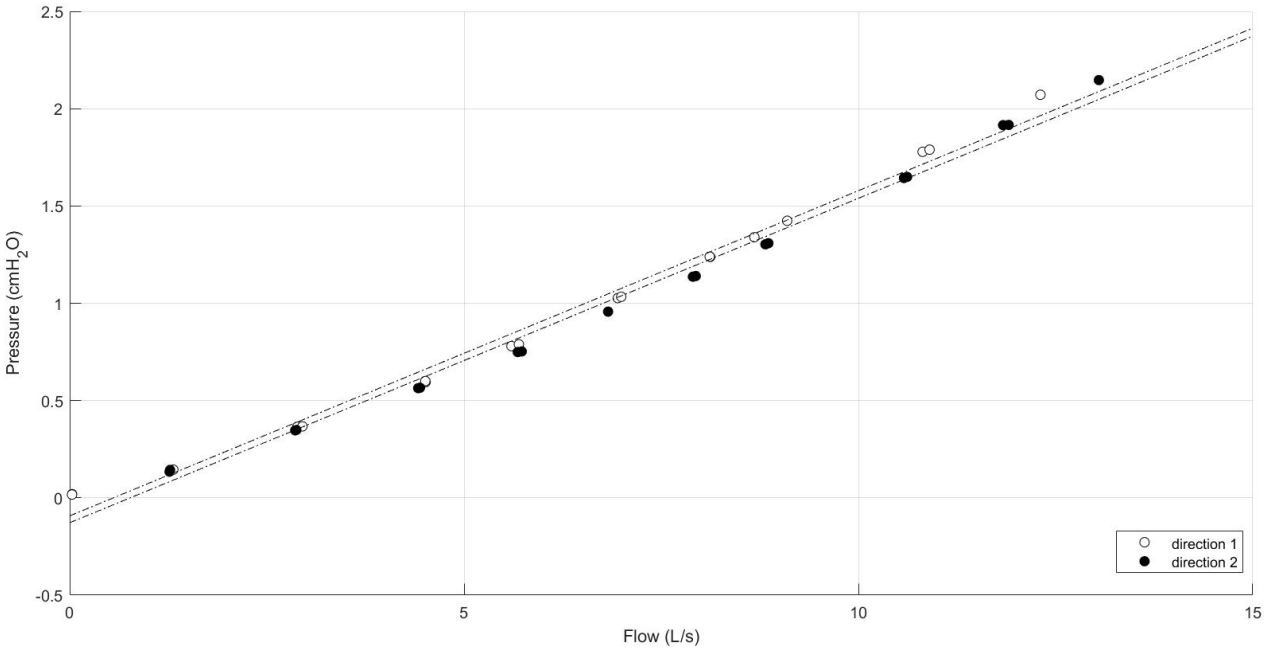

Figure 5.4 - Comparison between linear regression lines obtained from data collected in both direction 1 and 2.

Even though lines are not completely superimposed, they share a similar slope value. The maximum difference between the pressure values computed on the regression lines at the value of 10 L/s, which is a reasonable upper bound for the device application, it's 2.5 % (0.04 cmH_2O).

5.1.3 Mechanical Properties Evaluation

The last in vitro test, performed to evaluate the impedance calculation, was conducted on a test lung that resembles the horses' mechanical properties. The set-up is made of a carboy with a volume equal to 55.75 L used to simulate the compliance of the respiratory system and a test object used to represent inertive and resistive load. The test object is composed of 28 straws of length equal to 15 cm and a diameter of 2 mm. This set-up has a total resistance of 2.57 cmH2O·s/L, a compliance of 0.0385 L/cmH2O and an inertance value equal to 0.0274 cmH2O·s²/L. The values obtained are related to the dimension of the set-up built and are far from those computed on real horses: for example, to obtain a realistic value of compliance, at least 5 carboys equal to the one used in this test should be connected in parallel [11]. However, these values are considered acceptable for the set-up to be used in a bench test. In Figure 5.5 the set-up is schematized:

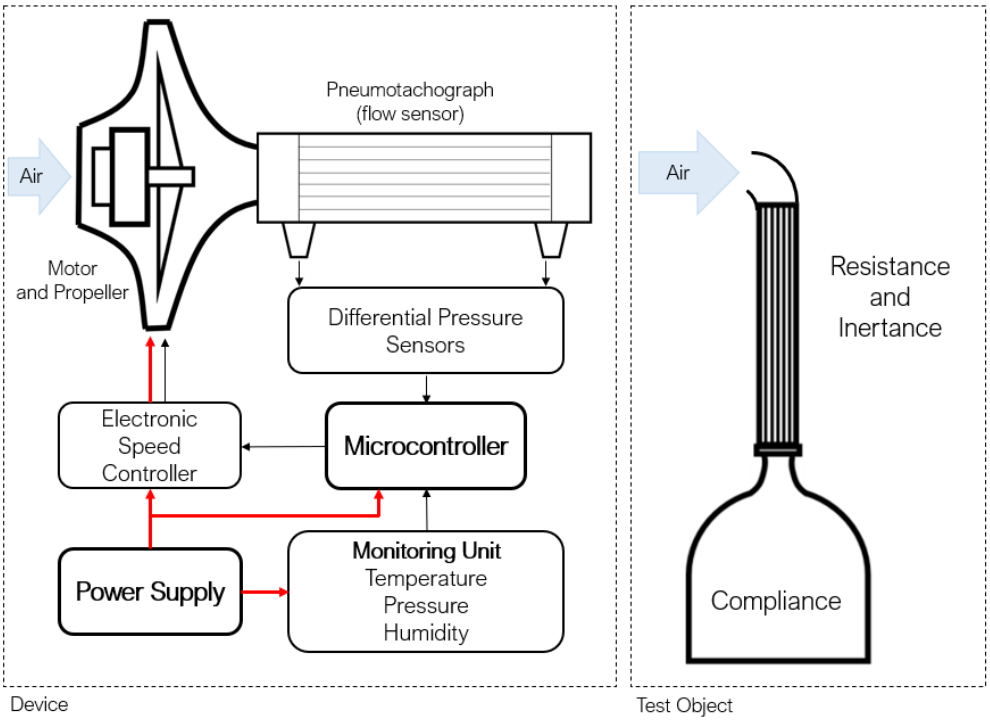

Figure 5.5 - Test lung scheme: the setup used for mechanical property evaluation is composed by a test object and a carboy placed in series.

The protocol consists of an acquisition exploiting the forced oscillation technique imposing the pressure sinusoids of 0.75 cmH_2O peak to peak amplitude superimposed to a 2 cmH_2O positive pressure. Specifically, the frequency range

starts from 1 Hz and ends at 7 Hz with steps of 1 Hz. The duration of each frequency has been set at 15 seconds in order to have sufficient data.

Theretical values of resistance and reactance have been computed for each frequency according to the model proposed by Franken et al. [39]. Results are reported in Figure 5.6:

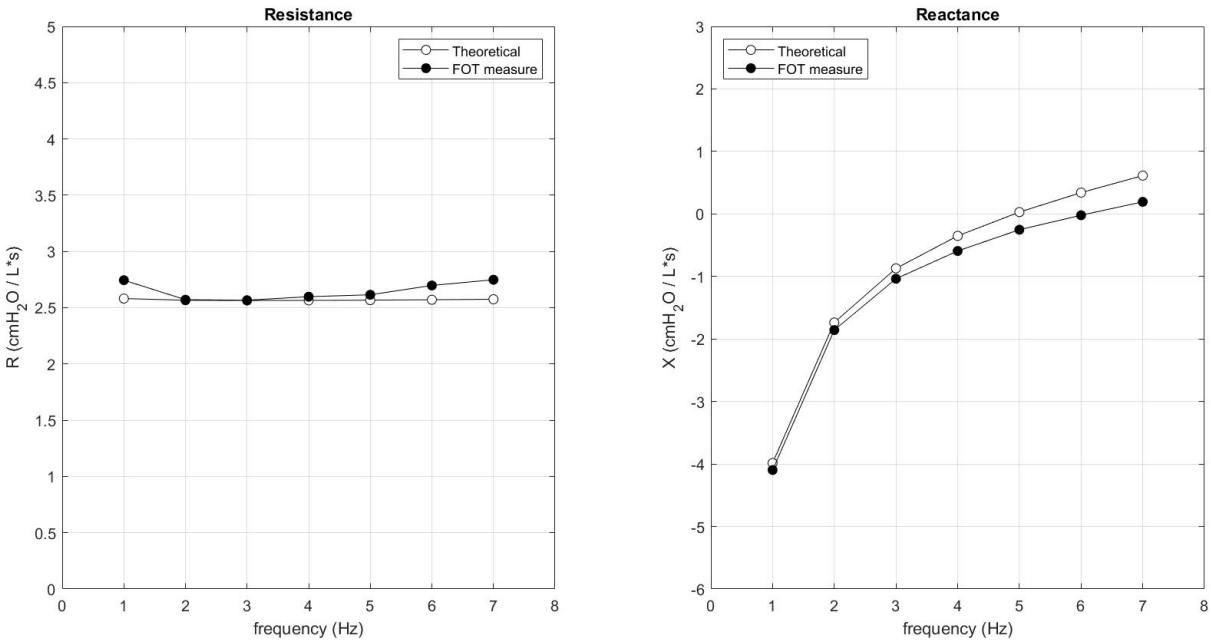

Figure 5.6 - Resistance and Reactance values comparison. Black circles represent empirical values, while white circles represent reference values computed with Franken model.

The average error has been computed for resistance and reactance:

- Average error on resistance: $\Delta R_{avg} = 0.0789\ cmH_2O \cdot {}^{s}/_{L}$
- Average error on reactance: $\Delta X_{avg} = 0.2433\ cmH_2O \cdot {}^{s}/_{L}$

The device resulted to be accurate enough to procede with in vivo tests.

5.2 In-Vivo Validation

The in-vivo acquisitions were performed at the faculty of veterinary medicine of Università degli Studi di Milano, Lodi. Tests were performed to understand whether the procedure of measure is feasible and to evaluate the quality of measured impedance by comparing collected data with veterinary assessment of horses

conditions. A further scope was the qualitative evaluation of the difference in measured respiratory impedances between healthy horses and asthmatic ones.

The study population is composed of 6 horses. Five healthy horses and one diagnosed with Severe Equine Asthma (SEA). Information about the equine population is reported in table 5.

Table 5 – Horse dataset for in-vivo validation

NAME	SEX	AGE	BREED	DIAGNOSIS
ZINGARA	F	13	Mixed	Healthy
FORTUNATO	M	29	Standardbred	SEA
VIOLA	F	6	Mixed	Healthy
CASSANDRA	F	4	Standardbred	Healthy
CRANBERRY	F	4	Standardbred	Healthy
VIRGIN	F	8	Standardbred	Healthy

The acquisition protocol consists of FOT recording over a range of frequencies going from 1 Hz to 7 Hz with a step of 1 Hz for 30 seconds each. Pressure oscillations were characterized by a peak-to-peak amplitude of 1 cmH_2O superimposed to a positive pressure of 3 cmH_20. Measurements were repeated three times on each subject. Each acquisition lasts about 6 minutes. Figure 5.7 depicts the device mounted and equipped with silicone seal and plastic conduit for pressure measurement during a measurement session.

Figure 5.7 - Picture of the device taken during the in-vivo validation.

The evaluation of mechanical properties strictly depends on the current lung volume, which in turn is determined by the pressure at airways opening. For this reason, the *intra-breath baseline control* was implemented. A qualitative evaluation of the effectiveness of the controller can be appreciated in figure 5.8 and 5.9, where changes in average air openings pressure between inspiration and expiration phase are reduced compared to *open-loop control* performed at low frequencies.

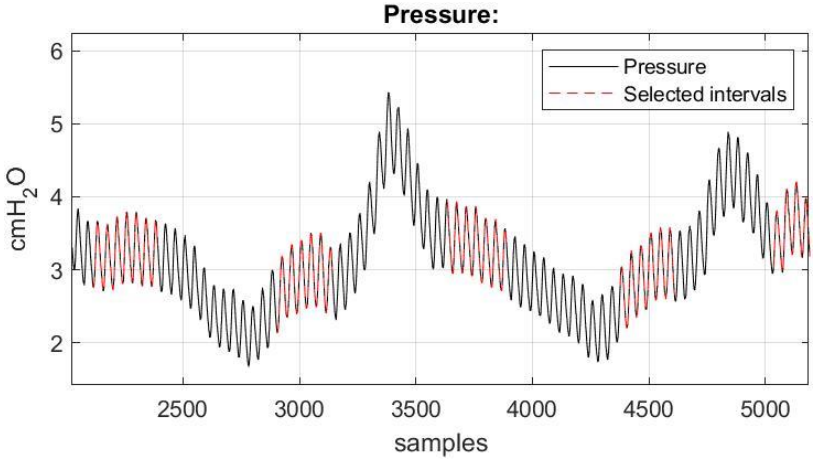

Figure 5.8 - Pressure waveform of a sinusoid pattern at 6 Hz. Closed loop control is applied. Intra breathing baseline compensation is active.

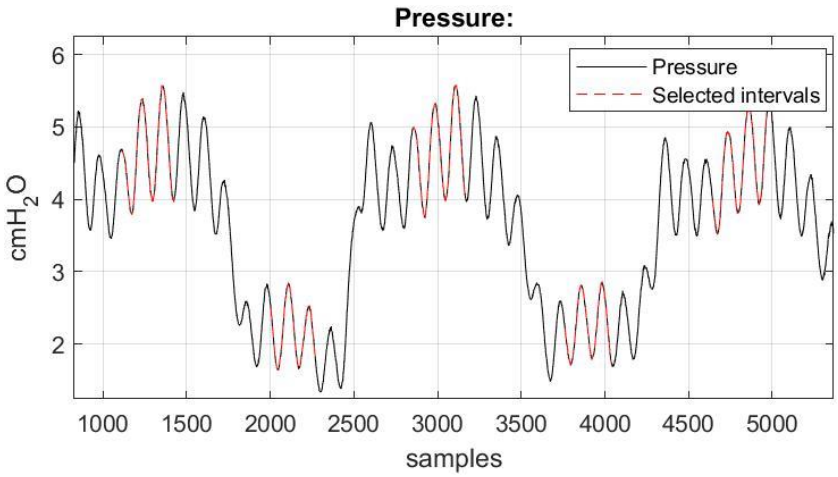

Figure 5.9 - Pressure waveform of a sinusoid pattern at 3 Hz. Open loop control is applied. No baseline compensation is active.

Impedance parameters were extracted using the automatic offline algorithm proposed in section 4.3.5. Resistance and reactance are computed started from filtered pressure and flow signals, in correspondence of the central section of both expiratory and inspiratory phases. Figure 5.10 reports examples of traces from the processing algorithm.

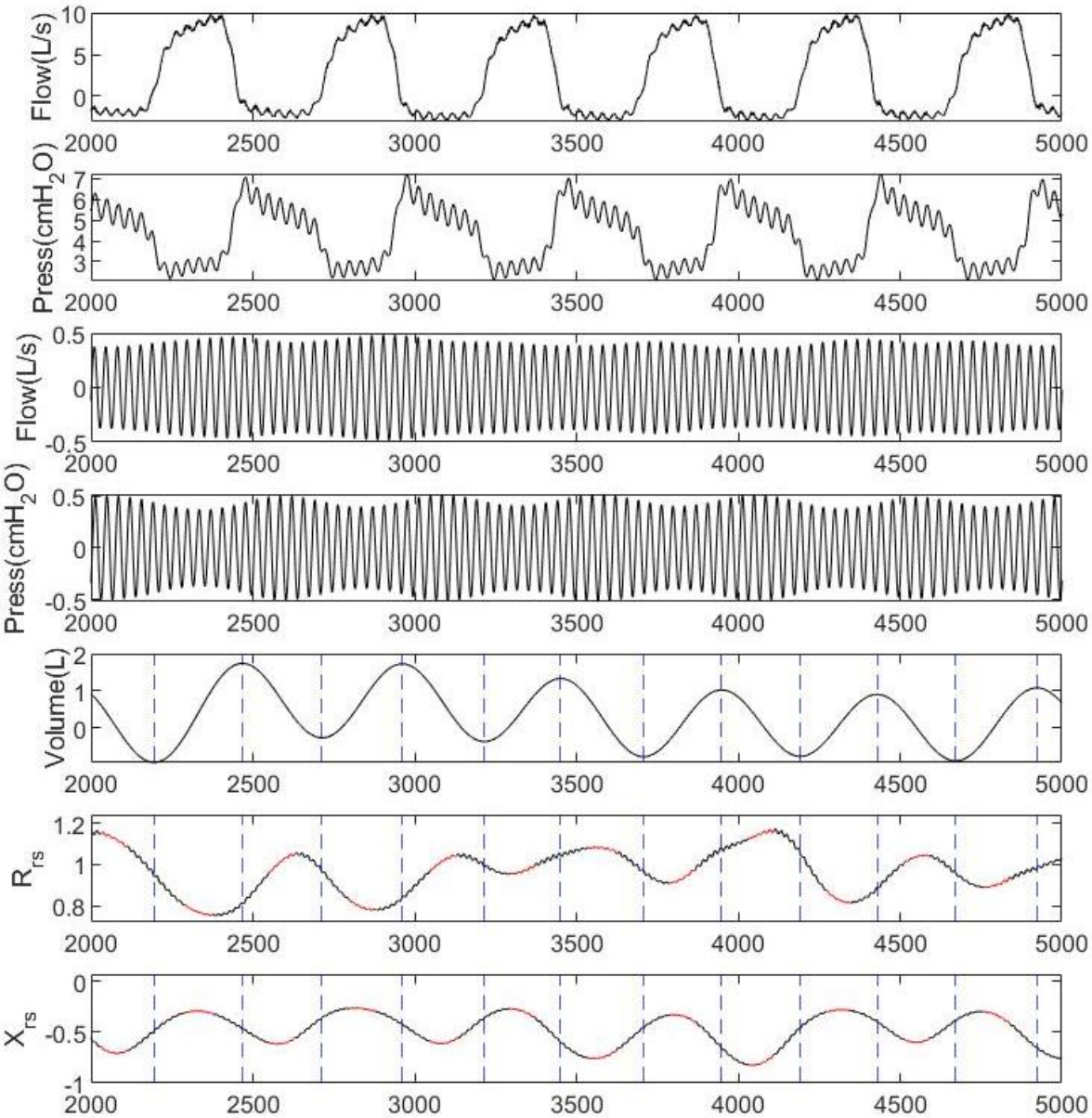

Figure 5.10 - From top to bottom: raw flow and pressure traces. Band-passed flow and pressure tracess. Volume trace and indication of maxima and minima. Resistance and reactance traces. Red sections are referred to the second third of each respiratory phases and are used to compute the average impedances.

Results

Resistance and reactance traces were computed for both the expiratory and inspiratory phases. Examples of traces extracted for a healthy horse are reported in figures 5.11 and 5.12.

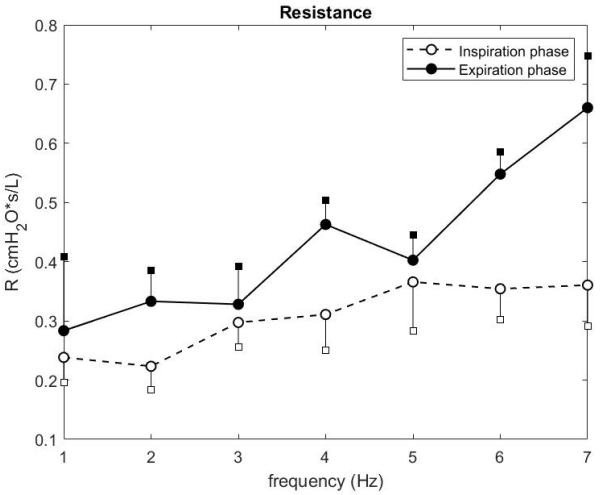

Figure 5.11 - Resistance trace of a healthy horse computed for inspiratory and expiratory phase. Average value and standard deviation over three repetitions.

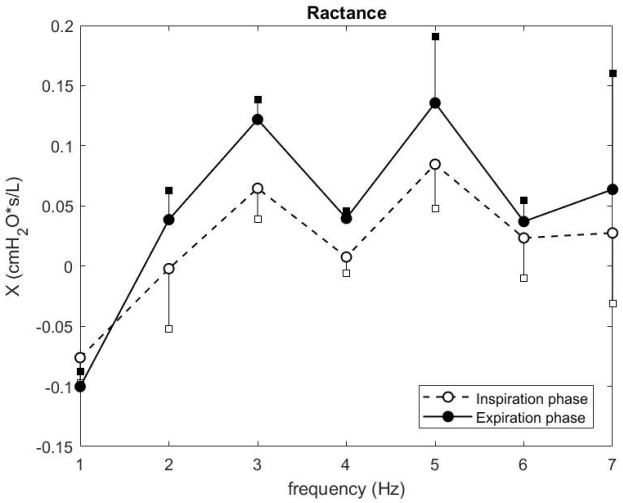

Figure 5.12 - Reactance trace of a healthy horse computed for inspiratory and expiratory phase. Average value and standard deviation over three repetitions.

Measurements were repeated three times among different days for each horse. Mean values are represented as circles, while standard deviation is represented as a square on one side of the curve; in this way was possible to assess the ability of the device to repeat the measure in a reliable way.

Figures 5.13 and 5.14 show the resistance and the reactance of the measurements on the six horses, expressed as mean (SD). Even if the number of asthmatic horses is limited, it is possible to appreciate a difference in resistance and reactance values between healthy and asthmatic horses. The results agree with findings in the literature; the shift in resistance is upward and more accentuated at lower frequencies, caused by an increased central airways resistance due to the presence of mucus within the airways. On the other hand, the reactance of the asthmatic horse decreases at mid frequencies compared to healthy horses due to the obstructive pathophysiology of asthma.

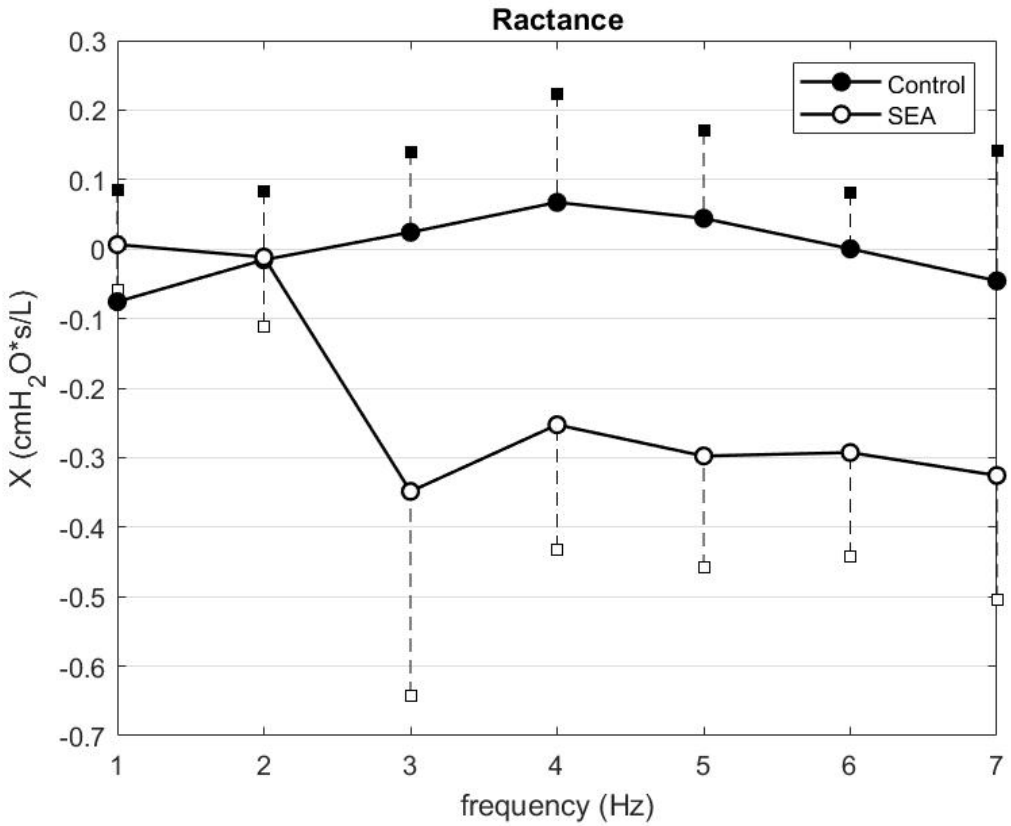

Figure 5.13 - Reactance values for control group and asthmatic one. Mean and standard deviation are reported.

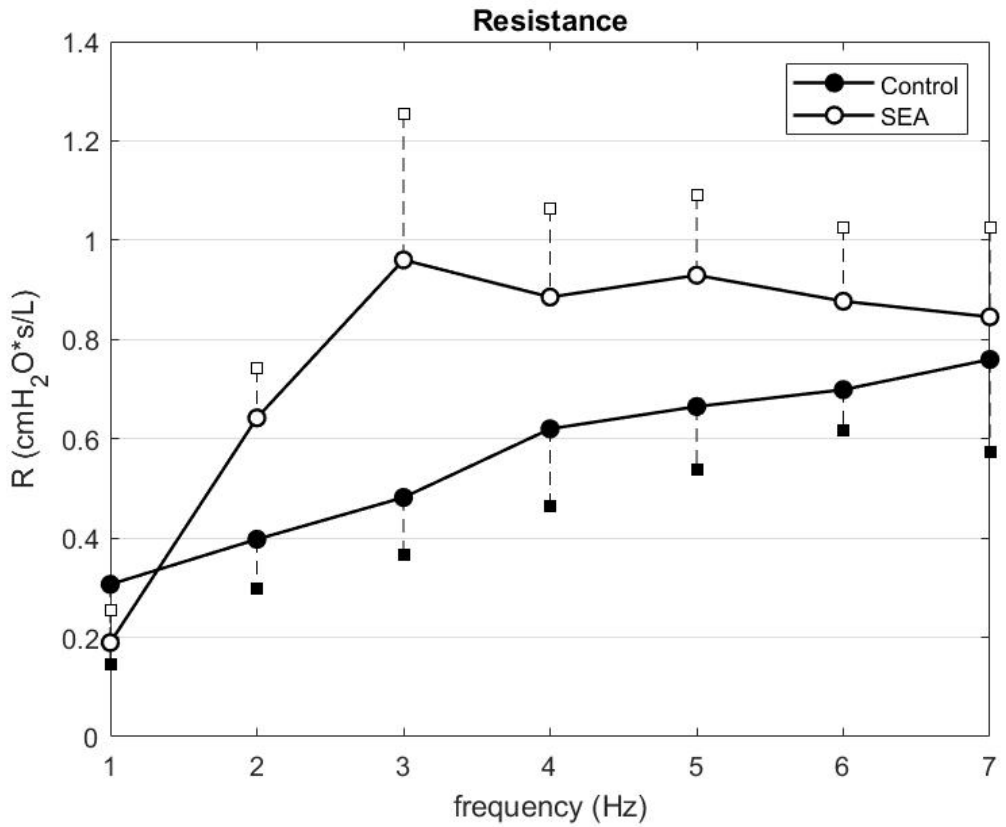

Figure 5.14 - Resistance values for control group and asthmatic one. Mean and standard deviation are reported.

Moreover, by analyzing the expiratory and inspiratory reactance separately, it is possible to compute the ΔXrs, that has been shown in humans to be an indicator of Expiratory Flow Limitation (EFL) in COPD patients. Figure 5.15 reports the ΔXrs of asthmatic and healthy horses for each stimulation frequency. As it is possible to see, there is no difference between the inspiratory and expirsatory reactances of healthy horses (ΔXrs ~ 0 for each frequency). In contrast, the asthmatic horse showed a higher ΔXrs, agreeing with EFL associated with human COPD and SEA in horses [50][51].

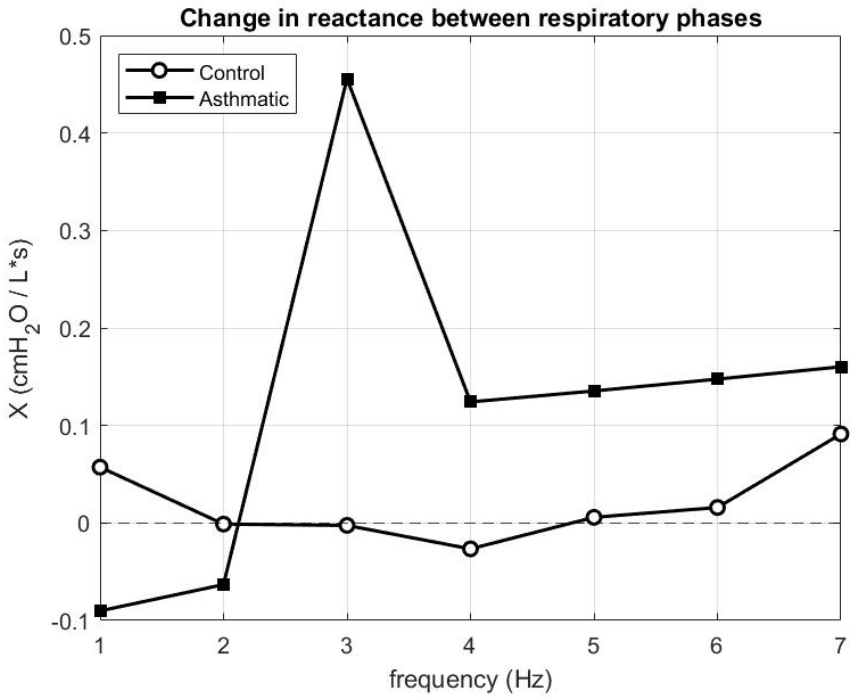

Figure 5.15 - Change in reactance between espiratory and inspiratory phase in both healthy horses, expressed as mean value over five subjects, and horse affected by SEA.

Even though the population of horses used for the in-vivo validation was small and only one asthmatic horse was included, the results confirmed the feasibility of extracting meaningful mechanical parameters using the developed device in an in-vivo context.

CHAPTER 6 CONCLUSIONS AND FURTHER DEVELOPMENTS

Equine asthma is a debilitating pathology that occurs in 80% of horses at least one time. Given the impact of such disorders on horses' physical performances, it is crucial to have access to early diagnosis systems that could be used for preventive treatment strategies. Because of the lack of similar commercially available devices, this thesis work aimed to design and realize a portable device for performing Forced Oscillation Technique tests on horses to assess lung mechanics in a non-invasive and objective way.

The device was developed and in-vitro validated at the TechRes Lab of Politecnico di Milano. The in-vitro tests demonstrated the possibility of transmitting and receiving data exploiting a Wi-Fi communication between the device and a specifically designed Graphical User Interface. Moreover, the mechanical tests showed good agreements between the mechanical properties of a test lung estimated using the device and the theoretical ones.

All the electronics, power supply, and necessary instrumentation have been designed to be fitted on a 3D printed mask that resembles the horse's face. The entire horse mask, air compression unit, and pneumotach were designed to constitute a solid, compact structure. The electronic PCB was designed to host all the necessary components minimizing area usage. The entire system is powered by a Lithium-Polymer battery, which can be easily removed from its case to be changed or charged. Wireless technology and portable power supply allow the device to be used in a context different from the ordinary medical room.

The portability and easiness of use of the developed device allowed a first batch of in-vivo measurements that consented to evaluate its performances in the field of application. In-vivo validation confirmed the feasibility of the procedure, showing that pressure oscillation doesn't interfere with horses' spontaneous breathing. Mechanical properties were correctly assessed in 6 horses, showing the possibility to obtain a reliable measure with a non-invasive, fast, and simple procedure. The possibility to

distinguish between healthy and impaired horses was explored, confirming the feasibility of the assessment.

Innovation of this work relies on the non-invasiveness and simplicity of the technique, allowing to perform tests in a non-controlled environment, which is fundamental for this application. Furthermore, the graphic user interface developed helps the clinician during the acquisition, extending the possibility also to a non-highly trained specialist to handle the test. These two characteristics of the device may allow wide use to monitor horses' lung mechanics, helping the clinician perform faster and more accurate and objective diagnoses.

Even if the number of asthmatic horses is limited, it is possible to appreciate a difference in resistance and reactance values between healthy and asthmatic horses. The results agree with findings in the literature; the shift in resistance is upward and more accentuated at lower frequencies, caused by an increased central airways resistance due to the presence of mucus within the airways. On the other hand, the reactance of the asthmatic horse decreases at mid frequencies compared to healthy horses due to the obstructive pathophysiology of asthma.

Further developments forsee a clinical study collaborating with the University of Montreal (Canada) and the Università Degli Studi di Milano. The protocol includes measurements on an extended sample of animals, which accounts for a large horses variability, including more asthmatic animals and a cohort of asymptomatic subjects. The study will also investigate the daily variability of the measure due to environmental factors.

From a technical point of view, further deveopements will extend the application domain to smartphones with internet access to increase the device portability even more. Moreover, data could be directly saved locally on the device itself, exploiting a microSD card, and retrieved or uploaded to a server that stores them in an ordered database for further analysis.

List of Figures

Figure 1.1 - Bronchial tree and Lung 18

Figure 1.2 - Equine lung volumes 19

Figure 1.3 - Respiratory airflow, oesophageal pressure, tidal volume. 20

Figure 1.4 - Flow and Tidal Volume in human and horse. 21

Figure 1.5 - FOT setup. 33

Figure 1.6 - Pressure and flow tracks recorded at the airway openings of an healthy subject during a 3Hz oscillation (top) and zoom of a 1s fragment of the two tracks obtained after digital filtering (bottom). 35

Figure 1.7 - Resistance and Reactance curves of a healthy subject. 36

Figure 1.8 - Shift in resistance and reactance curves caused by a peripheral airway obstruction. 37

Figure 1.9 - RC model. 38

Figure 1.10 - Resistance and reactance values: squares, clinical remission; circles, acute exacerbation; triangles, after bronchodilation. 41

Figure 2.1 - Device Architecture Scheme. 44

Figure 2.2 PCB scheme 46

Figure 2.3 Device Schematic 47

Figure 2.4 - Hall sensor and BEMF response. 51

Figure 2.5 - Emax LS2207. 52

Figure 2.6 - Three Phase H-Bridge 53

Figure 2.7 - Quadrants and motor operation. 54

Figure 2.8 - ESC architecture. 54

Figure 2.9 - Example of ESC circuit. 55

Figure 2.10- Motor Housing Superior Part. 56

Figure 2.11 - Motor Housing Inferior Part 56

Figure 2.12 - Pneumotachograph section (on the left). Differential pressure sensor (on the right). 58

Figure 2.13 - Absolute Pressure Sensors MS5637. 61

Figure 2.14 - Temperature and Humidity Sensor HIH6130. 61

Figure 2.15 - Power Supply scheme. 62

Figure 2.16 - Communication hierarchy scheme 64

Figure 2.17 - ESP32-D0WD-V3 block diagram. 67

Figure 2.18 - I2C connection scheme. 70

Figure 2.19 - I2C istruction example. 70

Figure 2.20 - SPI connection scheme. 71

Figure 2.21 - Horse mask design. Different colours identify different moduli: black for mask, green for PCB housing, red for power supply housing, grey and light blue for PNT and Motor module. 74

Figure 2.22 - Mask seal stamp, section. 77

Figure 2.23 - Mask seal stamp, front view. 77

Figure 3.1- Example of PID controller scheme 80

Figure 3.2 - ESP32 algorithm flowchart 85

Figure 3.3 - Motor control algorithm flowchart 89

Figure 4.1 - Electron Framework Architecture. 92

Figure 4.2 - Processes hierarchy. 94

Figure 4.3 - High level control scheme. Left: Developer mode. Right: Physician mode. 95

Figure 4.4 - Main process logic chart. 97

Figure 4.5 - Application Strating Window. 99

Figure 4.6 - “Start a new session” window. 100

Figure 4.7 - Settings Window – Physichian Mode. 101

Figure 4.8 - Settings Window – Developer Mode. 102

Figure 4.9 - Plots Window: example of pressure and flow tracks during measurement. 102

Figure 4.10 - Data Processing Scheme. 105

Figure 5.1 - Sinusoidal waveforms. From top to bottom: pressure, flow and PWM duty cycle. 108

Figure 5.2 - Pressure (left) and flow (right) periodgram for different sinusoid frequency. 109

Figure 5.3 - Pneumotachograph Linearity. Data in white have been collected in flow's direction 1; Data in black have been collected in the opposite direction. 110

Figure 5.4 - Comparison between linear regression lines obtained from data collected in both direction 1 and 2. 111

Figure 5.5 - Test lung scheme: the setup used for mechanical property evaluation is composed by a test object and a carboy placed in series. 112

Figure 5.6 - Resistance and Reactance values comparison. Black circles represent empirical values, while white circles represent reference values computed with Franken model. 113

Figure 5.7 - Picture of the device taken during the in-vivo validation. 115

Figure 5.8 - Pressure waveform of a sinusoid pattern at 6 Hz. Closed loop control is applied. Intra breathing baseline compensation is active. 116

Figure 5.9 - Pressure waveform of a sinusoid pattern at 3 Hz. Open loop control is applied. No baseline compensation is active. 116

Figure 5.10 - From top to bottom: raw flow and pressure traces. Band-passed flow and pressure tracess. Volume trace and indication of maxima and minima. Resistance and reactance traces. Red sections are referred to the second third of each respiratory phases and are used to compute the average impedances. 117

Figure 5.11 - Resistance trace of a healthy horse computed for inspiratory and expiratory phase. Average value and standard deviation over three repetitions. 118

Figure 5.12 - Reactance trace of a healthy horse computed for inspiratory and expiratory phase. Average value and standard deviation over three repetitions. 118

Figure 5.13 - Reactance values for control group and asthmatic one. Mean and standard deviation are reported. 119

Figure 5.14 - Resistance values for control group and asthmatic one. Mean and standard deviation are reported..... 119

Figure 5.15 - Change in reactance between espiratory and inspiratory phase in both healthy horses, expressed as mean value over five subjects, and horse affected by SEA. 120

List of Tables

Table 1 - Bluetooth and BLE characteristics 66

Table 2 - Wi Fi characteristics 67

Table 3 - PID controllers coefficients 84

Table 4 – PSI for FOT frequency range 109

Table 5 – Horse dataset for in-vivo validation 114

Bibliography

[1] J. W. Hotchkiss, S. W. J. Reid, e R. M. Christley, «A survey of horse owners in Great Britain regarding horses in their care. Part 2: Risk factors for recurrent airway obstruction», Equine Vet. J., vol. 39, n. 4, pagg. 301–308, lug. 2007.

[2] L. Couëtil e J. Hawkins, Respiratory Diseases of the Horse: A Problem-Oriented Approach to Diagnosis and Management. CRC Press, 2013.

[3] L. L. Couetil et al., «Inflammatory Airway Disease of Horses», pag. 7.

[4] M. Bullone e J.-P. Lavoie, «Asthma "of horses and men"—How can equine heaves help us better understand human asthma immunopathology and its functional consequences?», Mol. Immunol., vol. 66, n. 1, pagg. 97–105, lug. 2015.

[5] R. S. Pirie, «Recurrent airway obstruction: A review: Recurrent airway obstruction: a review», Equine Vet. J., vol. 46, n. 3, pagg. 276–288, mag. 2014.

[6] P. Tilley, J. P. Sales Luis, e M. Branco Ferreira, «Comparison of Skin Prick Tests with In Vitro Allergy Tests in the Characterization of Horses with Recurrent Airway Obstruction», J. Equine Vet. Sci., vol. 32, n. 11, pagg. 719–727, nov. 2012.

[7] E. Jose-Cunilleras, C. W. Kohn, A. Hillier, W. J. A. Saville, e G. Lorch, «Intradermal testing in healthy horses and horses with chronic obstructive pulmonary disease, recurrent urticaria, or allergic dermatitis», J. Am. Vet. Med. Assoc., vol. 219, n. 8, pagg. 1115–1121, ott. 2001.

[8] G. Lorch, A. Hillier, K. W. Kwochka, W. J. Saville, C. W. Kohn, e E. Jose-Cunilleras, «Results of intradermal tests in horses without atopy and horses with chronic obstructive pulmonary disease», Am. J. Vet. Res., vol. 62, n. 3, pagg. 389–397, mar. 2001.

[9] G. Nyman et al., «Pulmonary gas exchange correlated to clinical signs and lung pathology in horses with chronic bronchiolitis», Equine Vet. J., vol. 23, n. 4, pagg. 253–260, lug. 1991.

[10] A. Stopyra, P. Sobiech, e A. Wacławska-Matyjasik, «Acid-base indicators in the venous and arterial blood of horses affected by recurrent airway obstruction (RAO)», Pol. J. Vet. Sci., vol. 15, n. 3, gen. 2012.

[11] D. Navajas, R. L. Dellacà, e R. Farré, «Forced Oscillation Technique», in Mechanics of Breathing, A. Aliverti e A. Pedotti, A c. di Milano: Springer Milan, 2014, pagg. 137–148.

[12] S. S. Young e D. Tesarowski, «Respiratory mechanics of horses measured by conventional and forced oscillation techniques», J. Appl. Physiol., vol. 76, n. 6, pagg. 2467–2472, giu. 1994.

[13] S. S. Young, D. Tesarowski, e L. Viel, «Frequency dependence of forced oscillatory respiratory mechanics in horses with heaves», J. Appl. Physiol., vol. 82, n. 3, pagg. 983–987, mar. 1997.

[14] K.-D. Budras, Anatomy of the horse. Hannover: Schlütersche, 2012.

[15] C. L. Lafortuna e F. Saibene, «MECHANICS OF BREATHING IN HORSES AT REST AND DURING EXERCISE», pag. 16.

[16] T. Art e W. Bayly, «Lower airway function: response to exercise and training», Respir. Syst., pag. 15.

[17] A. M. Koterba, P. C. Kosch, J. Beech, e T. Whitlock, «Breathing strategy of the adult horse (Equus caballus) at rest», J. Appl. Physiol., vol. 64, n. 1, pagg. 337–346, gen. 1988.

[18] «The pattern of external respiration in the unanaesthetized animal», Proc. R. Soc. Lond. B Biol. Sci., vol. 159, n. 975, pagg. 325–347, gen. 1964.

[19] D. J. Marlin e C. M. Deaton, «Pulmonary Function Testing», pag. 21.

[20] N. E. Robinson et al., «Determinants of the Maximal Change in Pleural Pressure during Tidal Breathing in COPD-Affected Horses», Vet. J., vol. 157, n. 2, pagg. 160–165, mar. 1999.

[21] E. Oostveen et al., «The forced oscillation technique in clinical practice: methodology, recommendations and future developments», Eur. Respir. J., vol. 22, n. 6, pagg. 1026–1041, dic. 2003.

[22] D. Bizzotto e S. Dalla Gasperina, «A NEW DEVICE FOR THE MANAGEMENT OF RESPIRATORY SUPPORT AT BIRTH», Politecnico di Milano, 2017.

[23] C. Gulotta et al., «Monitoring the Temporal Changes of Respiratory Resistance: A Novel Test for the Management of Asthma», Am. J. Respir. Crit. Care Med., vol. 185, n. 12, pagg. 1330–1331, giu. 2012.

[24] A. Gobbi, R. L. Dellacá, G. King, e C. Thamrin, «Toward Predicting Individual Risk in Asthma Using Daily Home Monitoring of Resistance», pag. 3.

[25] S. S. Young e L. W. Hall, «A rapid, non-invasive method for measuring total respiratory impedance in the horse», Equine Vet. J., vol. 21, n. 2, pagg. 99–105, mar. 1989.

[26] S. Bickel, J. Popler, B. Lesnick, e N. Eid, «Impulse Oscillometry», Chest, vol. 146, n. 3, pagg. 841–847, set. 2014.

[27] H. J. Smith, P. Reinhold, e M. D. Goldman, «Forced oscillation technique and impulse oscillometry», in Lung Function Testing, R. Gosselink e H. Stam, A c. di European Respiratory Society, 2005, pagg. 72–105.

[28] E. van Erck, D. M. Votion, N. Kirschvink, T. Art, e P. Lekeux, «Use of the impulse oscillometry system for testing pulmonary function during methacholine bronchoprovocation in horses», Am. J. Vet. Res., vol. 64, n. 11, pagg. 1414–1420, nov. 2003.

[29] E. Van Erck et al., «Influence of breathing pattern and lung inflation on impulse oscillometry measurements in horses», Vet. J., vol. 168, n. 3, pagg. 259–269, nov. 2004.

[30] E. Viramontes, «BLDC Motor Control with Hall Effect Sensors Using the 9S08MP», pag. 13.

[31] R. Condit, «Brushed DC Motor Fundamentals», pag. 10, 2004.

[32] «AN885, Brushless DC (BLDC) Motor Fundamentals», pag. 20, 2003.

[33] P. J. Zhao e Y. Yu, «Brushless DC Motor Fundamentals Application Note», pag. 19, 2014.

[34] R. C. Becerra e M. Ehsani, «Four-Quadrant Brushless ECM Drive with Integrated Current Regulation», pag. 9.

[35] «Fiamm_Manuale_Tecnico.pdf». .

[36] «PSoC® 5LP: CY8C58LP Family Datasheet Programmable System-on-Chip (PSoC®)», n. 001, pag. 139.

[37] P. Dhaker, «Introduction to SPI Interface», pag. 5, 2018.

[38] S. R. Kim e Y. K. Rhee, «Overlap Between Asthma and COPD: Where the Two Diseases Converge», Allergy Asthma Immunol. Res., vol. 2, n. 4, pag. 209, 2010.

[39] H. FRANKEN, J. CLEMENT, M. CAUBERGHS, AND K. P. VAN DE WOESTIJNE, «Oscillationg Flow of a Viscous Compressible Fluid Through a Rigid Tube: A Theoretical Model», IEEE Transaction on Biomedical Engineering, VOL. BME-28, NO. 5, pagg. 416 - 420, 1981.

[40] I2C BUS specifications - https://i2c.info/i2c-bus-specification

[41] COMPUTER NETWORKS - ANDREW S. TANENBAUM, DAVID J. WETHERALL.

[42] Amit M. E. Arefin, Nava Raj Khatri, Nitin Kulkarni, Paul F. Egan. “Polymer 3D Printing Review: Materials, Process, and Design Strategies for Medical Applications”. Materials, Process, and Design Strategies for Medical Applications. Polymers 2021.

[43] B. A. Myers, “User Interface Software Technology,” ACM Computing Surveys, vol. 28, no. 1, pp. 189–191, 1996.

[44] T. C. Shan and W. W. Hua, “Taxonomy of Java web application frameworks,” Proceedings - IEEE International Conference on e-Business Engineering, ICEBE 2006, pp. 378–385, 2006.

[45] M. Jasim, Building Cross-Platform Desktop Applications with Electron. Birmingham, UK: Packt Publishing Ltd, 2017.

[46] S. Osterburg, “Electron,” 2019. [Available at https://www.stephanosterburg.com/electron].

[47] K. Kredpattanakul and Y. Limpiyakorn, “Transforming javascript-based web application to cross-platform desktop with electron,” Lecture Notes in Electrical Engineering, vol. 514, pp. 571–579, 2019.

[48] “Electron | Build cross-platform desktop apps with JavaScript, HTML, and CSS.” [Available at https://www.electronjs.org/].

[49] Bizzotto, D., Paganini, S., Stucchi, L., Avallone, M. P., Ramirez, E. M., Pompilio, P. P., Ferrucci, F., Lavoie, J. P., & Dellacà, R. L. (2022). A portable fan-based device for evaluating lung function in horses by the forced oscillation technique. Physiological measurement, 43(2), 10.1088/1361-6579/ac522e. https://doi.org/10.1088/1361-6579/ac522e

[50] Dellacà R L et al 2004 Detection of expiratory flow limitation inCOPDusing the forced oscillation technique Eur. Respir. J. 23 232–40

[51] Stucchi L, Ferrucci F, Bullone M, Dellacà R L and Lavoie J P 2021 Within-breath oscillatory mechanics in horses affected by severe equine asthma in exacerbation and in remission of the disease Animals 12 4